UNIVERSITY OF OKLAHOMA

GRADUATE COLLEGE

DENSITY CHANGES AND COMPOSITIONAL PATH DURING CO_2 INJECTION

A THESIS

SUBMITTED TO THE GRADUATE FACULTY

in partial fulfillment of the requirements for the

Degree of

MASTER OF SCIENCE

By

SON HOANG NGUYEN
Norman, Oklahoma
2016

DENSITY CHANGES AND COMPOSITIONAL PATH DURING CO_2 INJECTION

A THESIS APPROVED FOR THE
MEWBOURNE SCHOOL OF PETROLEUM AND GEOLOGICAL ENGINEERING

BY

_____
Dr. Mashhad Fahes, Chair

_____
Dr. Ahmad Sakhaee-Pour

_____
Dr. Maysam Pournik

DEDICATION

To my advisor, family and friends

ACKNOWLEDGEMENTS

I would like to thank my academic advisor, Dr. Mashhad Fahes, for her dedicative guidance and support. She supports me in and out of school with her prudent wisdom about school and about life. I would also like to thank Dr. Maysam Pournik and Dr. Ahmad Sakhaee-Pour for serving in my committee.

I am grateful to Department of Petroleum Engineering for funding me. Thanks to my friends, colleagues and faculty in this university, I have had a truly valuable experience during my time here.

Finally, thanks my family for their love and support.

TABLE OF CONTENTS

LIST OF TABLES

LIST OF FIGURES

ABSTRACT

CO_2 EOR has been used for a couple of decades as it improves oil recovery. With more than 50% of original oil in place (OOIP) remaining inside reservoir after primary and secondary stage, more and more companies start to apply CO_2 EOR on their fields. In the time when CO_2 is building up in the atmosphere at an alarming rate, the sequestration of CO_2 underground becomes more and more attractive.

In the reservoir, at depth whose pressure is high, CO_2 becomes supercritical, a condition at which CO_2 is not liquid nor gas but has properties of both. Supercritical CO_2 can fill up a container like gas but has high density like liquid (Sidiq & Amin, 2010). At reservoir condition, CO_2 becomes miscible with hydrocarbon. When CO_2 dissolves in hydrocarbon, it increases density of the mixture unlike methane or nitrogen. Scientists have discovered this density effect in the 1970s but they did not study the phenomenon thoroughly. This study models the effect of the density increase using Soave-Redlich-Kwong EOS with CMG simulator software. This phenomenon is confirmed through experimental data. Experimental results then help regression to tune oil model. Finally, this regressed/modified model is imported into CMG BUILDER to study the compositional flow path. The 2D simulation shows the instability in compositional flow. This instability alters significantly the CO_2 flow path and recovery performance. At higher reservoir pressure, the increase in density is greater. At higher permeability, the reservoir is more sensitive to density effect. Both of density increase and permeability play an important role in the gravity instability of flow path.

1. INTRODUCTION

1.1. Introduction

CO_2 is a significant greenhouse gas that traps heat within Earth's atmosphere. It is a product of human activities such as deforestation and burning fossil fuels. It is also released from nature such as respiration and volcanic eruption. Over the past decades, the amount of CO_2 in the atmosphere has increased over 100 parts per million (ppm) rising from 300 ppm in 1950 to over 400 ppm today (Fig. 1.1) (NASA, 2016). This causes global warming and natural disasters. Researchers have figured out a way to store CO_2 underground called carbon sequestration. This process is proposed as a way to slow down CO_2 building up in the atmosphere. This long-term storage of CO_2 is believed to mitigate climate change. In enhanced oil recovery, CO_2 flooding is a valuable technique because it does not only improve oil recovery, it also helps sequester a great amount of CO_2 inside the reservoir. Our understanding of how CO_2 interacting with hydrocarbon is still limited. Therefore, it is essential to study CO_2 and its behaviors at reservoir condition, so that we can have an accurate prediction of what happens during CO_2 flooding. CO_2 increases density of crude oil when dissolved and this creates instability in its flow path. Reservoir permeability and pressure plays an important role in this instability. This complication in flow path alters bottom hole pressure (BHP), oil production rate and total oil recovery.

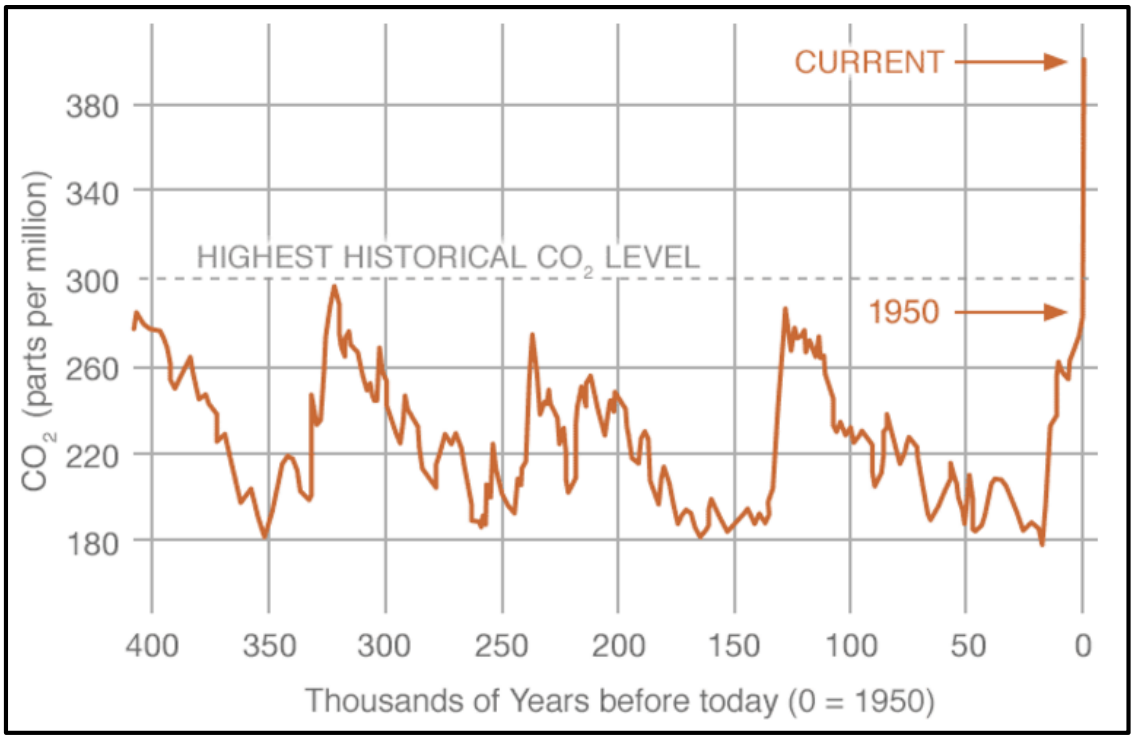

Figure 1.1 – Seasonal cycle of CO_2 levels during the last three glacial cycles. CO_2 level has increased more than 100 ppm since 1950.

1.2. CO_2 Flooding History

CO_2 is one of the most abundant gas on Earth (EPA, 2016). The idea of using this gas to recover oil is dated back to as early as 1920s (Beecher & Parkhurst, 1926). Many attempts have been made to have a better understanding of CO_2 EOR. In 1974, Holms and Josendal studied the mechanism of oil displacement by CO_2. They investigated different types of displacement such as miscible, immiscible and multiple-contact miscible drive of CO_2. They carried out CO_2 flooding to displace different types of oil at different conditions. Throughout the experiments, it was discovered that some of the properties of CO_2 promoted oil recovery. CO_2 enhances recovery by (a) solution gas drive, (b) reduction of viscosity and (c) miscible gas drive. They also compared the recovery mechanism of CO_2 and liquefied petroleum gas (LPG). However, LPG cannot become miscible directly at

reservoir pressure. Furthermore, LPG requires light hydrocarbon in the reservoir for the displacement to be effective. On the other hand, CO_2 can achieve miscibility with heavy oil or residual oil. This is particularly helpful in oil recovery in depleted reservoirs.

In 1982, Svreek and Mehrotra set up some apparatus to investigate the relationship between gas solubility and viscosity/density in bitumen. They carried out the experiment with several gases such as CO_2, CH_4 and N_2 at different conditions. They found out that the solubility is the greatest with CO_2 following by CH_4 and the least with N_2. This leads to CO_2 being the best candidate for oil viscosity reduction. When measuring gas saturated density, they discovered that density of CO_2 saturated bitumen exhibited a different trend to that of CH_4. While density of bitumen decreases with added CH_4, density of CO_2 saturated bitumen increases. This discovery helps explain some phenomena in CO_2 flooding projects as well as opens doors for potential applications.

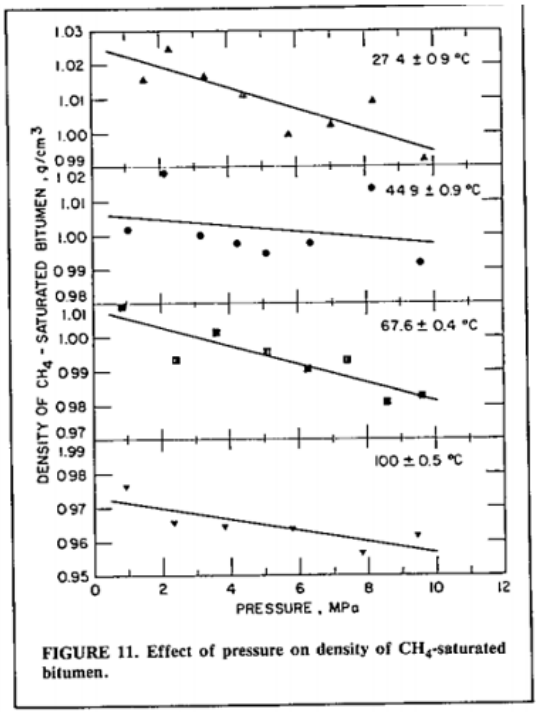

FIGURE 11. Effect of pressure on density of CH_4-saturated bitumen.

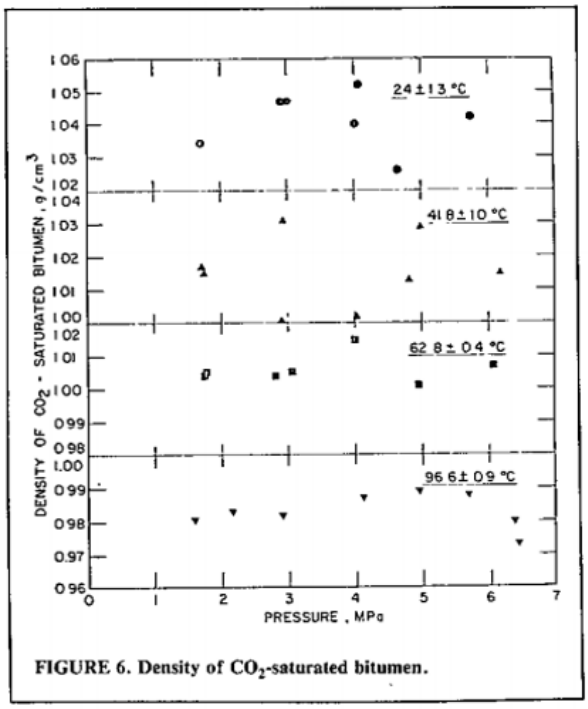

FIGURE 6. Density of CO_2-saturated bitumen.

Figure 1.2 — CO_2 saturated bitumen density tends to increase as pressure increases (more CO_2 in the system). On the other hand, CH_4 decreases density of bitumen as pressure increases (more CH_4 in the system).

There are many fields being developed for CO_2 flooding. Some of which are working and prove their success. There are 4 biggest fields; the largest is the SACROC which was developed in 1981. This is a carbonate reservoir of the Kelly-Snyder field in Scurry county, West Texas. The project has the four-pattern flood. The area is 600 acres and contains about 19 million barrels of oil. The CO_2 flooding comes after and uses the same setup as water flooding. The well pattern is an inverted 9 spot with spacing of 40 acres. The result is an increase in production rate that results in about 1.7 MMSTB additional oil recovered. This accounts for 9% of the OOIP in the area.

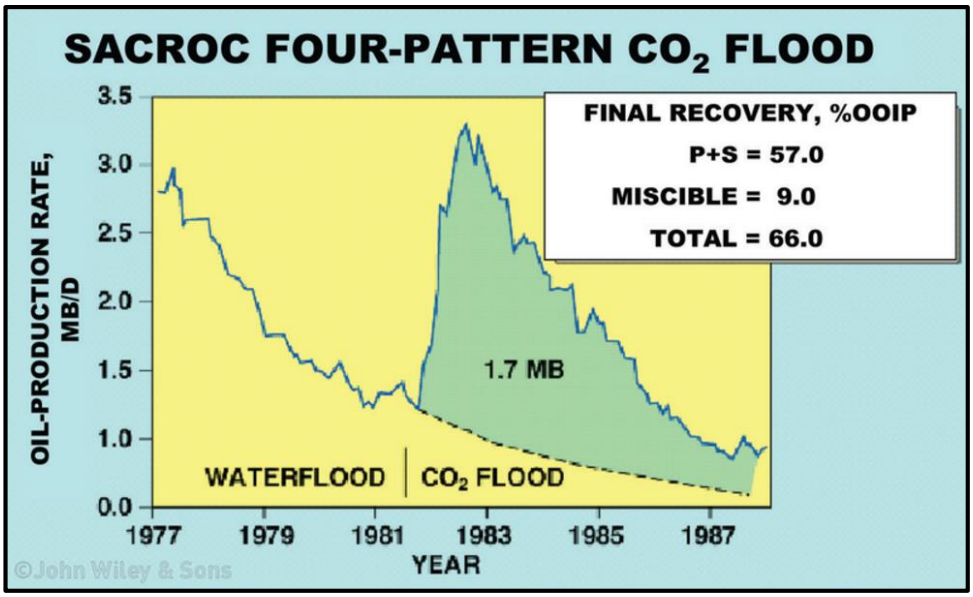

Figure 1.3 — Additional recovery in SACROC field using CO_2 EOR is as much as recovery at secondary stage

Another case is the Means San Andres Unit. Again, the CO_2 flooding comes after water flooding using 20-acre spacing in an inverted 9-spot pattern. The project was developed on an area of 7830 acres. The project uses 2:1 WAG ratio and 0.6 HCPV of CO_2. Fig. A.1 shows that CO_2 miscible flooding results in 15% more of OOIP (Langston, Hoadley, & Young, 1988). This is a great result for CO_2 flooding however this is due to great work of reservoir management program.

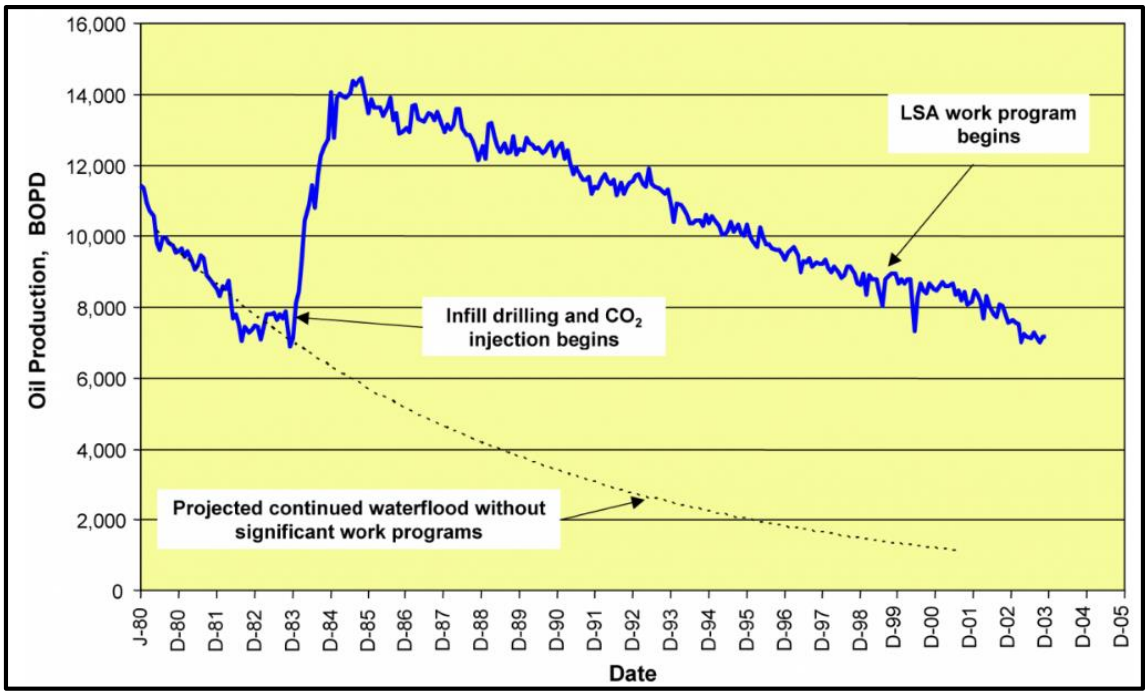

Figure 1.4 – Means San Andres performance

The case in Denver unit is also a great example which started in 1983. This is a larger CO_2 flooding project. It covers an area of 28,000 acres and is estimated to have 2.1 billion barrels of oil (Tanner, Baxley, & Crump III, 1992). As shown in Fig. 1.4, oil production would have had declined significantly if it wasn't for CO_2 injection. In this case WAG is implemented after some time of continuous CO_2 injection. Different water-gas ratio is tested at different parts of the field to find the optimal ratio. Oil rate was maintained as soon as WAG started. However, WAG performs worse than continuous CO_2 injection site. Overall the project performed well. We can see that CO_2 injection clearly is a winner in terms of oil production compared to only-water injection or WAG.

To this date, there are as many as 123 projects using CO_2 EOR in the U.S. They prove CO_2 injection to be a big success. In 2012, oil recovered by CO_2 EOR is almost half of the total oil produced from EOR in the U.S. (Fig. 1.5).

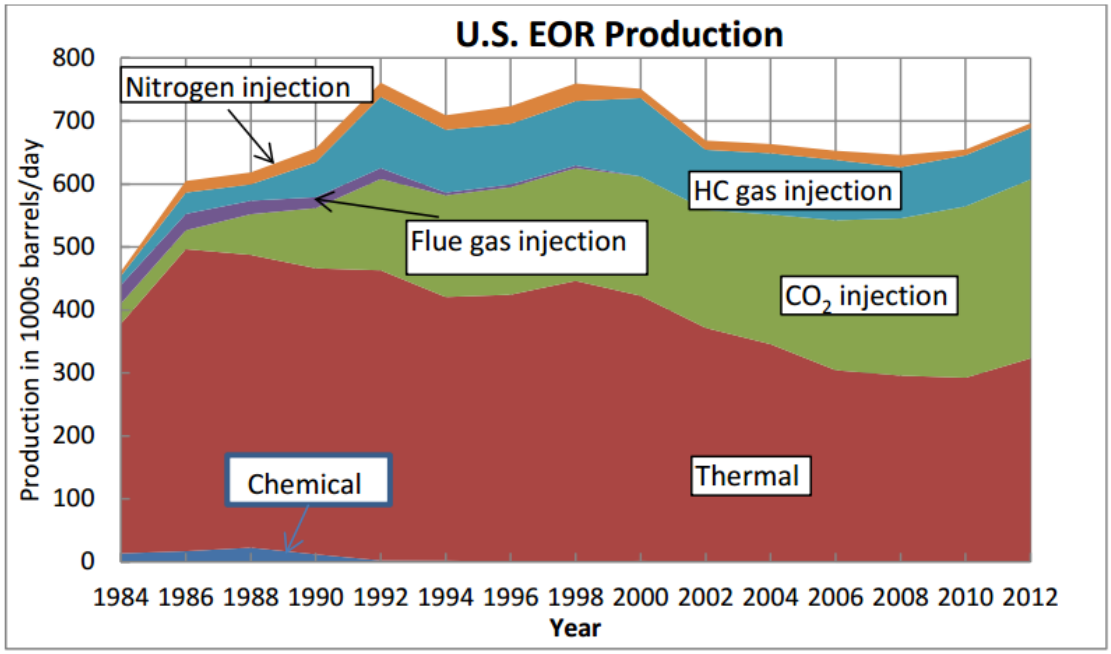

Figure 1.5 – More and more oil recovery comes from CO_2 EOR and it contributes to almost half of U.S. EOR production in recent years. (Koottungal, 2012)

Most of CO_2-EOR projects have been applied in light to medium gravity oils. The table below summarizes 123 projects in the US in 2013 (Verma & Warwick, 2012)

Table 1.1 - Suitable oil for CO_2 EOR has API ranges from 30° to 44°

Number of projects	Lithology	Porosity (percent)	Perm. (md)	Depth (feet)	Gravity (°API)	Viscosity (cp)	Temp. (°F)
			Miscible				
42	ss.	7–26	16–280	1,600–11,950	30–45	0.6–3.0	82–257
2	ss./ls.-dol.	10	4–5	5,400–6,400	35	1	170–181
41	dol.	7–5	2–28	4,000–11,100	28–42	0.6–6.0	86–232
12	dol./ls.	3–12	2–5	4,900–6,700	31–44	0.4–1.8	100–139
6	ls.	4–20	5–70	5,600–6,800	39–43	0.4–1.5	125–135
1	dol./trip. chert	13.5	9	8,000	40	NA	122
7	tripolite	18–24	2–5	5,200–7,500	40–44	0.4–1.0	101–123
1			inadequate data				
			Immiscible				
8	ss.	17–30	30–1,000	1,500–8,500	11–35	0.6–45	99–198
1	dol.	17	175	1,400	30	6	82

1.3. Past Evidence

In the past, there are several experiments that measure mixture of CO_2 and oil. Some of them were to study the density effect while the others came by this effect by accident.

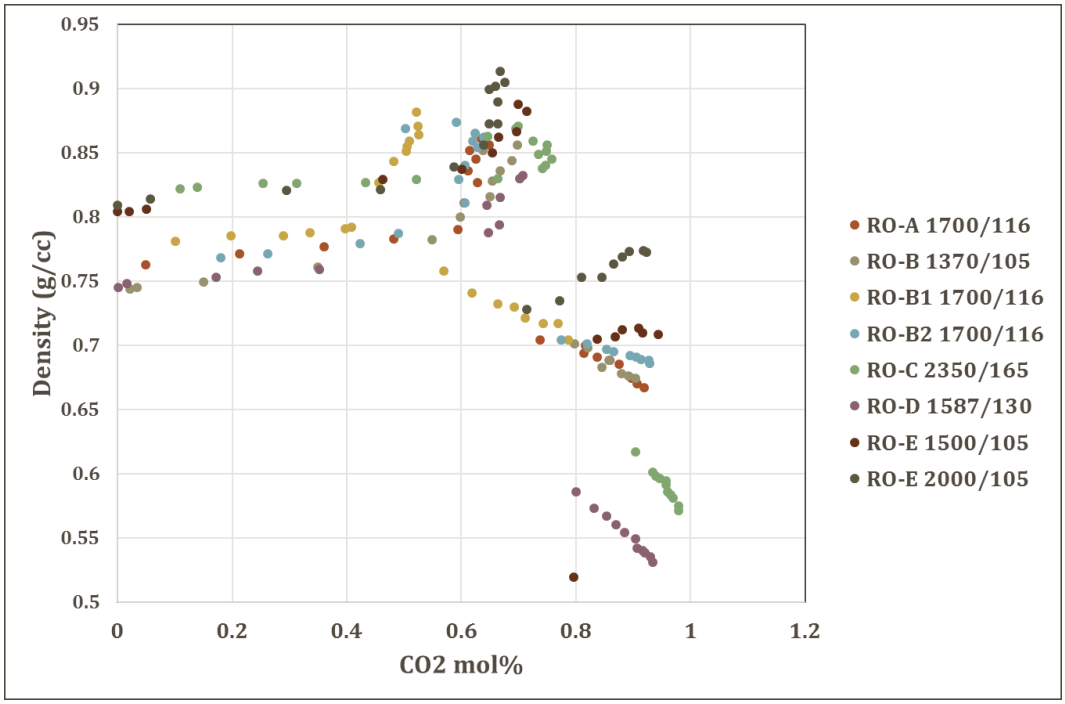

Figure 1.6 – Densities of West Texas oils when mixed with CO_2 at various conditions (RO-A 1700/116 means oil RO-A at 1700 psia and 116 F)

The density changes from CO_2 dissolution in different oils are different but the trends are similar (Figure 1.6). Oil densities increase with added CO_2. This trend is quite linear until around 60 percent mole of CO_2. At this point, the mixture splits into 2 phases: liquid and gas. Densities of liquid phase increase at a higher rate since light components are vaporized into gas phase.

Table 1.2 – These oils showed that densities increase when mixed with CO_2

Type of oil	Where from	API	Density (g/cc)	T ($F^{o)}$	P (psi)	Year
RO-A (live)	West Texas	54	0.763	105	1370	1993
RO-B (live)		59	0.744	116	1700	
RO-B1 (live)		50	0.781	116	1700	
RO-B2 (live)		53	0.768	116	1700	
RO-C (live)		41	0.822	165	2350	
RO-D (live)		58	0.745	130	1587	
RO-E1 (live)		44	0.804	105	1500	
RO-E2 (live)		43	0.809	105	2000	
RO-E (live)		45	0.802	105	1150	
STO-A (live)		49	0.784	109	1500	
Reservoir oil	Bakken	27	0.894	400	14.7	1995
Stock tank oil		15	0.963	107	14.7	
Live oil	N/A	31	0.87	170	2535	1988
Weyburn 1 (dead)	Weyburn	30	0.875	141	14.7	2000
Weyburn 2 (dead)		36	0.842	138	14.7	
Weyburn 3 (dead)		32	0.864	140	14.7	
Weyburn 1 (live)		29	0.882	141	700	
Weyburn 2 (live)		36	0.845	138	700	
Weyburn 3 (live)		31	0.871	141	700	
Stock tank oil	PORT NECHES FILED	38	0.835	165	14.7	2002
Live oil	PORT NECHES FILED	35	0.850	165	2700	

1.4. Is CO_2 from Acidizing a Problem?

CO_2 at reservoir condition has potential to affect oil properties and its flow path. This emerges a problem when a formation goes through acidizing and produces CO_2 as a byproduct. The following chemical reaction illustrates the essential process of what happens during acidizing

$$2HCl + CaCO_3 \rightarrow CaCL_2 + CO_2 + H_2O$$

Now let's take a closer look at the equation and apply that to a simple case. The case is as follow:

Using HCl 15% to acidize 100% carbonate rock with porosity of 15%. The formation is 100% oil saturated. The volume of acid injected is 100 gallons for each foot of formation. The wellbore radius is 0.28 ft. Reservoir condition is 150 °C and 5000 psia.

With the stoichiometry of HCl and $CaCO_3$ equal to 2 and 1 respectively, the amount of mineral consumed by a given amount of acid is calculated by

$$\beta_{100\%} = \frac{v_{mineral} MW_{mineral}}{v_{acid} MW_{acid}} = \frac{1 * 100.1}{2 * 36.5} = 1.37 \ \frac{lb\ CaCO_3}{lb\ HCl}$$

β is gravimetric dissolving power in mass basis and v is the stoichiometry.

Using HCl 15%, the power is reduced to

$$\beta_{15\%} = \beta_{100\%} * 15\% = 0.206 \ \frac{lb\ CaCO_3}{lb\ HCl}$$

From here we can easily convert mass dissolving power to volumetric dissolving power

$$X = \beta \frac{\rho_{acid}}{\rho_{mineral}} = 0.206 * \frac{66.8 \frac{lb}{ft^3}}{169 \frac{lb}{ft^3}} = 0.081 \ \frac{ft^3 CaCO_3}{ft^3 HCl}$$

So every cubic feet of acid can dissolve 0.081 cubic feet of the formation.

Now, with the injection rate of 100 gallons (or 13.4 ft^3) per feet assuming that HCl reacts immediately with formation, it is simple to calculate the distance of acid front before being spent. The volume of rock dissolved is:

$$V_{carbonate} = X_{15} * V_{acid} = \frac{0.081 \frac{ft^3 CaCO_3}{ft^3 HCl} * 13.37\ ft^3 HCl}{1 - 0.15} = 1.28\ ft^3 CaCO_3$$

Specific gravity of HCl 15% is 1.07 according to Perry's Chemical Engineers' Handbook. (Green & Perry, 2016). Mass of HCl in 15% solution

$$V_{HCl} = 1.07 * 62.4 * 13.4\ ft^3 * 15\% = 134\ lb\ HCl$$

Mass of water in solution before reaction

$$V_{water\_before} = 1.07 * 62.4 - 134 = 759\ lb$$

Mass of water produced

$$V_{water} = \frac{nHCl}{2} * MW_{water} = \frac{\frac{134}{36.5}}{2} * 18 = 33\ lb$$

After the reaction, the total amount of water in 1 ft. of formation is

$$V_{water\ total} = 759 + 33 = 792\ lbs$$

At reservoir condition, this is equivalent to 24.4 ft^3 of water.

Similarly, the amount of CO_2 produced is

$$V_{CO_2} = \frac{nHCl}{2} * MW_{CO_2} = \frac{\frac{134}{36.5}}{2} * 44 = 80.7\ lb$$

Or at reservoir condition would be equivalent to 2.4 ft^3.

Using density data from NIST at reservoir condition, we can calculate the amount of CO_2 dissolved in water to be 0.5 ft^3 which leaves 1.9 ft^3 of CO_2 in 1 ft. of formation which extends to 0.42 ft. into the reservoir. This amount of CO_2 is too small to have any

significant effects on oil property when dissolved, thus it should not cause any problems in the formation of interest after acidizing treatment in terms of density changes.

2. EXPERIMENTAL WORK

2.1. Experimental Setup

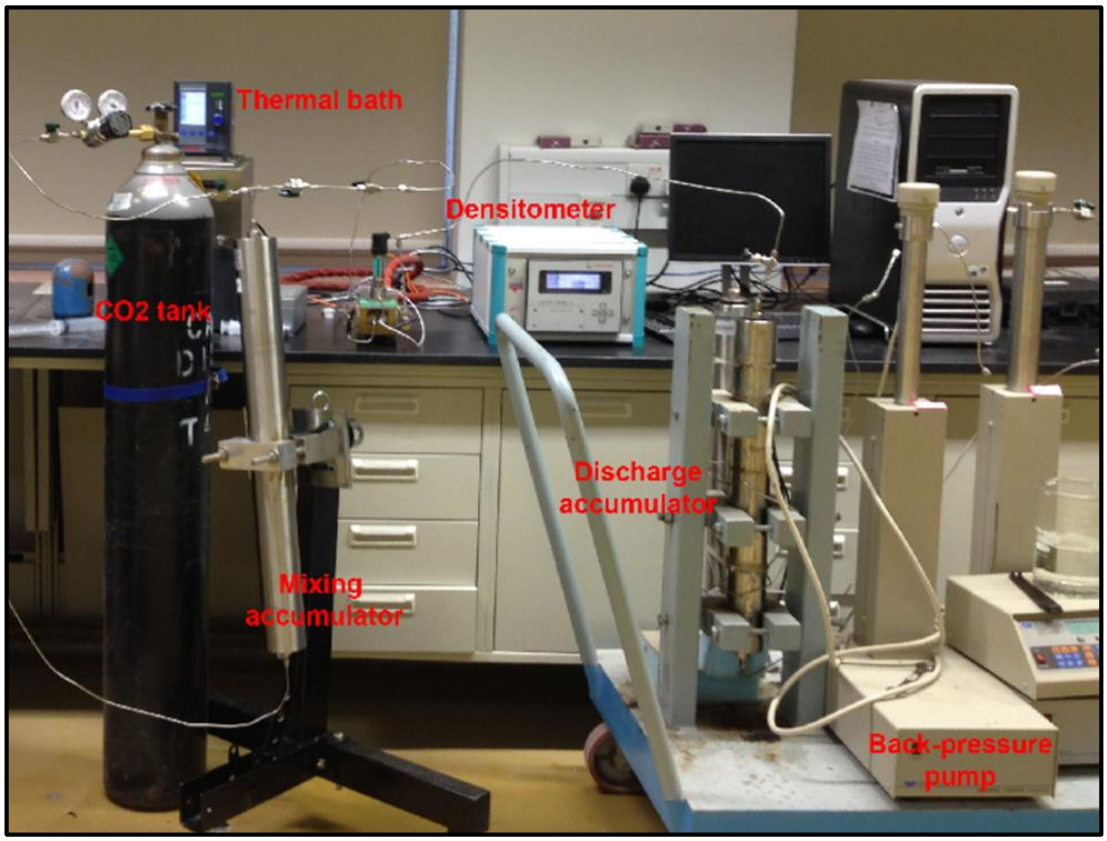

Figure 2.1 –Setup in the lab with all equipment

Equipment:

- Pump for creating desired pressure (inlet pump)
- Pump for back pressure (outlet pump)
- CO_2 tank
- Accumulator for mixing
- Accumulator for discharge
- Densitometer
- Thermal bath

The schematic can be drawn as follow:

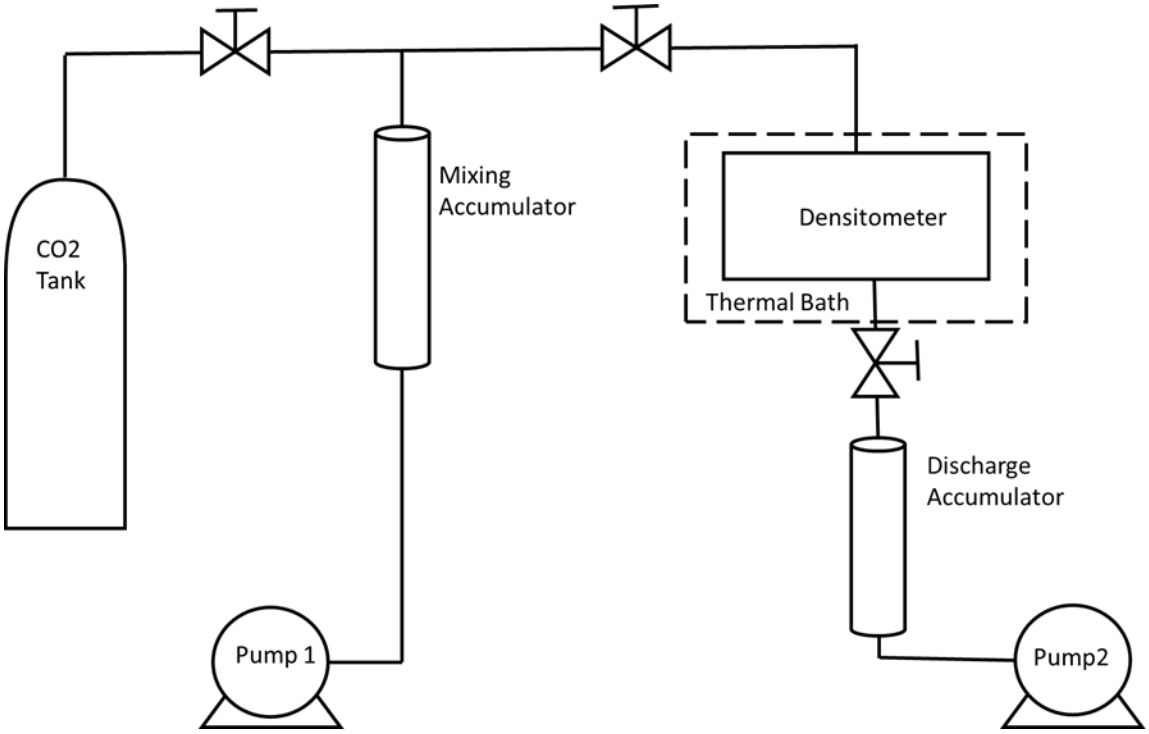

Figure 2.2 – Schematic of experimental setup

The experiment is run at 122^{o} F and 3000 psia.

2.2. Experimental Procedure

In general, the oil is mixed with CO_2 in mixing accumulator, then the mixture is run through the densitometer, whose temperature is controlled by a thermal bath, for density measurement. Discharging the mixture from densitometer to another accumulator is accompanied by a pump for back pressure.

CO_2 tank connects to bottom of mixing accumulator. To figure out the mixing ratio, volume of crude oil and free volume in mixing accumulator is calculated. This free

volume later will be occupied by CO_2 gas. CO_2 is injected to accumulator at pressure set on CO_2 tank valve. Based on the temperature and pressure inside the accumulator, it is possible to figure out how much CO_2 is injected into the accumulator from the tank. Finally, inlet pump increases pressure inside accumulator to dissolve CO_2 into the oil.

Figure 2.3 - T connection on top of mixing accumulator

On top of the mixing accumulator, there is a T connection to let the mixture go into the densitometer (to the right) after receiving CO_2 (from the left) like shown in Fig. 2.3.

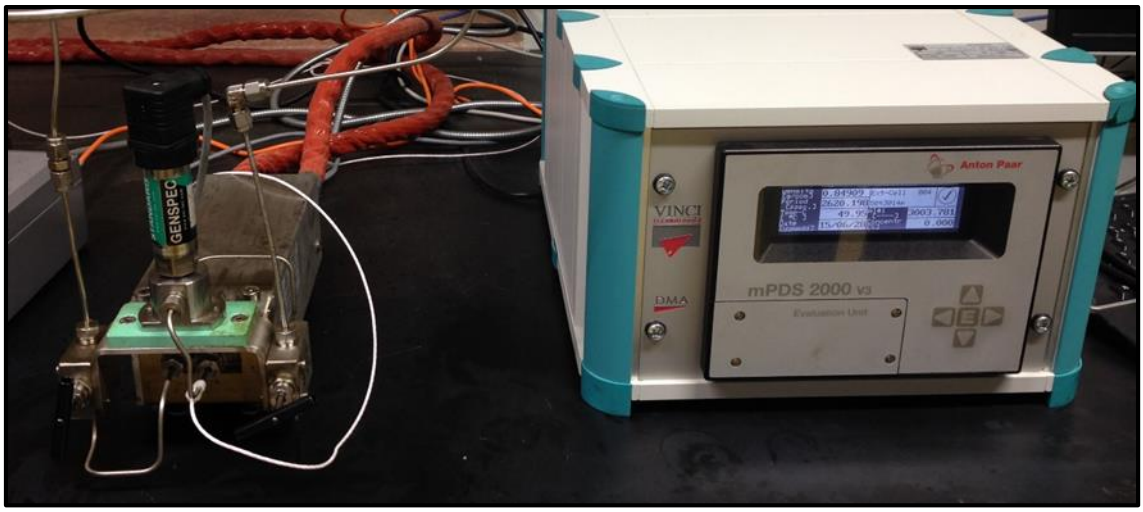

Figure 2.4 – Densitometer controller and its chamber (left)

A thermal bath is used to control the fluid temperature inside the densitometer chamber. After new mixture comes inside densitometer chamber, new density can be recorded. (Fig. 2.4)

To discharge old mixture, another accumulator is used. A pump is connected to this accumulator to provide back pressure so that oil composition is protected when transferring (Fig. 2.5).

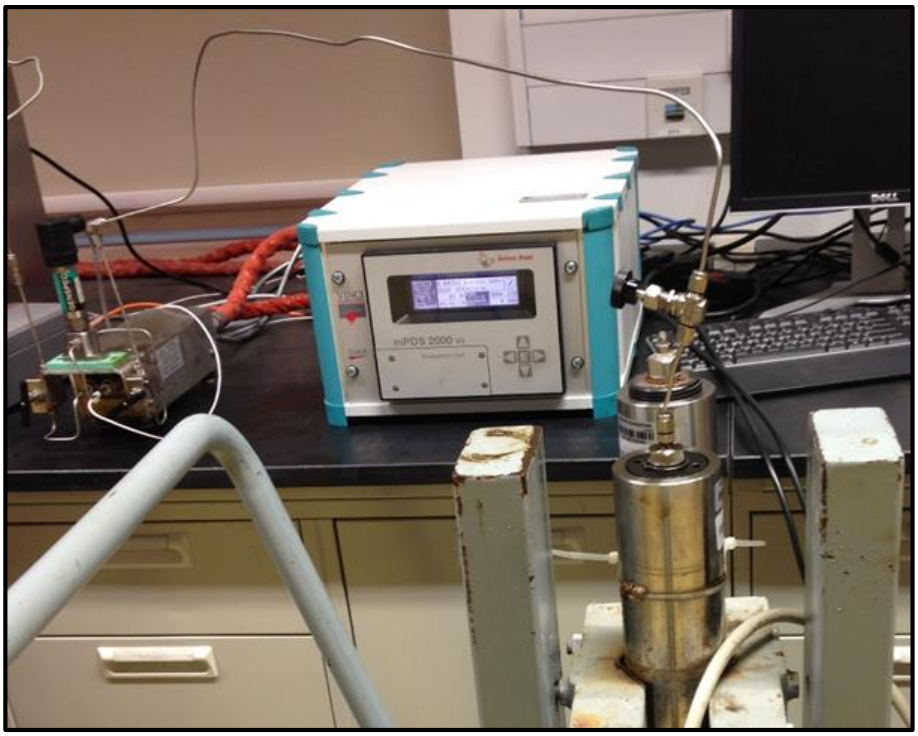

Figure 2.5 - Accumulator for discharge connects to outlet pump at the bottom

2.3. Experimental Results

Density of CO_2/Oil mixture is recorded according to CO2 content. The result is plotted as CO_2 mole fraction (Fig. 2.6) and weight fraction (Fig. 2.7).

Oil A

CO_2 Mole Fraction	Density (g/cc)	Density Increase (%)
0.0000	0.8485	0.0000
0.0839	0.8495	0.120
0.2011	0.8518	0.388
0.3048	0.8542	0.668
0.4019	0.8550	0.768
0.4780	0.8568	0.981
0.5590	0.8582	1.146
0.6498	0.8601	1.370
0.7075	0.8609	1.464
0.7611	0.8600	1.353
0.7971	0.8643	1.862
0.8276	0.8657	2.028
0.8534	0.8676	2.253
0.8733	0.8727	2.855

Oil B

CO_2 Mole Fraction	Density (g/cc)	Density Increase (%)
0.0000	0.8445	0.000
0.1422	0.8461	0.189
0.2251	0.8479	0.403
0.3116	0.8492	0.560
0.3629	0.8497	0.618
0.4109	0.8536	1.080
0.4902	0.8513	0.804
0.5369	0.8560	1.356
0.5798	0.8573	1.515
0.6254	0.8588	1.693
0.6943	0.8560	1.358
0.7400	0.8591	1.729
0.7867	0.8597	1.800
0.8521	0.8535	1.061

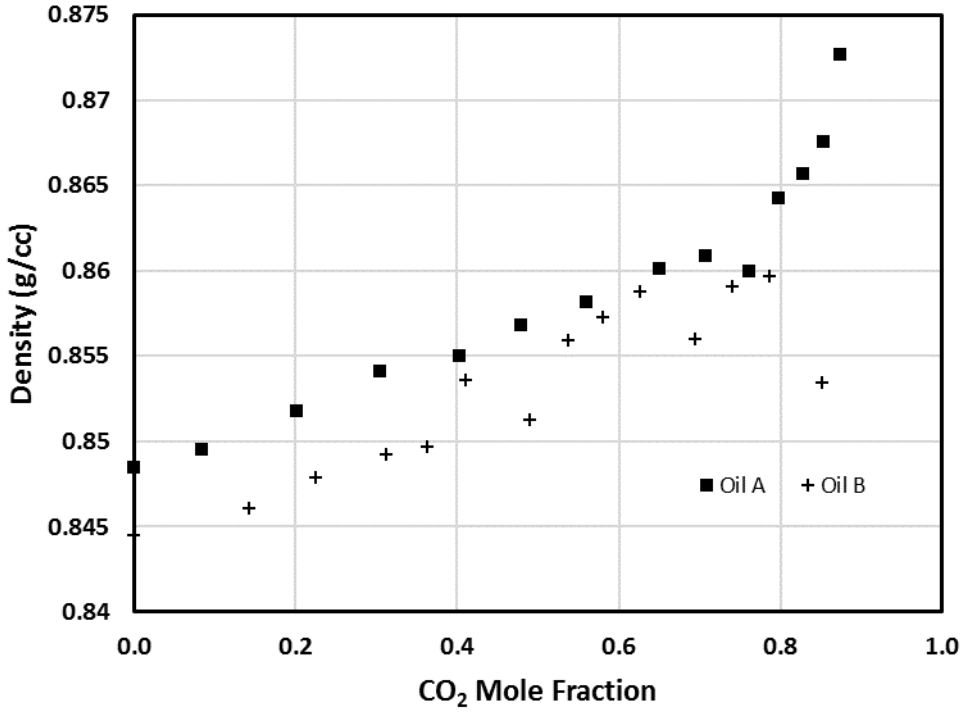

Figure 2.6 - Density of mixture increases as more CO_2 enters the system

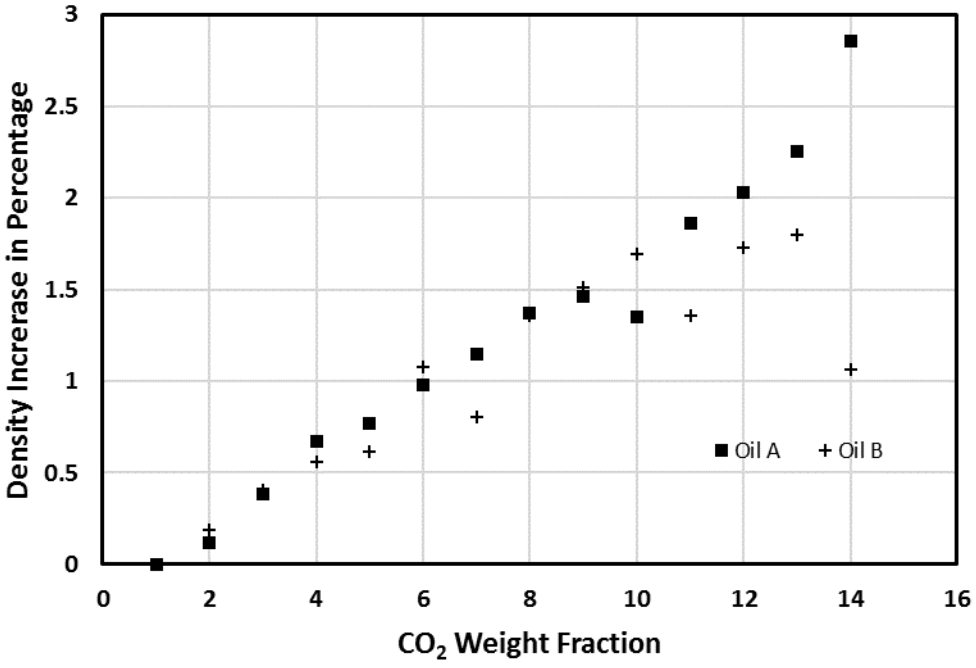

Figure 2.7- Density of mixture increases as more CO_2 enters the system

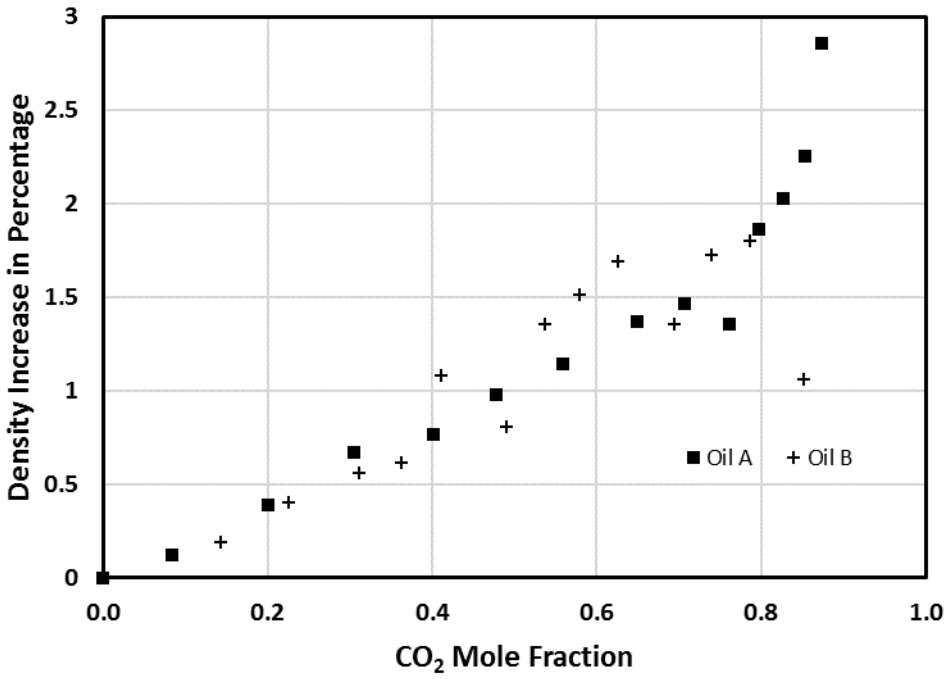

Figure 2.8 - Density increases as much as 3 percent

Overall, density of mixture increases with more CO_2 content. The trend line is linear up to 70 percent then has a break on both oils. When put together, Oil A and Oil B shows different trend lines (Fig. 2.6). However, when density is normalized to density-gain-in-percentage versus CO_2 mole fraction, the two data sets lie on top of each other showing great agreement (Fig. 2.8).

3. SIMULATION WORK

3.1. Equations of State and Volume Shift

To predict properties of a pure substance at different conditions, the industry has been using equations of state (EOS). This equation can illustrate the behavior of fluid at 2 phase or 1 phase region. Several EOS have been proposed such as Van der Waals, Soave-Redlich-Kwong, Benedict-Webb-Rubin and Peng-Robinson, etc. Some EOS perform better than others with different types of oil or some perform better with mixtures than others (Firoozabadi, 1989). Mixture of HC requires each parameter to change according to mixing rule to apply EOS, but the EOS still cannot predict very well. EOS have been compared in many papers. All the results get to the point that there is no one best EOS for reservoir fluids at different conditions. Some surpass others in predicting certain properties while other can excel at a certain reservoir fluid.

One of the most widely used EOS is Soave-Redlich-Kwong EOS. This is an improved version of van der Waals EOS, which was introduced in 1976. This EOS greatly improves density prediction. The EOS is as follow

$$P = \frac{RT}{V_m - b} - \frac{a(T)}{V_m(V_m + b) + b(V_m - b)} \quad (1)$$

Where

$$a(T_c) = 0.45724 \frac{(RT_c)^2}{P_c}$$

$$b = 0.0778 \frac{RT_c}{P_c}$$

For temperature dependent parameter

$$a(T) = a(T_c)\alpha(T)$$

Where $\alpha(T)$ is a dimensionless function of reduced temperature and acentric factor

$$\alpha(T) = \left\{1 + m\left[1 - \sqrt{\frac{T}{T_c}}\right]\right\}^2$$

With

$$m = 0.3746 + 1.5423\omega - 0.2699\omega^2$$

Equation (1) can be rewritten as

$$Z^3 - (1 - B)Z^2 + (A - 3B^2 - 2B)Z - (AB - B^2 - B^3) = 0 \qquad (2)$$

Where

$$A = \frac{aP}{R^2T^2}$$

$$B = \frac{bP}{RT}$$

$$Z = \frac{Pv}{RT}$$

Jhaveri and Youngren (1984) used a modification by Peneloux el al. to include a third parameter to correct offset in volume prediction. This method is recommended in mixture of oil and CO_2. This parameter does not affect any properties of the oil system. It only changes phase volume by shifting volume axis. The modified equation is as follow

$$(Z + C)^3 - (1 - B)(Z + C)^2 + (A - 3B^2 - 2B)(Z + C) - (AB - B^2 - B^3) = 0 \quad (3)$$

Where

$$C = sB$$

With *s* being the volume shift parameter.

The equation **(2)** or **(3)** yields 1 or 3 roots depending on the number of phases in the system. If the system has 2 phase, the biggest root is the compressibility for gas phase and the smallest root corresponds to compressibility of liquid. (Pénelou, Rauzy, & Fréze, 1981).

Even though many researchers enjoy the simplicity of the PR EOS, the EOS cannot predict well at C_{10+}. There were some attempts to fix this problem, but this involves adding a fourth parameter, which makes it too complicated.

3.2. Fluid Modeling

The main concern in this study is CO_2 and its behaviors, which cause the density of CO_2/oil mixture to increase. By default, in CMG WINPROP, more CO_2 in an oil composition results in density decreases. This can be fixed by running regression on CO_2 volume shift using CO_2 density at different pressures. Data of CO_2 density at 116^{o} F is acquired from National Institute of Standards and Technology (NIST). The default volume shift of CO_2 is 0.0833. After regression, new volume shift is found to be 0.238, which gives a much better prediction around 3000 psia- the pressure the experiment is carried out. This is very close to the volume shift suggested in Thermodynamics and Applications of Hydrocarbons Energy Production, which is 0.25 (Firoozabadi, 2015). With the new volume shift, CO_2 dissolution in oil makes the mixture density increase.

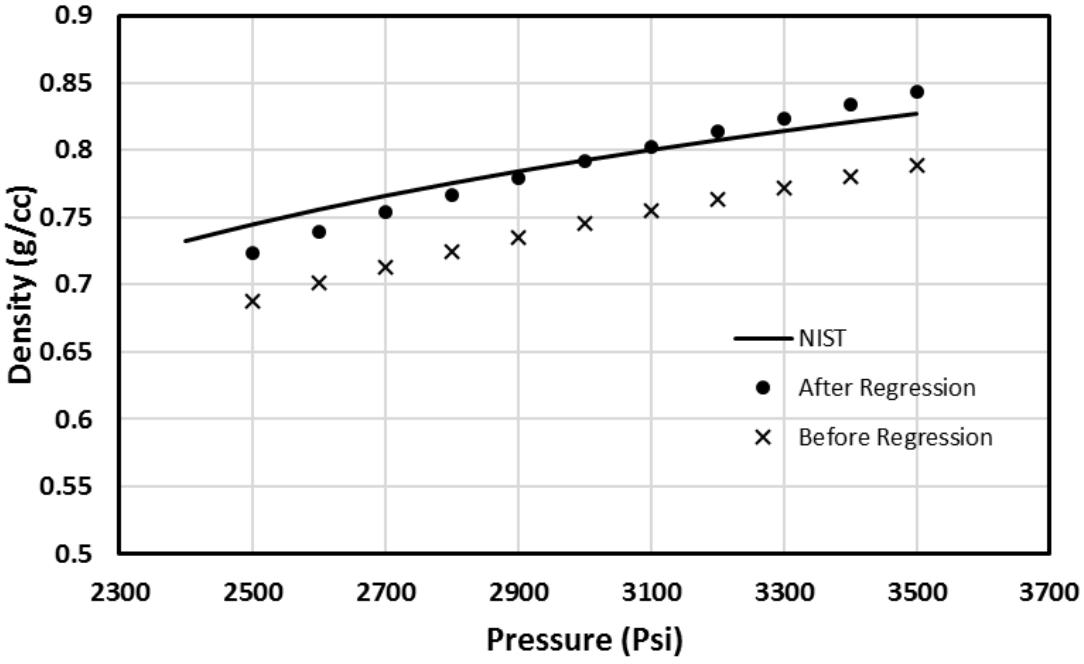

Figure 3.1 – Density of CO_2 at 122 °F versus pressure. The densities generated using default volume shift and modified volume shift are compared with data from NIST.

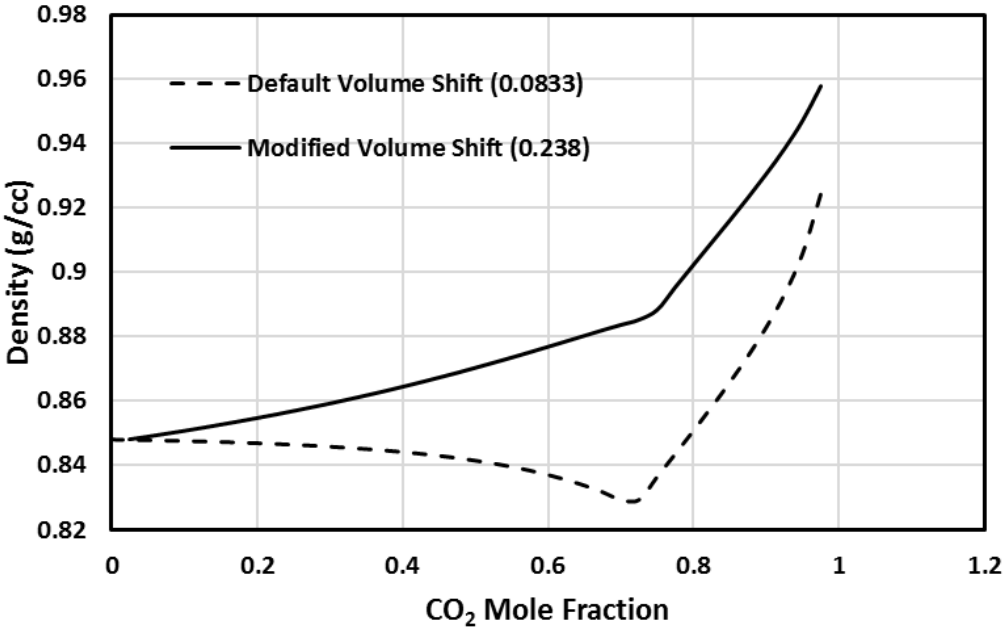

Figure 3.2 – Densities of CO_2/oil mixture versus CO_2 composition using default and modified volume shift. The default volume shift does not account for the increase in density.

The oil model to be used for simulation is based on density data from oil A. We use WINPROP to match experiment data on volume shifts and binary interaction coefficients. Using chromatography, oil A composition is revealed as shown in Table 3.1.

Table 3.1 - Oil A composition (Mole Fraction)

Component	Composition	Component	Composition	Component	Composition	Component	Composition
CH4	0	MC-Hex	1.5310	FC13	4.3316	FC25	1.2323
C2H6	0	TOLUENE	0.8215	FC14	3.8275	FC26	1.2136
C3H8	0	FC7	3.6034	FC15	3.9395	FC27	1.0642
IC4	0	Eth-Ben	0.6535	FC16	3.3981	FC28	1.0456
NC4	0	O-Xyl	0.6348	FC17	2.8753	FC29	1.0082
Neo-C5	0.0187	MP-Xyl	1.6057	FC18	2.6139	FC30	0.8588
IC5	1.8671	FC8	4.4436	FC19	2.5579	FC31	0.8402
NC5	3.2487	TM-Ben	0.7282	FC20	2.1845	FC32	0.7842
MC-Pen	1.4376	FC9	3.6221	FC21	1.9604	FC33	0.6908
BENZENE	0.2614	FC10	5.2838	FC22	1.7177	FC34	0.6535
CYCLO-C6	1.0456	FC11	5.2651	FC23	1.5683	FC35	0.5975
FC6	5.7132	FC12	4.5743	FC24	1.4003	C36+	10.8103

Running this whole composition in simulation is time consuming; therefore, lumping is necessary. The result of lumping is in Table 3.2.

Table 3.2 - Composition of oil A after lumping (dead oil at separator condition)

Component	Composition
C_1	0
C_2	0
C_3	0
C_4	0
C_5	0.05134
C_6	0.08458
C_7	0.05956
C_8	0.11688
C_{9-22}	0.40851
C_{21+}	0.27446

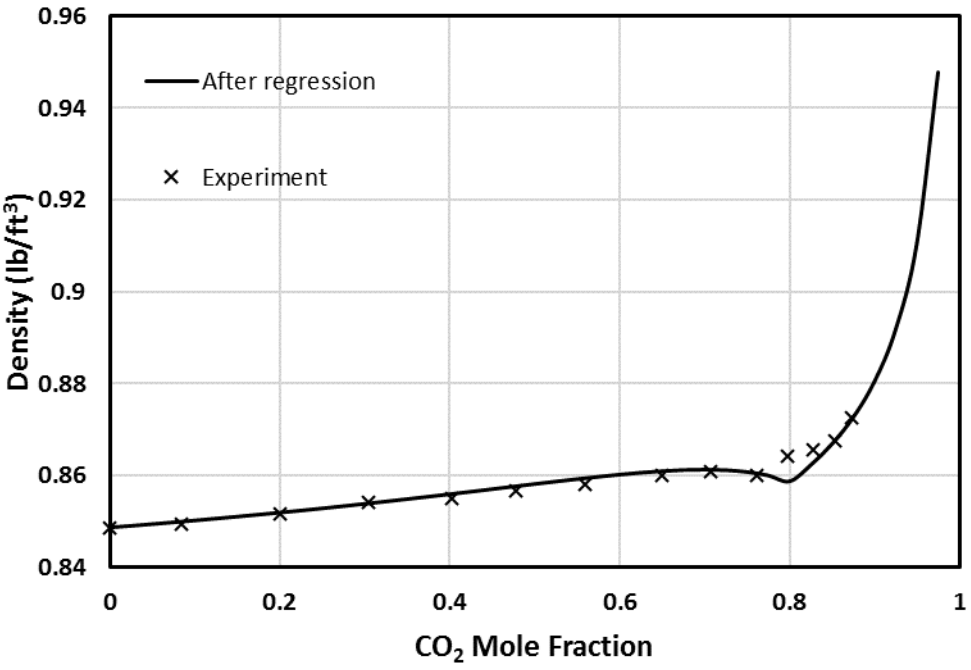

Figure 3.3 – Densities calculated after regression fit experimental densities well.

Since this is dead oil, the light components (C_1 to C_4) are absent. Light components are well defined in WINPROP, but that is not the case for heavy and lumped components. Therefore, we regress density data on volume shift and binary interaction coefficient of heavy components. After that, light components are added matching its live composition to run simulation using CMG BUILDER.

Table 3.3 - Composition of oil A (live oi at reservoir condition)

Component	Composition
C_1	14.3123
C_2	8.2546
C_3	7.9334
C_4	5.2611
C_5	3.2983
C_6	5.4332
C_7	3.8260
C_8	7.5081
C_{9-22}	26.2423
C_{21+}	17.6308

Table 3.4 - Volume shift values

Components	Default Volume shift	Modified Volume Shift
C1	0.0234	0.0234
C2	0.0605	0.0605
C3	0.0825	0.0825
C4	-0.0643	-0.0643
C5	-0.0345	-0.0345
C6	-0.0067	-0.0067
C7	0.0175	0.0175
C8	0.0446	-0.0977
C10-20	0.1348	-0.1540
C21+	0.2809	0.2441
CO2	0.0833	0.238

At different pressures, CO_2/oil mixture still displays the increase in density with added CO_2. However, the increase slope is different. The density increase of the mixture at 3000 psia is higher than that at 1700 psia (Fig. 3.4). Because the increase is greater, more instability is expected at 3000 psia. This will be investigated in the next section.

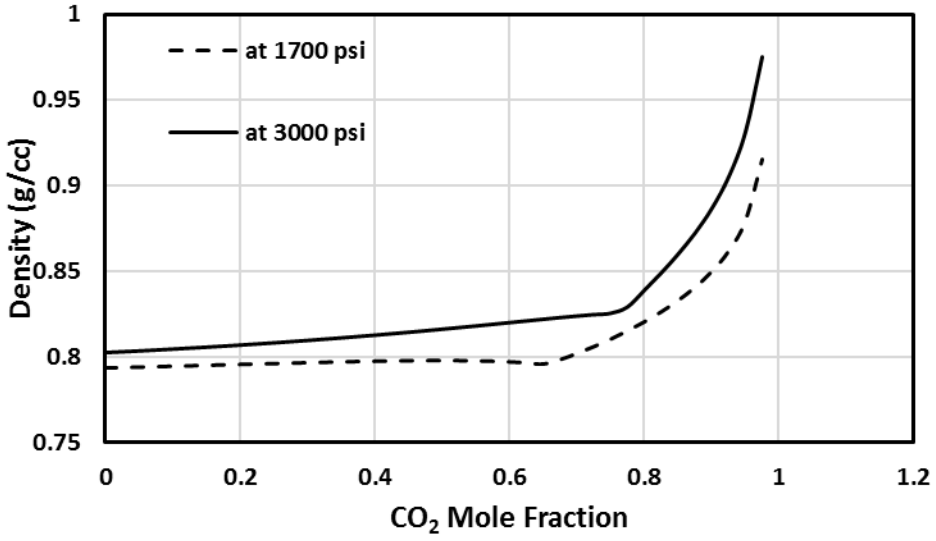

Figure 3.4 – Density increase at 3000 psia is greater than that at 1700 psia. This increase alters the flow path significantly at 3000 psia.

3.1. Validation of the Fluid Model by a Correlation

After getting the characterized fluid, it is necessary to validate the model through a correlation. There are several correlations to calculate the density of CO_2/oil mixture. However, most of them only predict density at saturation pressure. At different pressure, the amount of CO_2 dissolved is different (saturated solubility). So, there are 2 changing parameters: pressure and CO_2 dissolution. They both increase density of the oil mixture. The experiment in this study is carried out at constant condition (122 $^{\circ}$F and 3000 psia) but with different amount of CO_2. Therefore, a correlation that allows density calculation at constant pressure and temperature is required. This part is to validate our work in CMG WINPROP.

There is one correlation (Marra, Poettmann, & Thompson, 1981) that predicts density of oil at constant condition with changing CO_2 content. It shows great agreement with experimental data from Texas oils. One of the oil, RO-B, is calculated with this

correlation and compared to its actual measurement (Fig. 3.5). The correlation shows great agreement. This means the correlation should work for oil with similar density.

For oil model in this study, light components are added to match its live version. The live oil generated from CMG WINPROP has API of 43°. Since the Texas oil (RO-B) has similar API gravity (45°), it is reasonable to use this correlation to verify the oil model.

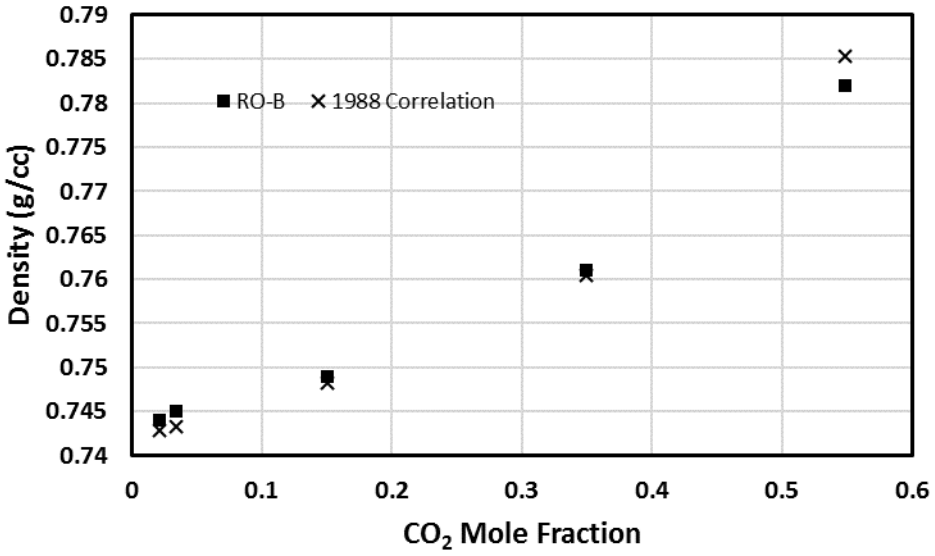

Figure 3.5 - The correlation from 1988 has a very good match with West Texas oil RO-B

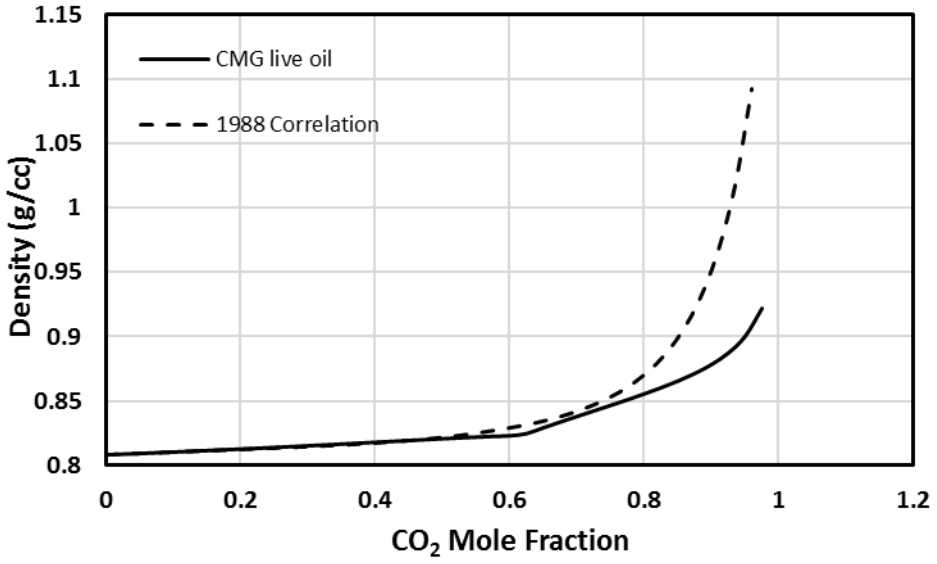

Figure 3.6 - CMG WINPROP and correlation from 1988 agree on mixture density up to 70 percent then breaks apart.

Comparing data from CMG and the correlation, there is a good agreement from 0 to 70 percent mole of CO_2 (Fig. 3.6). After 70 percent of CO_2, the predictions have great disagreement. This happens because in reality, at around 70 percent of CO_2, the mixture splits into 2 phases. The correlation does not account for that so all the weight of the gas phase is added into the weight of the mixture causing it to jump up. The CMP WINPROP accounts for the split so the density of liquid phase has moderate increase at 70 percent CO_2 concentration.

3.2. Simulation Model

To study the compositional flow path of the injection, CO_2 flooding is run in a 2D reservoir model using compositional simulator CMG-GEM and reservoir simulator CMG-BUILDER. There are two oil models: one with regression and another one without regression. The one with regression (modified volume shift) shows the increase in density

while the other one shows a decrease in density. The two models are integrated in CMG BUILDER for simulation. The reservoir model has a length of 1200 ft., depth of 200 ft. and width of 20 ft. the grid block system is 240 grids in length x 10 grids in depth x 1 grid in width. The reservoir is homogeneous with permeability of 1000 mD. Porosity is 20 percent and constant throughout the life of reservoir. Simulation are run at two different reservoir pressure 1700 psia and 3000 psia. Injector is at one end and producer is at the other end of the reservoir. There are two well layouts. The first one is with injector on top and producer at the bottom. The second one is opposite, which is injector at the bottom and producer on top. In addition, we run simulation with formation permeability of 100 mD to study effect of permeability on flow path. Therefore, there are six cases using two oil models (with and without regression) to compare the results.

Table 3.5 – The simulation has six cases with different reservoir conditions and wells layouts

Case	Permeability (mD)	Reservoir Pressure (psia)	Well layout
1	100	1700	Top Injecter, Bottom Prodcuer
2	100	3000	Top Injecter, Bottom Prodcuer
5	100	1700	Bottom Injector, Top Producer
6	100	3000	Bottom Injector, Top Producer
3	1000	1700	Top Injecter, Bottom Prodcuer
4	1000	3000	Top Injecter, Bottom Prodcuer
5	1000	1700	Bottom Injector, Top Producer
6	1000	3000	Bottom Injector, Top Producer

3.3. Results

There are two well layouts: (1) Top injector and bottom producer and (2) bottom injector and top producer (Fig. 3.7). With default volume shift, density of oil mixture does not increase with CO_2 solubility. This makes the flow path gravity stable (no fingering). On

the other hand, with modified volume shift, flow path is unstable and shows fingering. This happens at both 1700 psia and 3000 psia (Fig. 3.8 and Fig. 3.9).

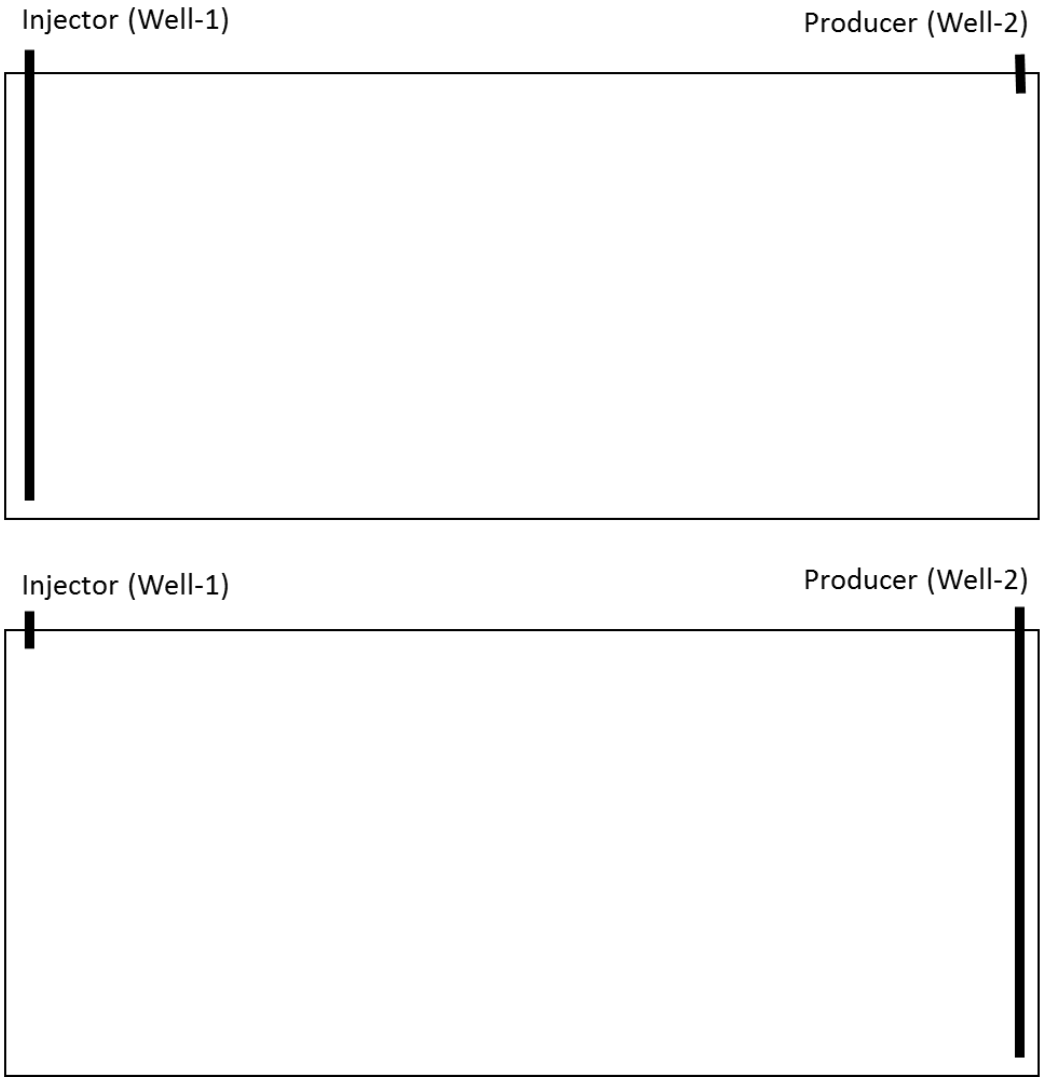

Figure 3.7 – Layout 1 (top) with bottom injector and top producer. Layout 2 (bottom) with top injector and bottom producer

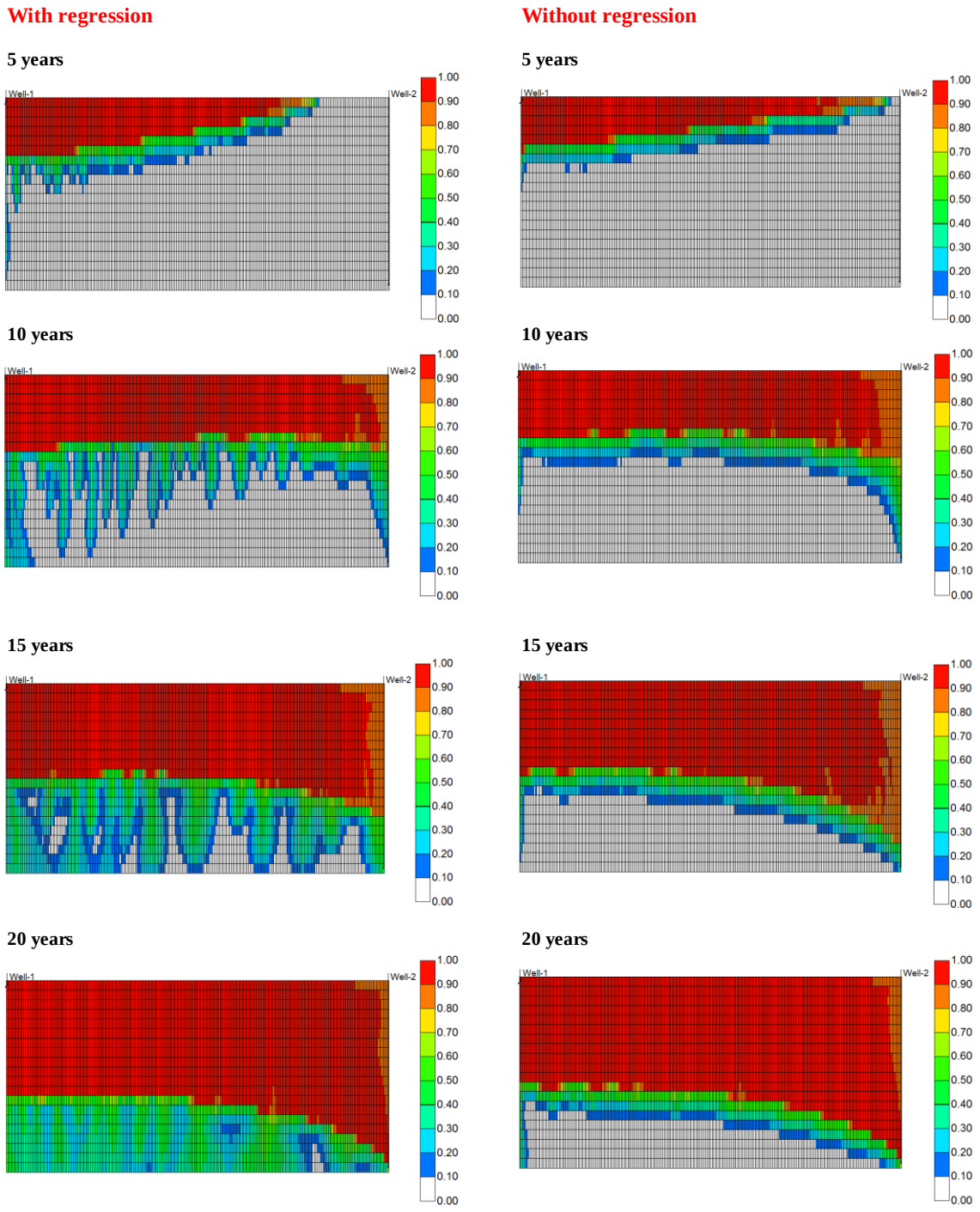

Figure 3.8 – Global CO_2 composition (mole fraction) at different time. K = 1000 mD and P = 1700 psia with top injector and bottom producer. On the left with modified volume shift, flow path shows instability while default volume shift (on the right) shows steady and stable flow path.

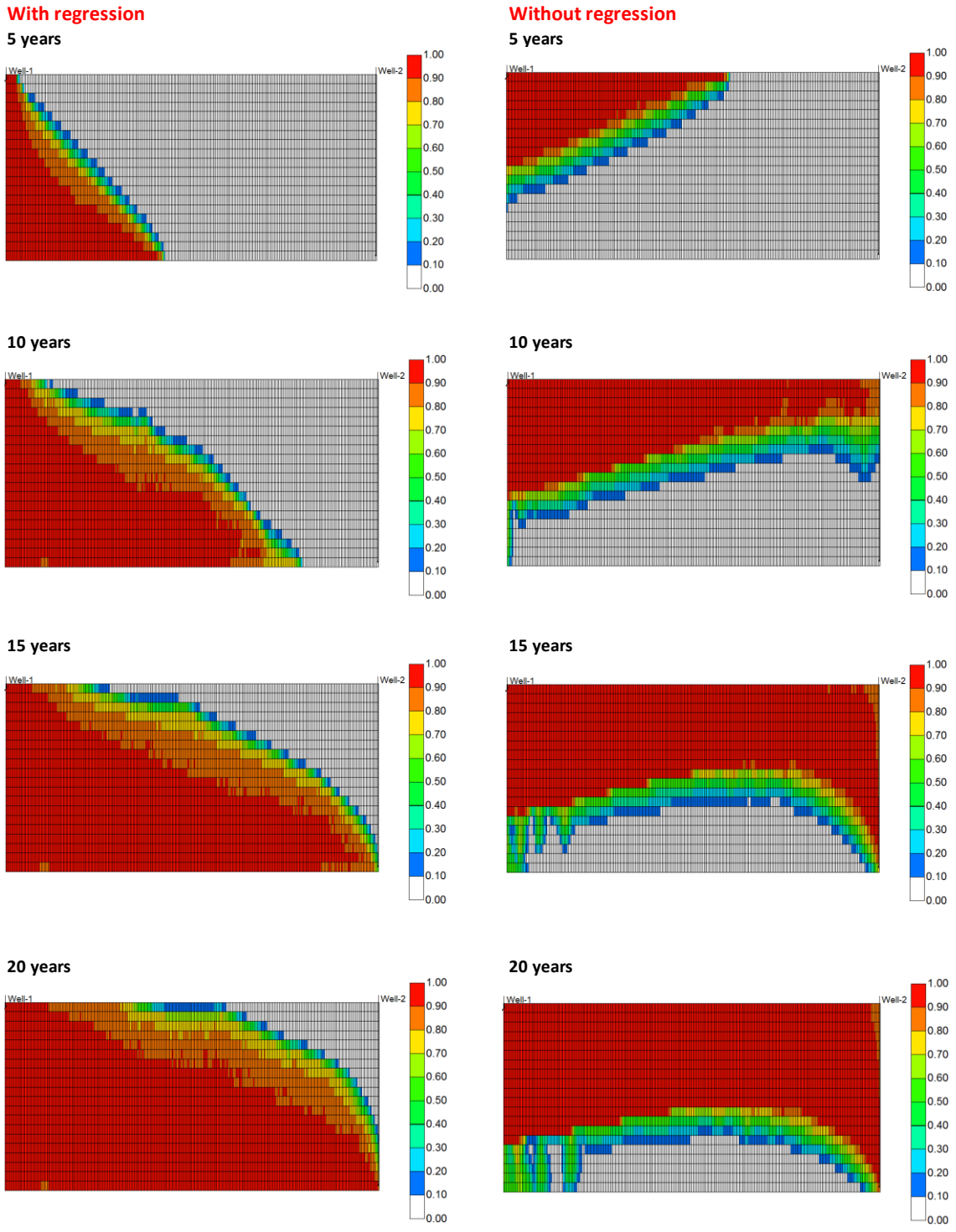

Figure 3.9 – Global CO_2 composition (mole fraction) at different time. K = 1000 mD and P = 3000 psia with top injector and bottom producer. Modified oil model (left) shows CO_2 saturated oil sinks down to bottom. With default volume shift, the flow path is stable.

In both cases with layout 1, with modified volume shift of CO_2, there is instability due to gravity in Fig. 3.8 and Fig 3.9. However, depending reservoir pressure, the instability in flow path is quite different. At 1700 psia, as more CO_2 being injected, the fingering becomes more severe (the CO_2 fingers become longer and bigger). At 3000 psia, there is an interesting flow pattern; as CO_2 enters oil system, the new composition immediately sinks down to the bottom. This could be due to two reasons: (1) at 3000 psia, CO_2 solubility is higher thus, makes density increase greater and (2) density of gas phase at 3000 psia is much greater (almost equal to oil density) than that at 1700 psia. At both pressures, due to injector being on top, gravitational force pulls CO_2 saturated oil downward, this makes injection pressure lower and higher injection rate (Fig. A.4 and A.5 in Appendix) compared to default oil model. Top injection also allows CO_2 to be distributed more thoroughly throughout the reservoir. Modified oil model shows later CO_2 breakthrough (Fig. A.7) but equal oil flow rate with default oil model. This results in 10 percent higher cumulative production (Fig. A.9).

In cases with layout 2, the trend is similar to the cases with layout 1. For modified oil model: at 1700 psia, there is fingering; and at 3000 psia, density increase keeps the heavy mixture at the bottom (Fig. A.17). The default oil model shows stable flow path (Fig. A.23).

To study the effect of formation permeability on this density changes, formation permeability is set to be 100 mD. At 1700 psia, the density increase is not significant enough to create instability (Fig. A.44). However, at 3000 psia, the saturated CO_2 oil

sinks to middle (instead of sinking to the bottom when permeability of 1000 mD) of the reservoir and flows to producing well without any fingering (Fig. A.37). This case has a later CO_2 breakthrough. This means permeability plays an important role in oil flow path. At higher permeability, reservoir is more sensitive to density changes. In a low permeability formation, small change in density does not alter flow path.

4. CONCLUSIONS AND FUTURE WORKS

4.1. Conclusions

This study investigates the abnormal behavior of CO_2 when dissolved in crude oil. Density of CO_2/oil mixture increases as CO_2 content increases. By default, commercial simulator cannot predict this trend accurately. To correct this, we can modify the volume shift of CO_2 by running regression using CO_2 densities at different pressures. The volume shift of CO_2 in this study is found to be 0.238, which is close to 0.25 as confirmed in other studies. This density increase alters flow path of oil, which changes BHP, flow rates and total recovery. At higher reservoir pressure, CO_2 solubility is greater, which makes instability more severe. In addition, at higher permeability, reservoir becomes more sensitive to density changes. It lets heavier composition to sink down faster, which alters flow path significantly. Understanding the effect of CO_2 on crude oil at different reservoir conditions makes predicting oil flow path more accurately.

4.2. Future Works

To this day, no one can explain the density increase effect of CO_2 in crude oil. Lasangan and Smith (1993) had proposed a theory that strong molecular force might be the cause. This can be verified by Molecular Dynamic simulation. More experimental data is necessary as well, such as how CO_2 interacts with different hydrocarbon groups at various conditions. Real 3D reservoir modelling is also important to find the best well pattern, injection and production schedule.

REFERENCES

Beecher, C. E., & Parkhurst, I. P. (1926, December 1). Effect of Dissolved Gas upon the Viscosity and Surface Tension of Crude Oil. *SPE J*.SPE-926051-G. http://dx.doi.org/10.2118/926051-G.

EPA. 2016. *Overview of Greenhouse Gases*. EPA, 27 November 2016, https://www.epa.gov/ghgemissions/overview-greenhouse-gases (accessed 1 December 2016)

Firoozabadi, A. 2015. *Thermodynamics And Applications Of Hydrocarbons Energy Production,* first edition. New York: McGraw-Hill.

Green, D., & Perry, R. (2007). *Perry's Chemical Engineers' Handbook*, eighth edition. New York: McGraw-Hill.

Holm, L. W., & Josendal, V. A. 1974. Mechanisms of Oil Displacement By Carbon Dioxide. *SPE J*. SPE-4736-PA. http://dx.doi.org/10.2118/4736-PA

Jhaveri, B. S., & Youngren, G. K. 1984. Three-Parameter Modification Of The Peng-Robinson Equation Of State To Improve Volumetric Predictions. *SPE Res Eval & Eng*. SPE-13118-PA. http://dx.doi.org/10.2118/13118-PA

Koottungal, L. 2012. 2012 Worldwide EOR survey. *Oil and Gas Journal*, volume 110, issue 4, April 2, tables C, D, and E.

Langston, M.V., Hoadley, S.F., and Young, D.N. 1988. Definitive CO2 Flooding Response in the SACROC Unit. Presented at the SPE Enhanced Oil Recovery Symposium, Tulsa, Oklahoma, 16-21 April 1988. SPE-17321-MS. http://dx.doi.org/10.2118/17321-MS

Lansangan, R. M., & Smith, J. L. 1993. Viscosity, Density, and Composition Measurements of CO2/West Texas Oil Systems. *SPE J*. SPE-21017-PA. http://dx.doi.org/10.2118/21017-PA

Marra, R. K., Poettmann, F. H., & Thompson, R. S. 1988. Density of Crude Oil Saturated With CO2. *SPE J*. http://dx.doi.org/10.2118/16350-PA

NASA. 2016. Global Climate Change. NASA, 25 November 2016. http://climate.nasa.gov/vital-signs/carbon-dioxide/ (accessed 25 November 2016).

Pénelou, A., Rauzy, E., & Fréze, R. 1981. *A consistent correction for Redlich-Kwong-Soave volumes* (Vol. 8). Amsterdam: Elsevier Scientific Publishing.

Sidiq, H. H., & Amin, R. 2010. Supercritical CO2/Methane Relative Permeability Investigation. Presented at SPE International Conference on CO2 Capture, Storage, and Utilization, New Orleans, Louisiana, 10-12 November. SPE-137884-MS. http://dx.doi.org/10.2118/137884-MS.

Stiles, L., & Magruder, J. 1992. Reservoir Management in the Means San Andres Unit. *J Pet Technol 44 (4): 469-475*. SPE-20751-PA. http://dx.doi.org/10.2118/20751-PA

Svrcek, W. Y., & Mehrotra, A. K. 1982. Gas Solubility, Viscosity And Density Measurements For Athabasca Bitumen. *J Can Pet Technol*. SPE-82-04-02. http://dx.doi.org/10.2118/82-04-02

Tanner, C., Baxley, P., & Crump III, J. 1992. Production Performance of the Wasson Denver Unit CO2 Flood. *Presented at the SPE/DOE Enhanced Oil Recovery Symposium.* Tulsa, Oklahoma, 22 April. SPE-24156-MS. http://dx.doi.org/10.2118/24156-MS

Verma, M., & Warwick, P. D. 2012. Development philosophy of an assessment methodology for hydromcarbon recovery potential using CO2 EOR associated with carbon sequestration. Presented at the 33rd Symposium on IEA EOR, Regina, Saskatchewan, Canada, 22 April.

APPENDIX A

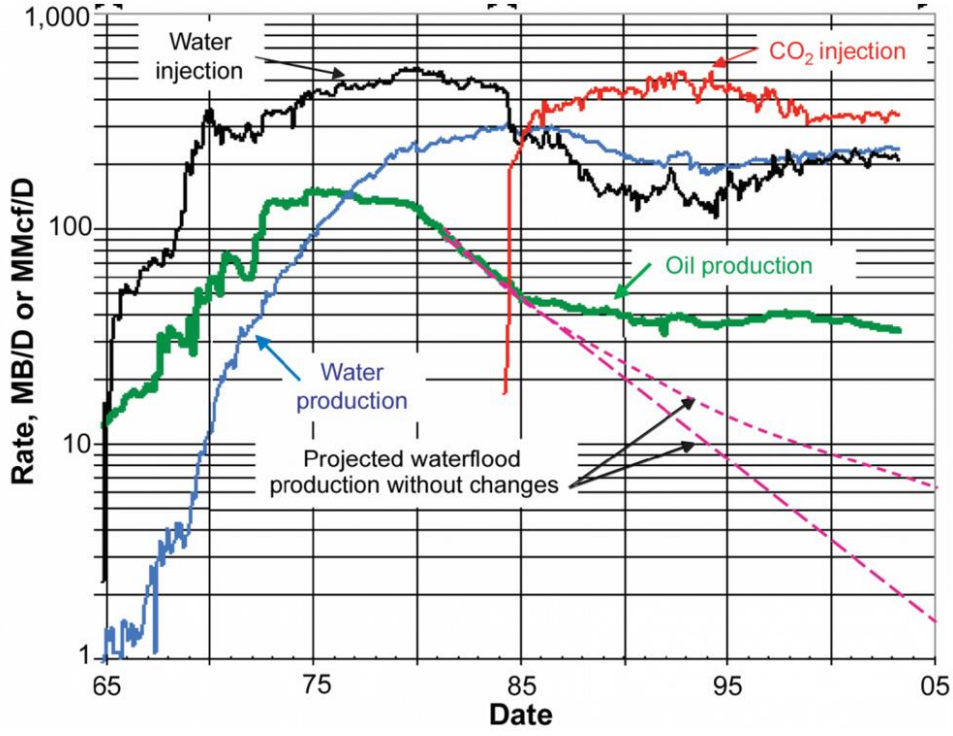

Figure 0.1 - Production performance with different recovery stage of Denver unit (Stiles & Magruder, 1992)

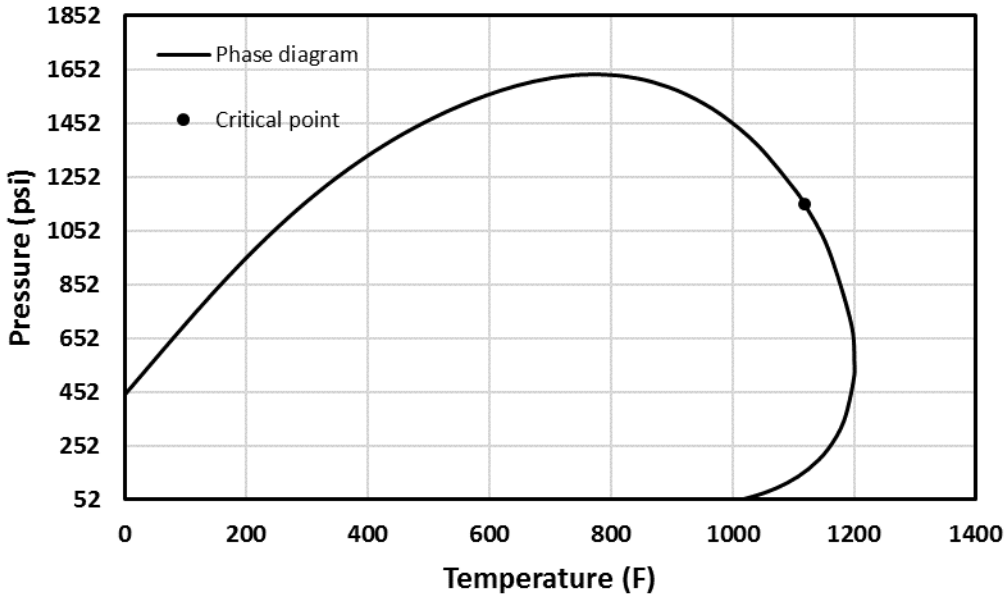

Figure 0.2 Phase diagram of live oil A

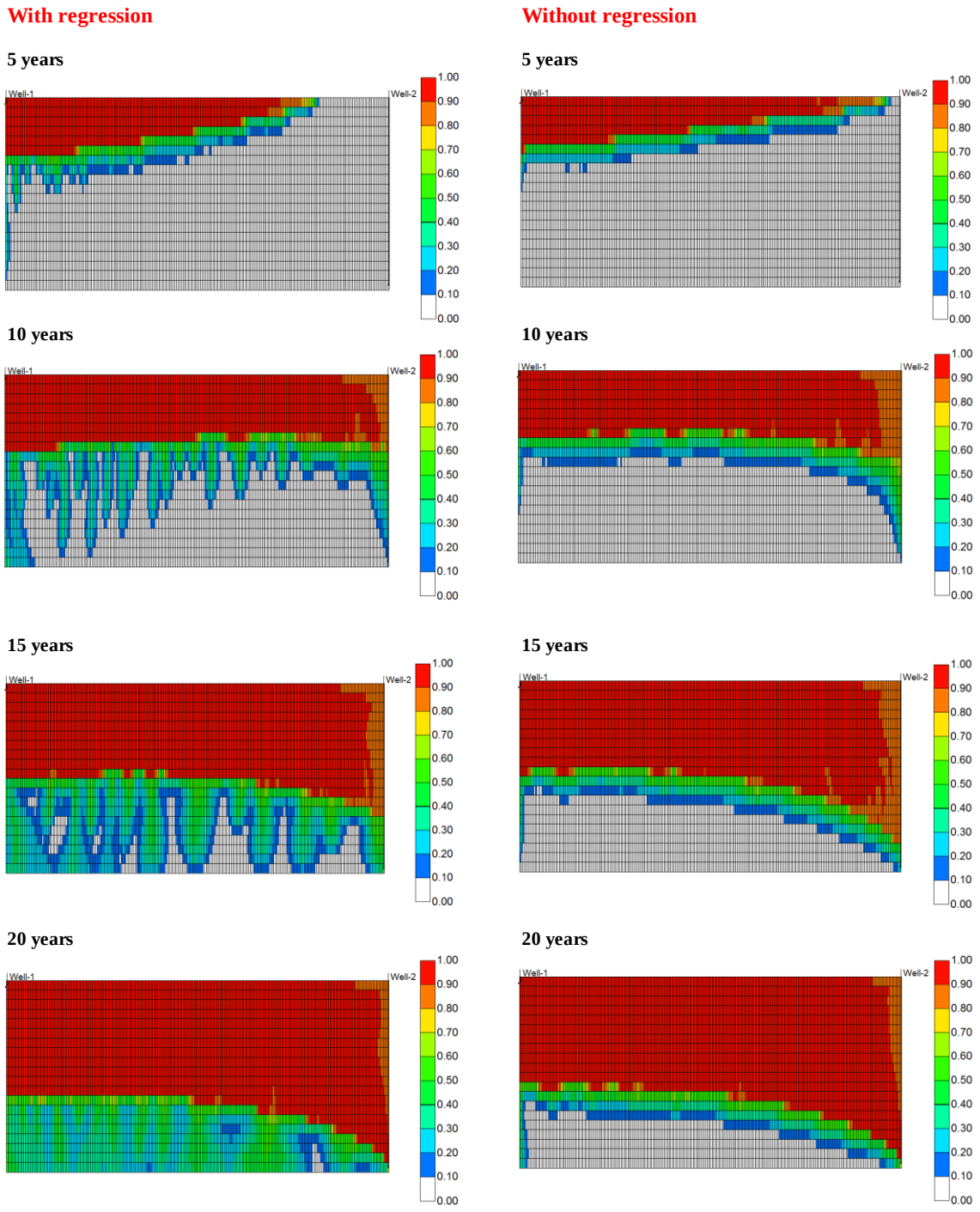

Figure 0.3 – k = 1000 mD. P = 1700 psia with top injector and bottom producer

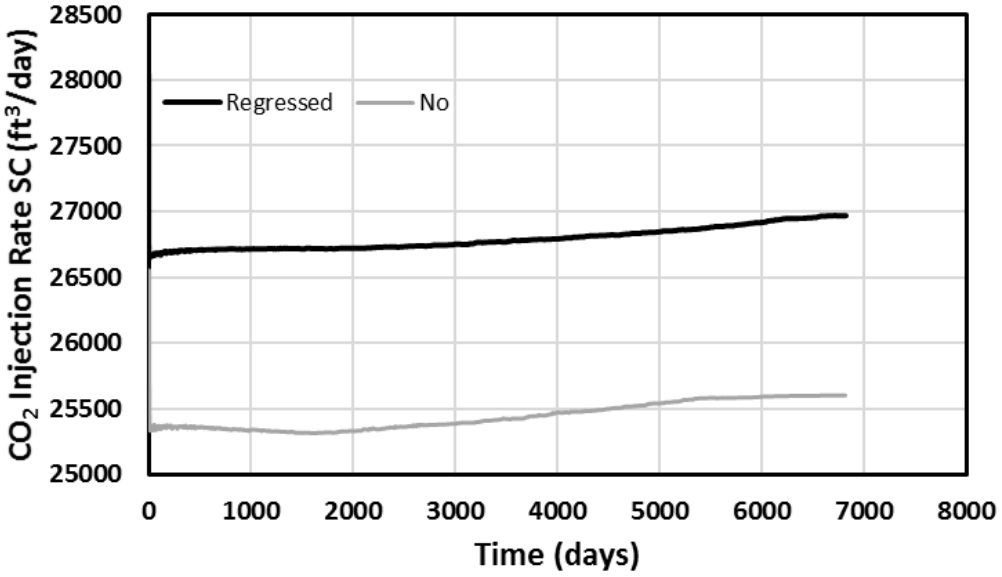

Figure 0.4 – Result of Fig. A.3

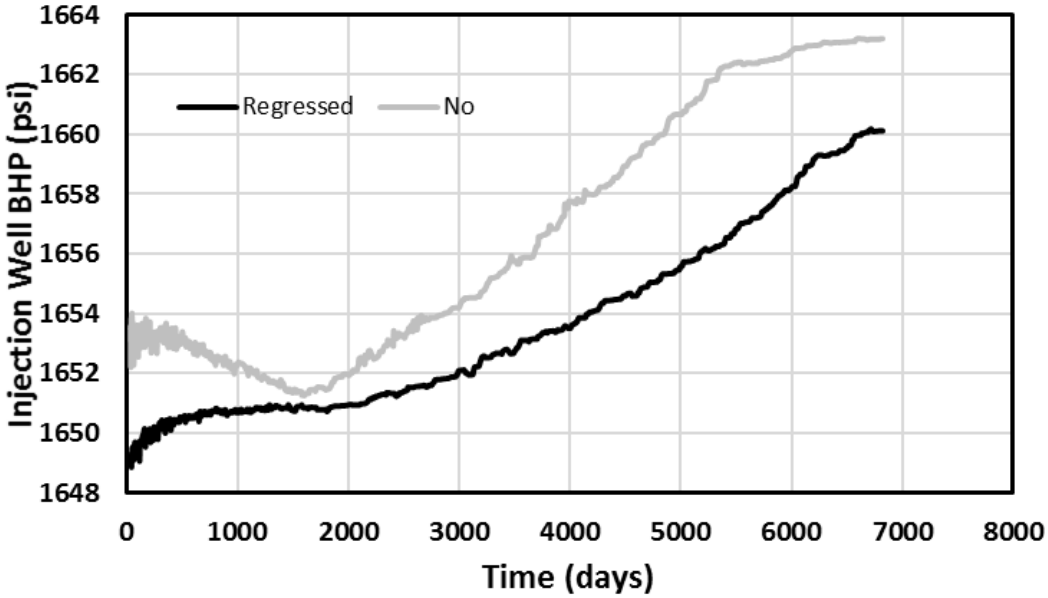

Figure 0.5 – Result of Fig. A.3

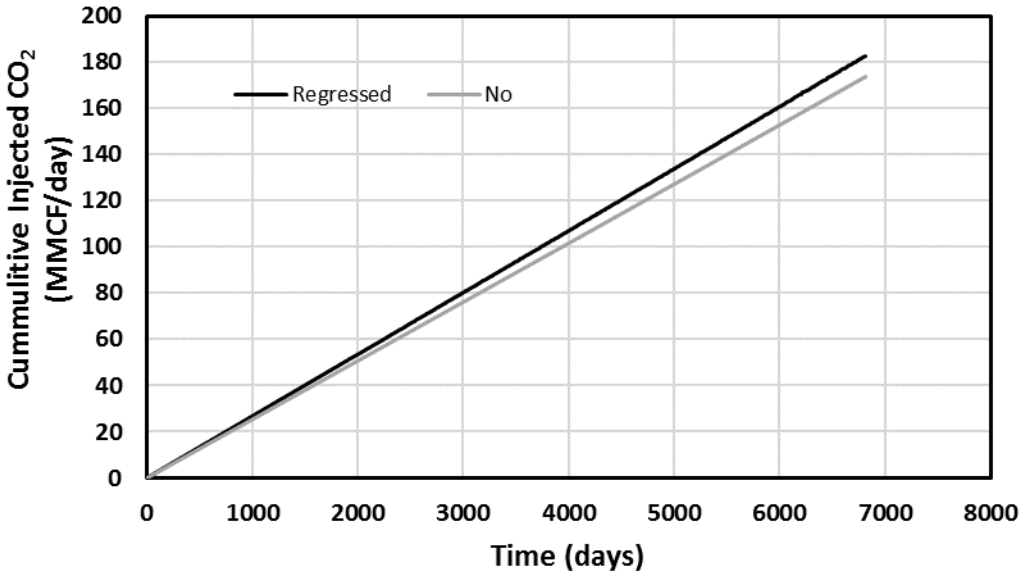

Figure 0.6 – Result of Fig. A.3

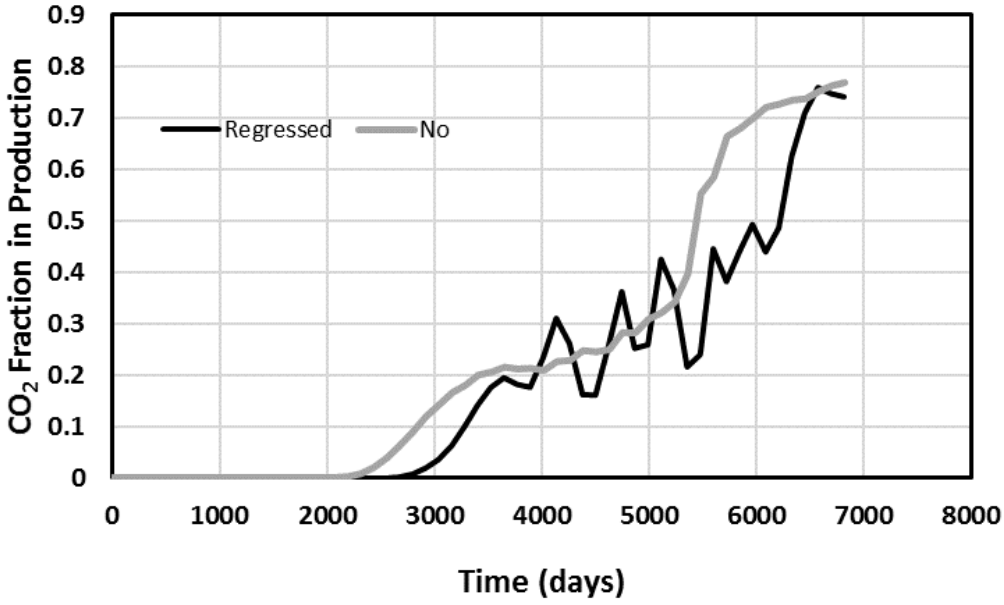

Figure 0.7 – Result of Fig. A.3

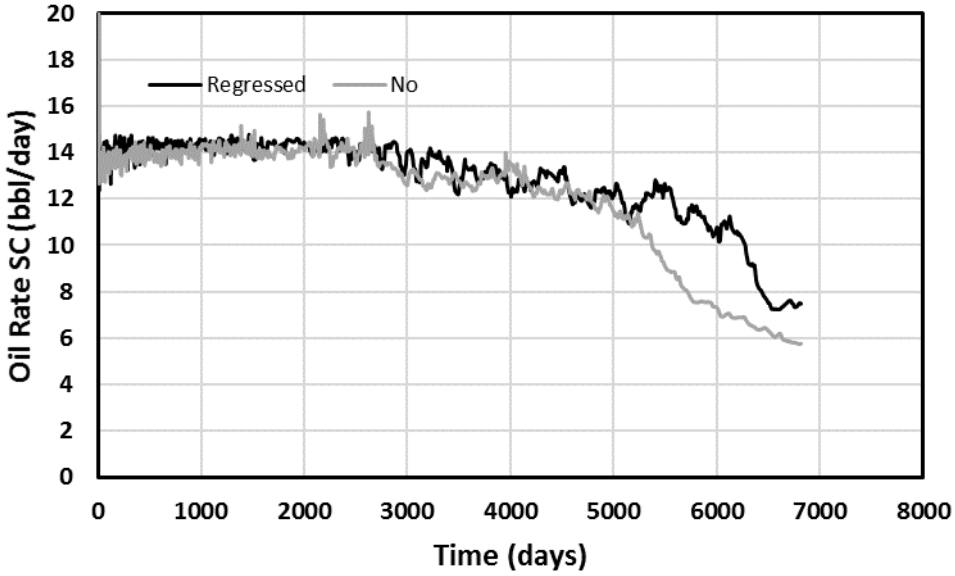

Figure 0.8 – Result of Fig. A.3

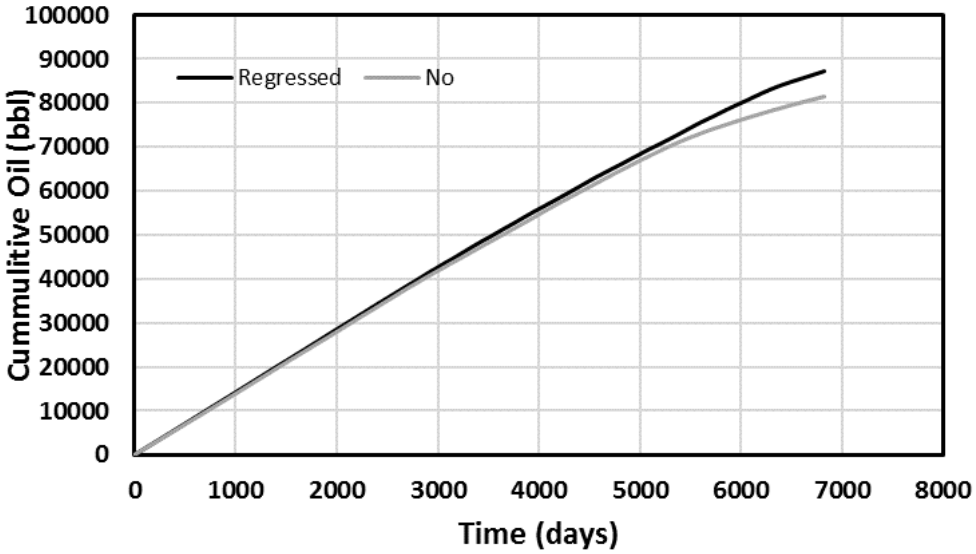

Figure 0.9 – Result of Fig. A.3

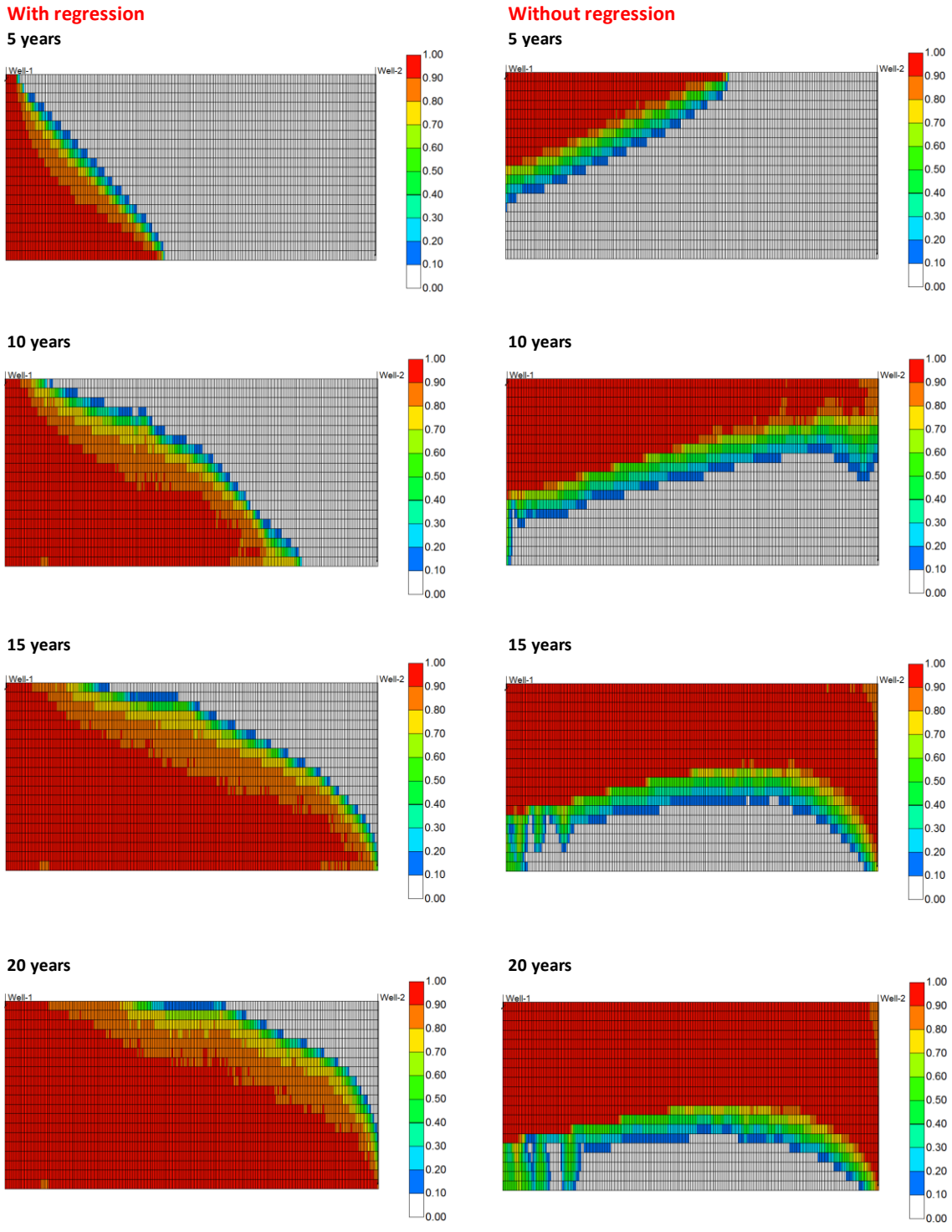

Figure 0.10 – K = 1000 mD and P = 3000 psia with top injector and bottom producer

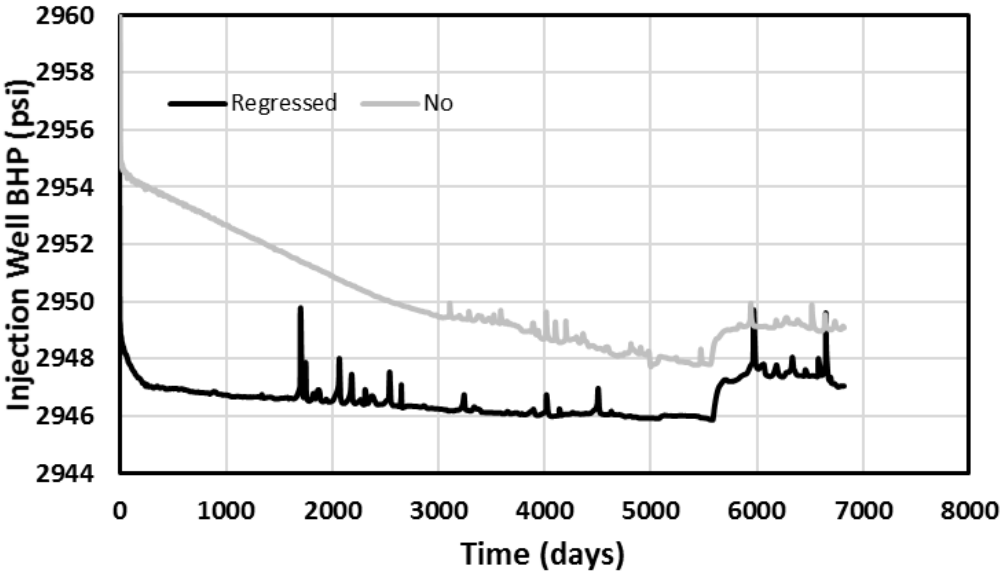

Figure 0.11 – Result of Fig. A.10

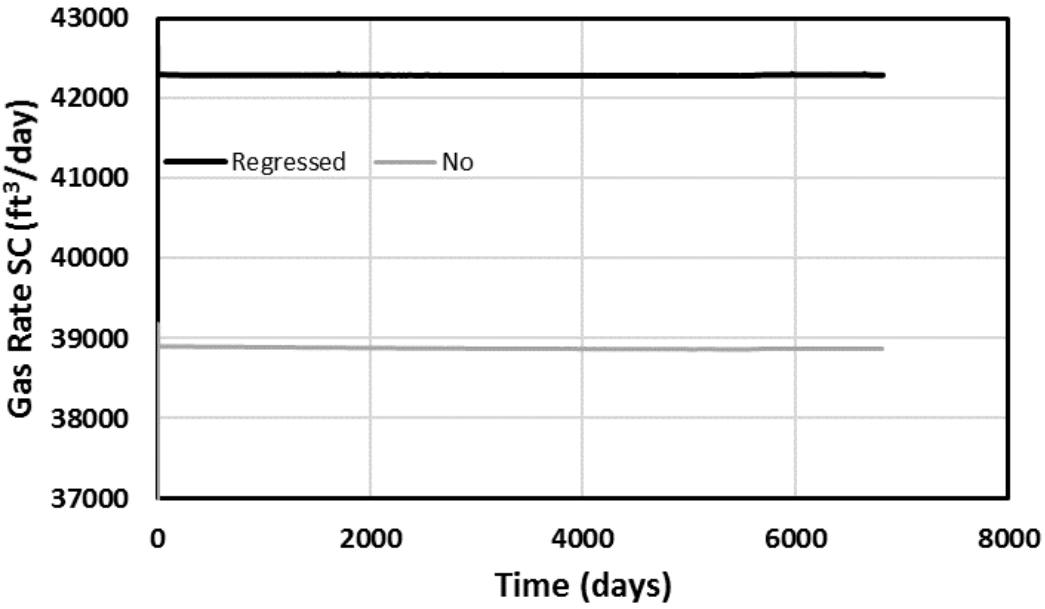

Figure 0.12 – Result of Fig. A.10

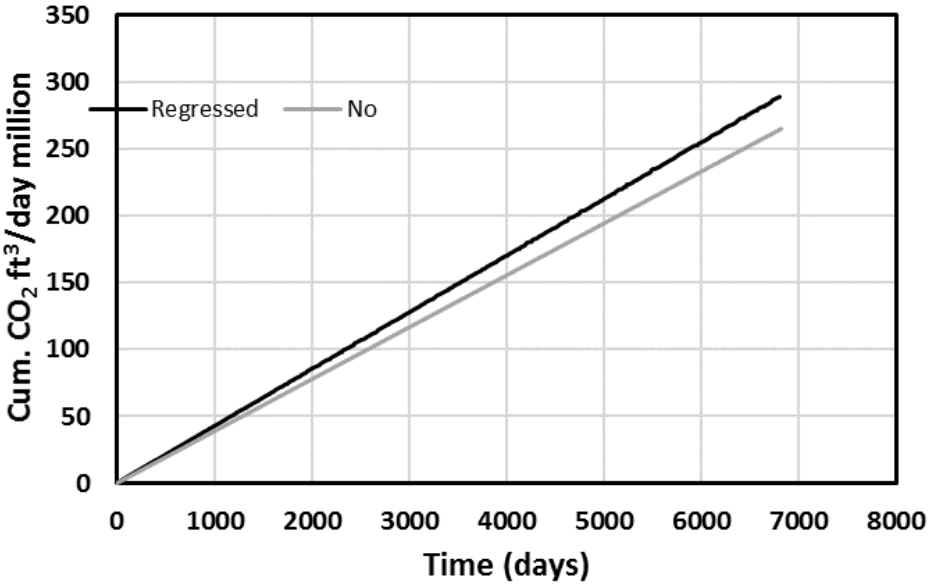

Figure 0.13 – Result of Fig. A.10

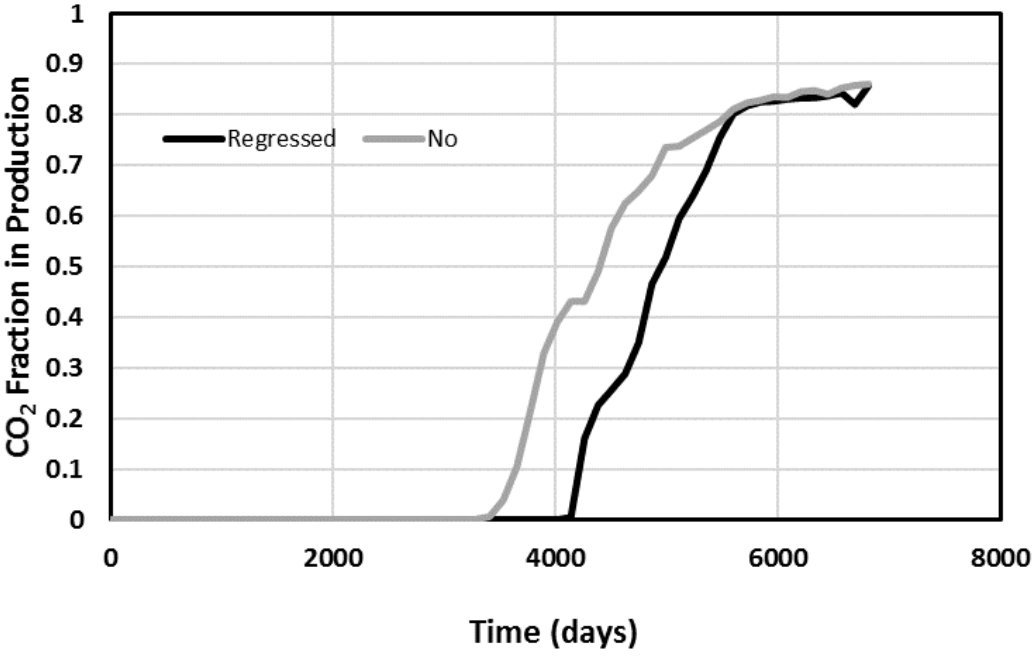

Figure 0.14 – Result of Fig. A.10

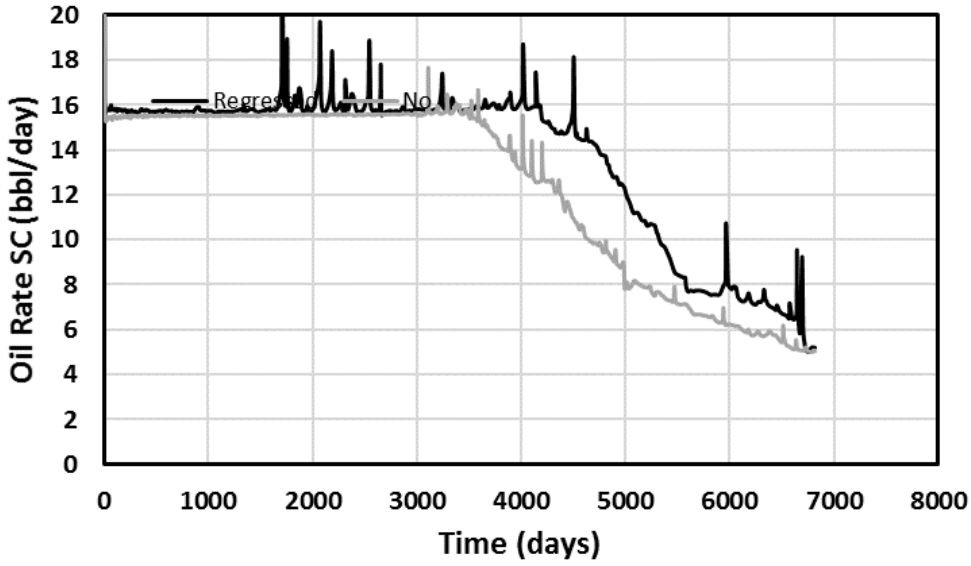

Figure 0.15 – Result of Fig. A.10

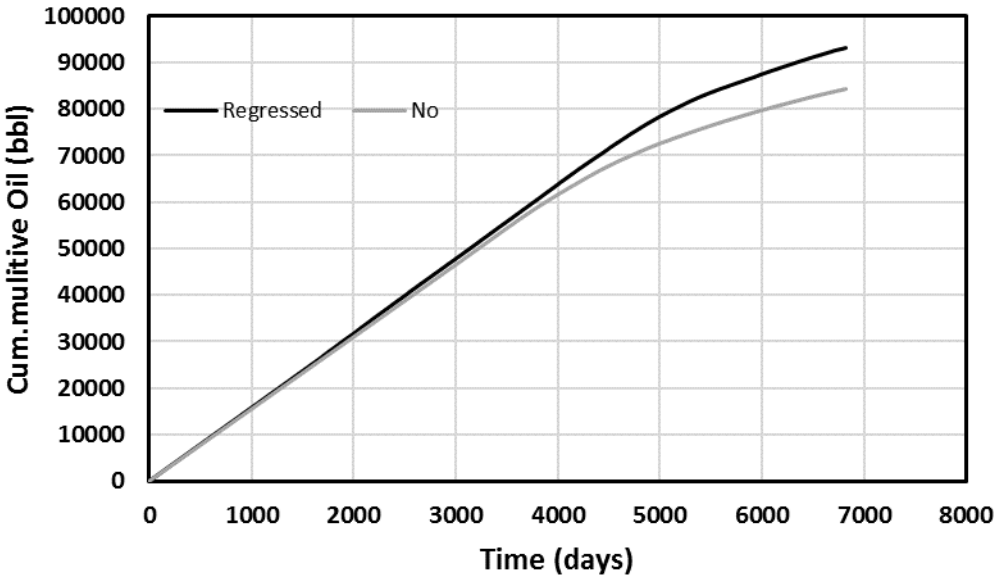

Figure 0.16 – Result of Fig. A.10

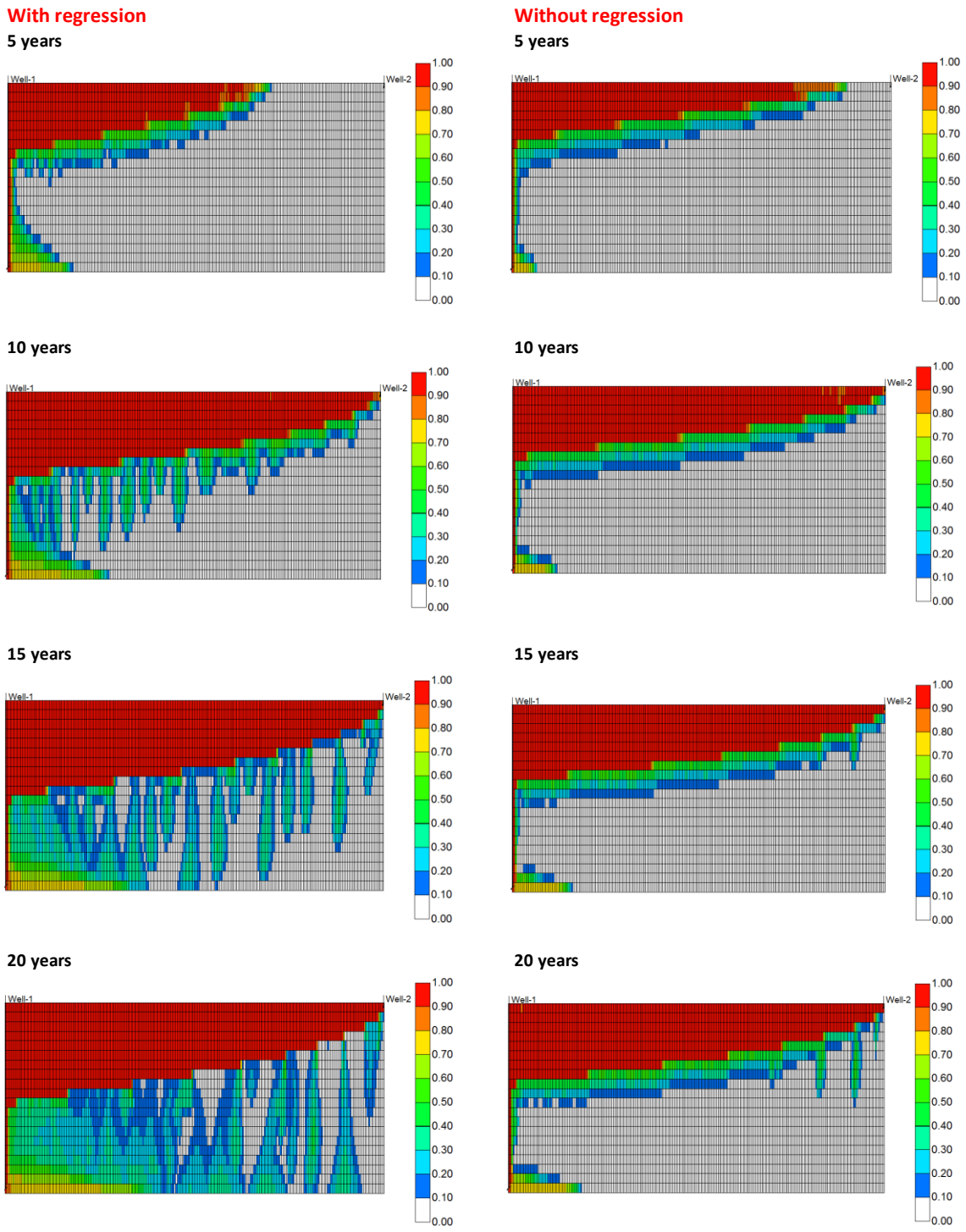

Figure 0.17 – K = 1000 mD and P = 1700 psia with bottom injector and top producer (layout 2)

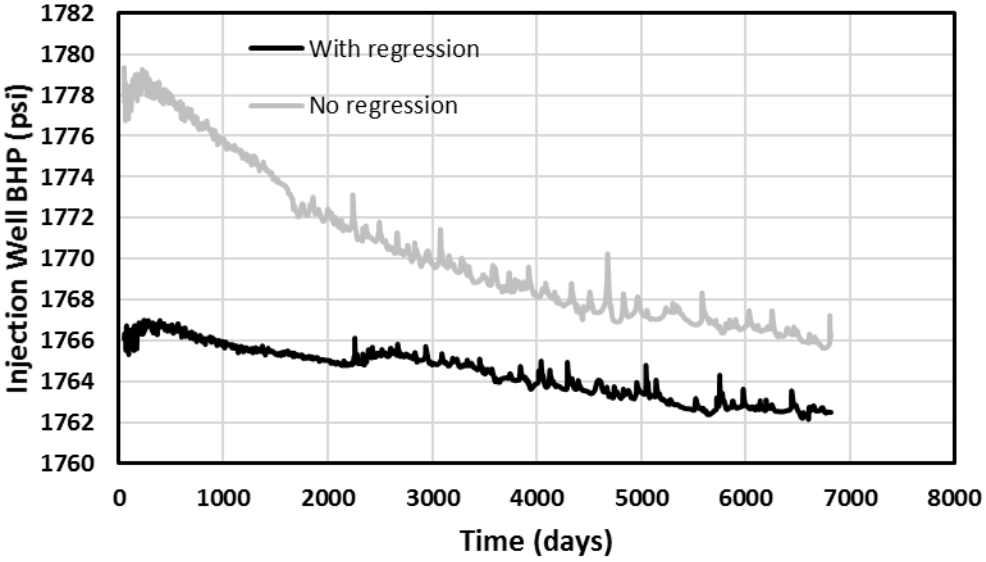

Figure 0.18 – Result of Fig. A.17

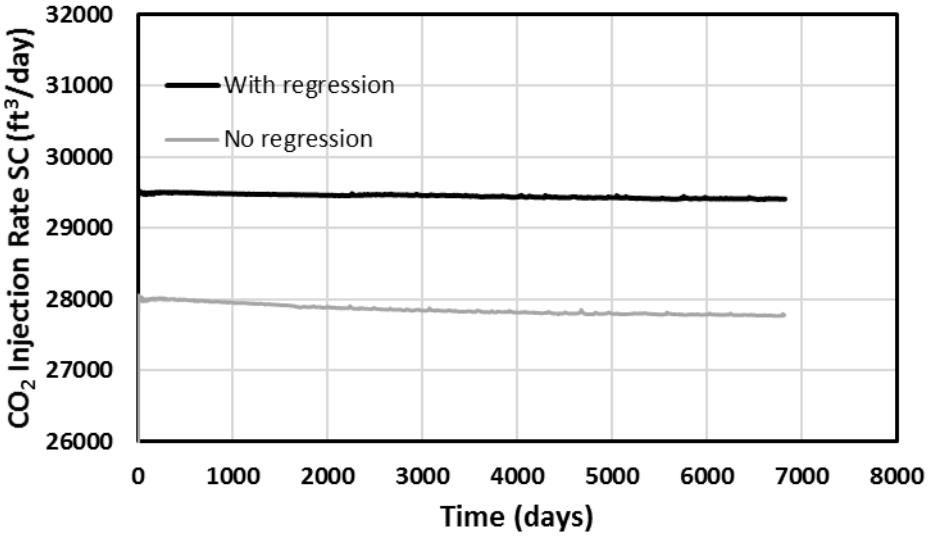

Figure 0.19 – Result of Fig. A.17

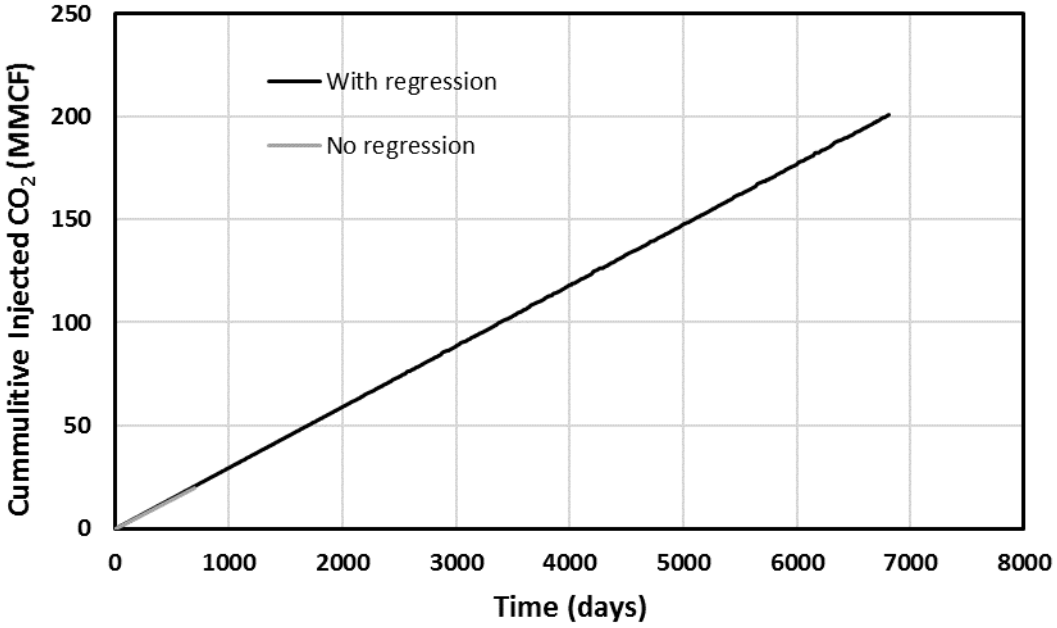

Figure 0.20 – Result of Fig. A.17

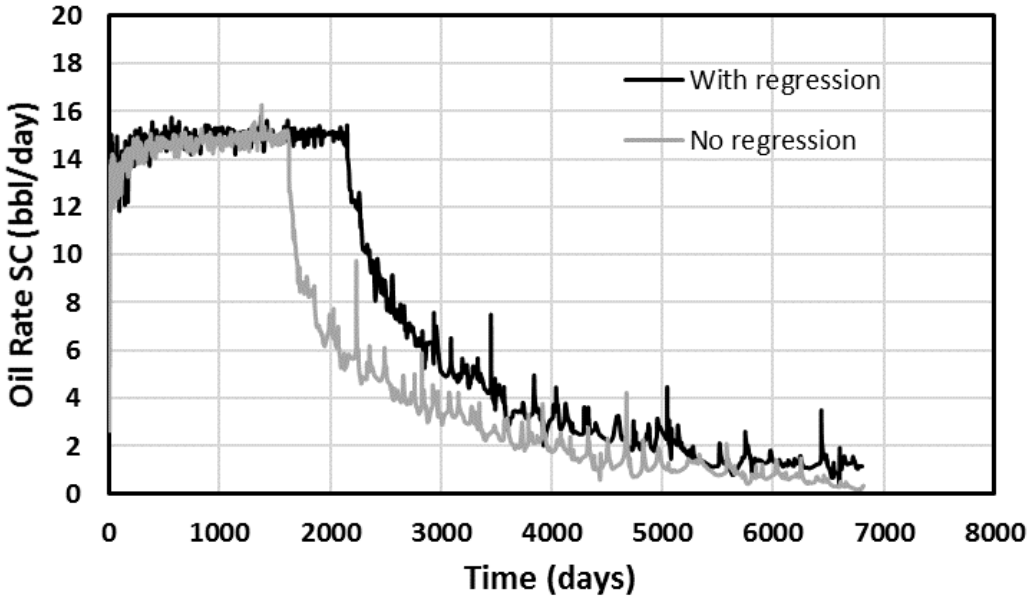

Figure 0.21 – Result of Fig. A.17

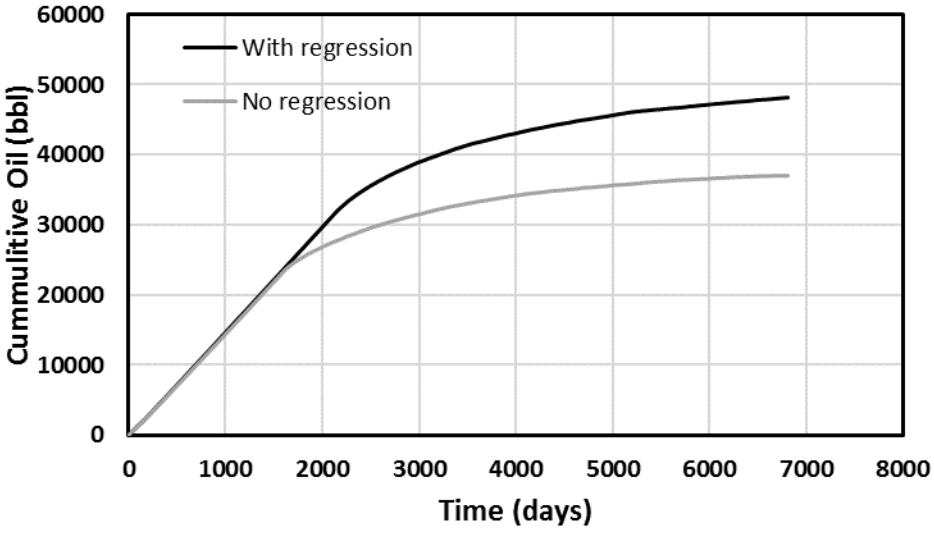

Figure 0.22 – Result of Fig. A.17

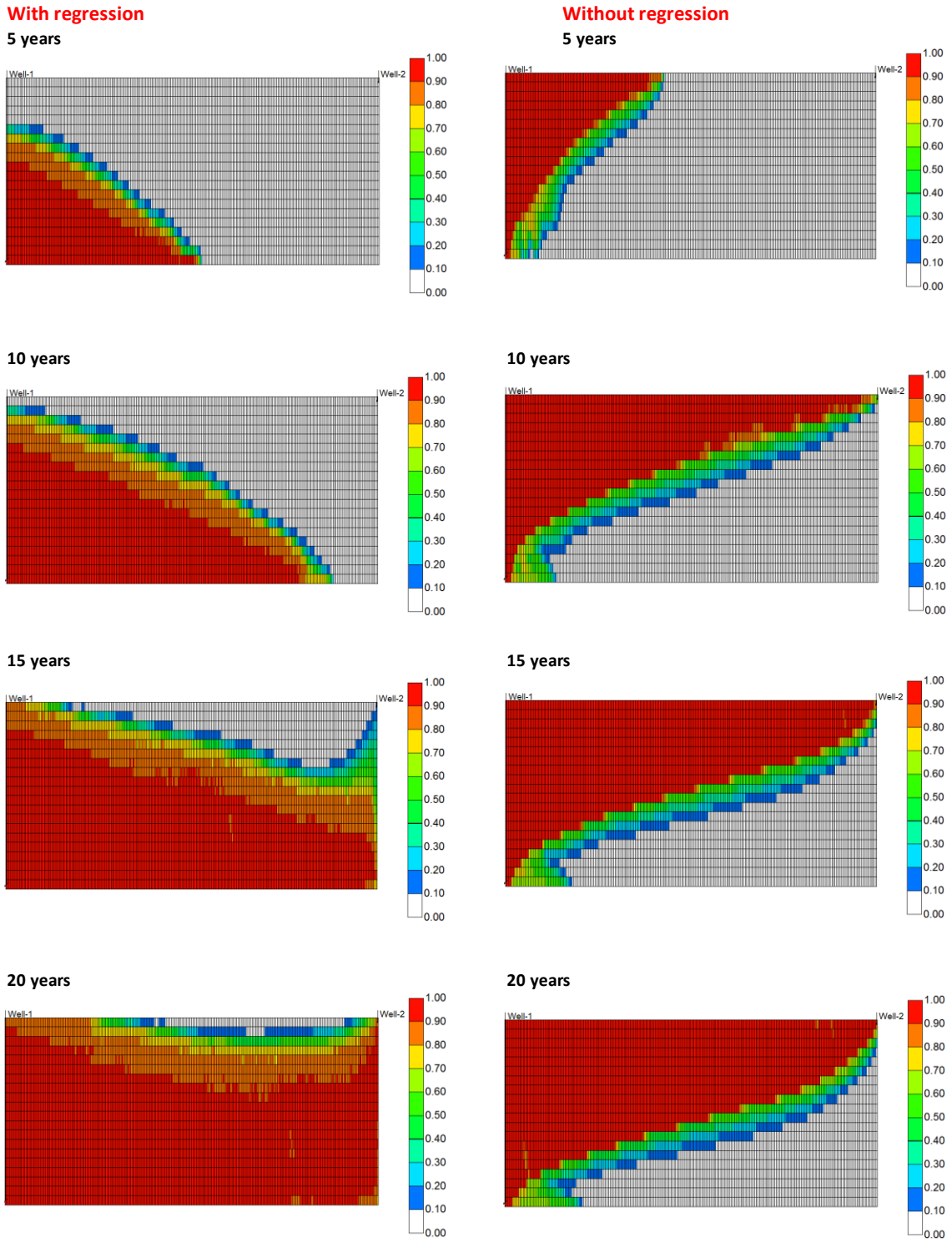

Figure 0.23 - K = 1000 mD and P = 3000 psia with bottom injector and top producer (layout 2)

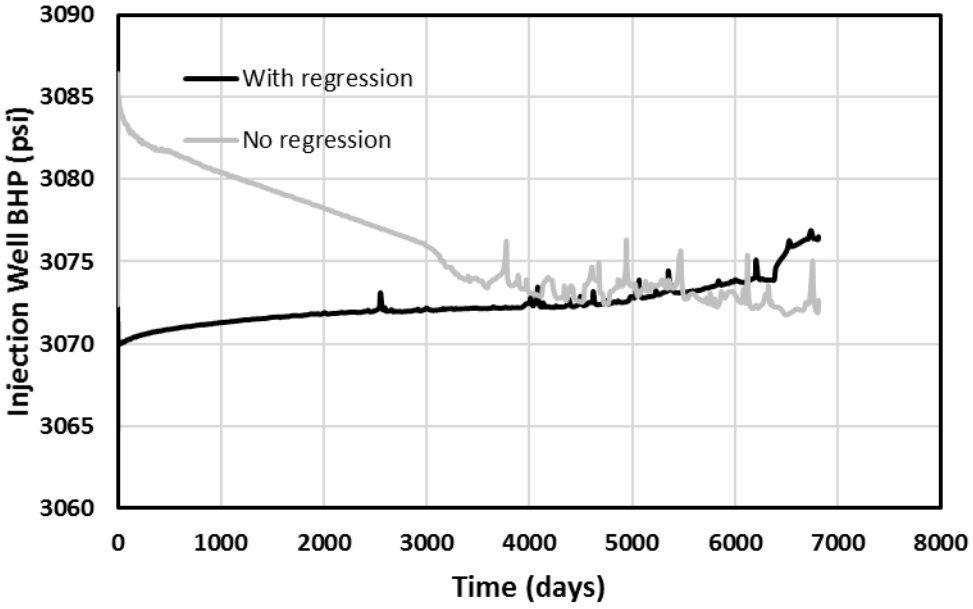

Figure 0.24 – Result of Fig. A.23

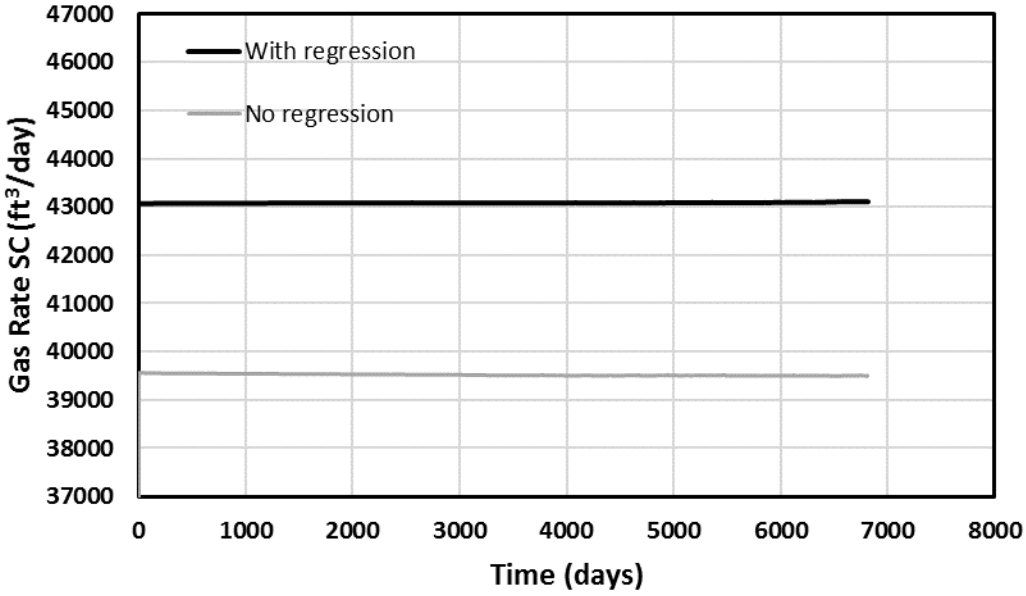

Figure 0.25 – Result of Fig. A.23

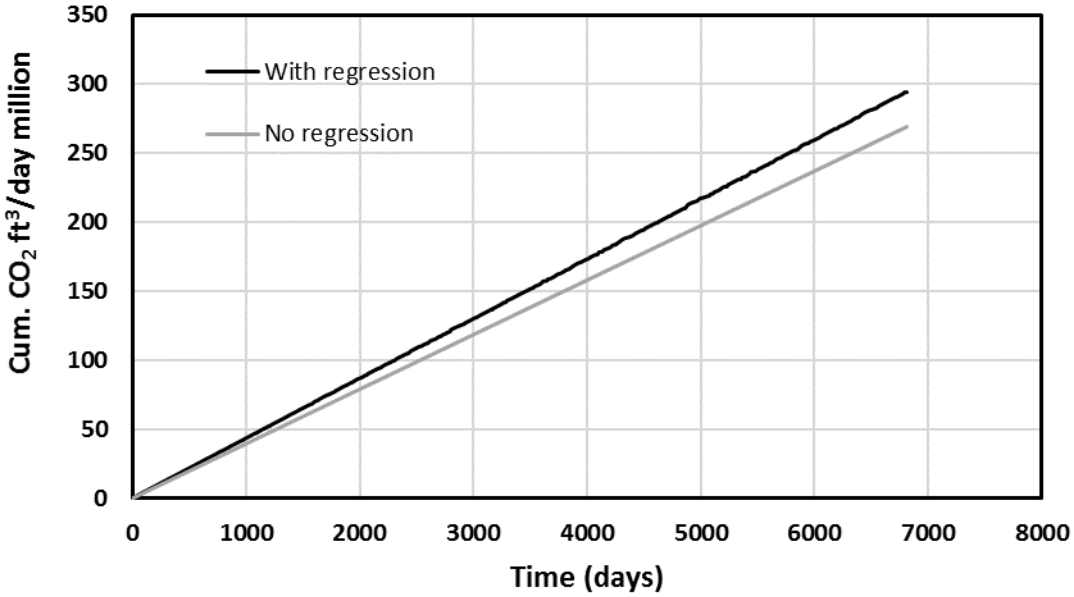

Figure 0.26 – Result of Fig. A.23

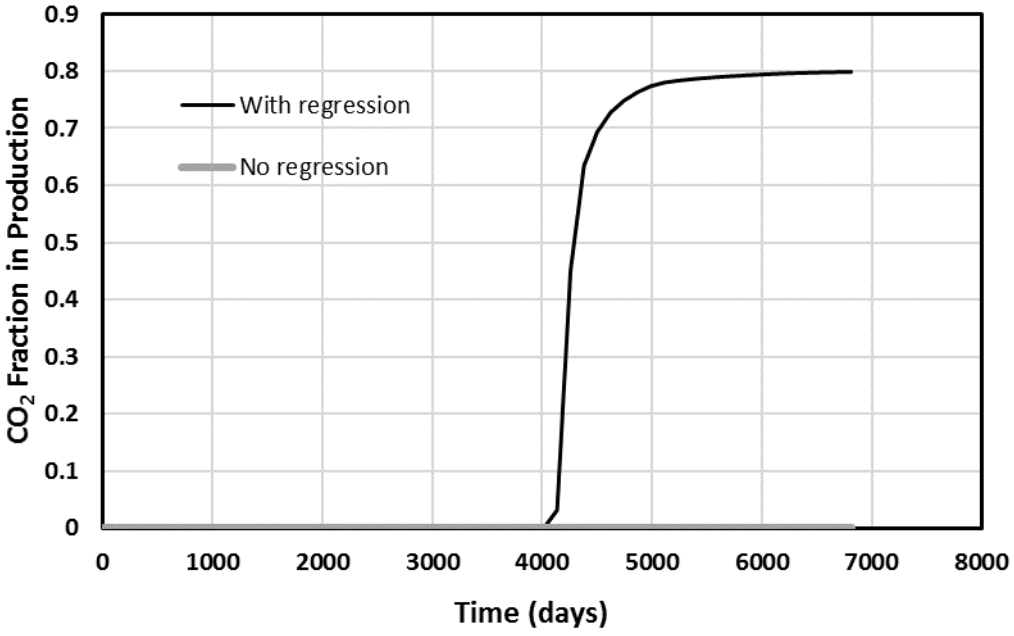

Figure 0.27 – Result of Fig. A.23

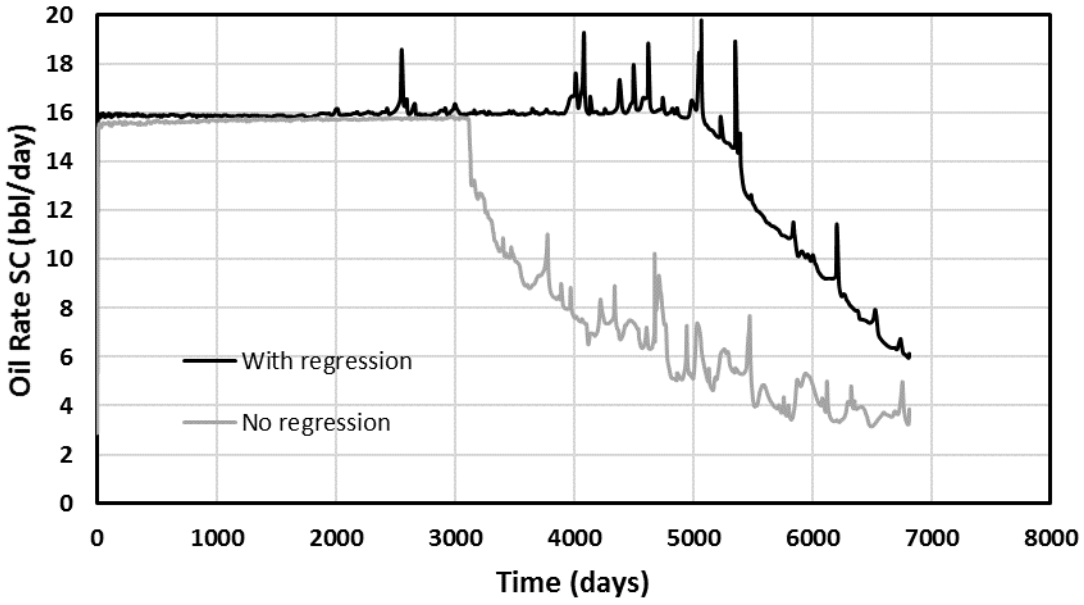

Figure 0.28 – Result of Fig. A.23

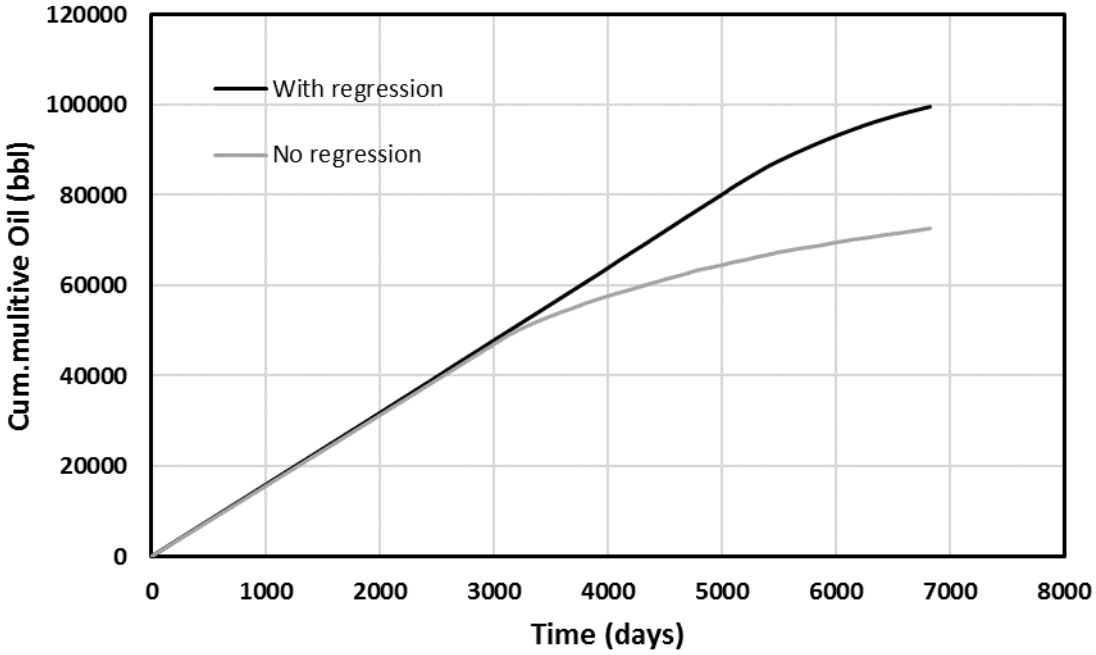

Figure 0.29 – Result of Fig. A.23

100 mD and 1700 psi

With regression

Without regression

5 years

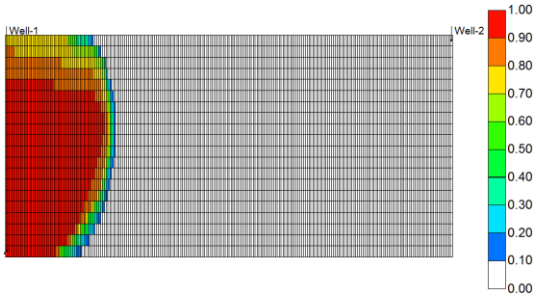

5 years

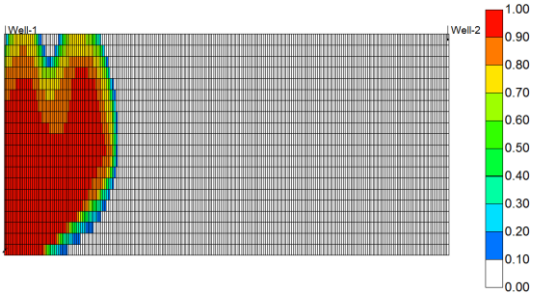

10 years

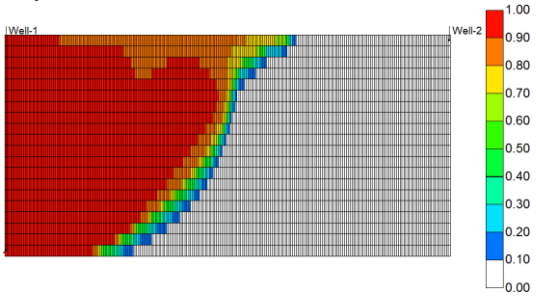

10 years

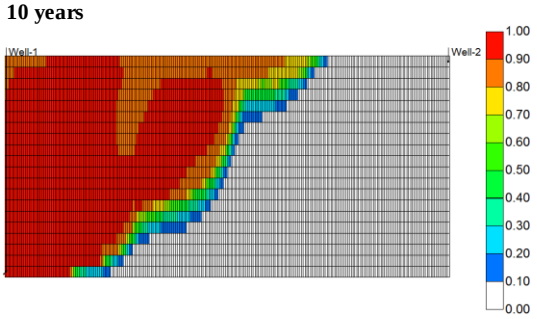

15 years

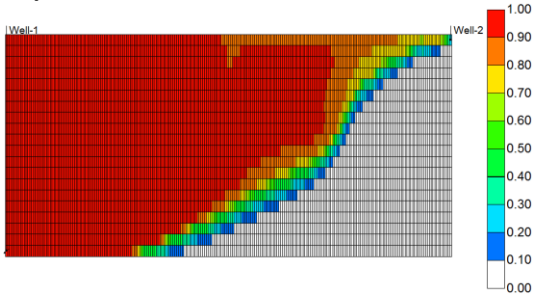

15 years

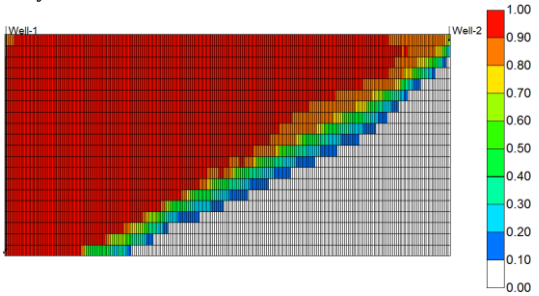

20 years

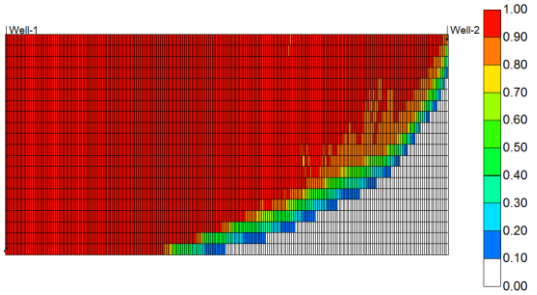

20 years

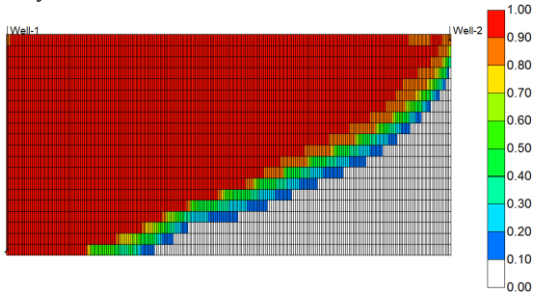

Figure 0.30 – K = 100 mD and P = 1700 psia.

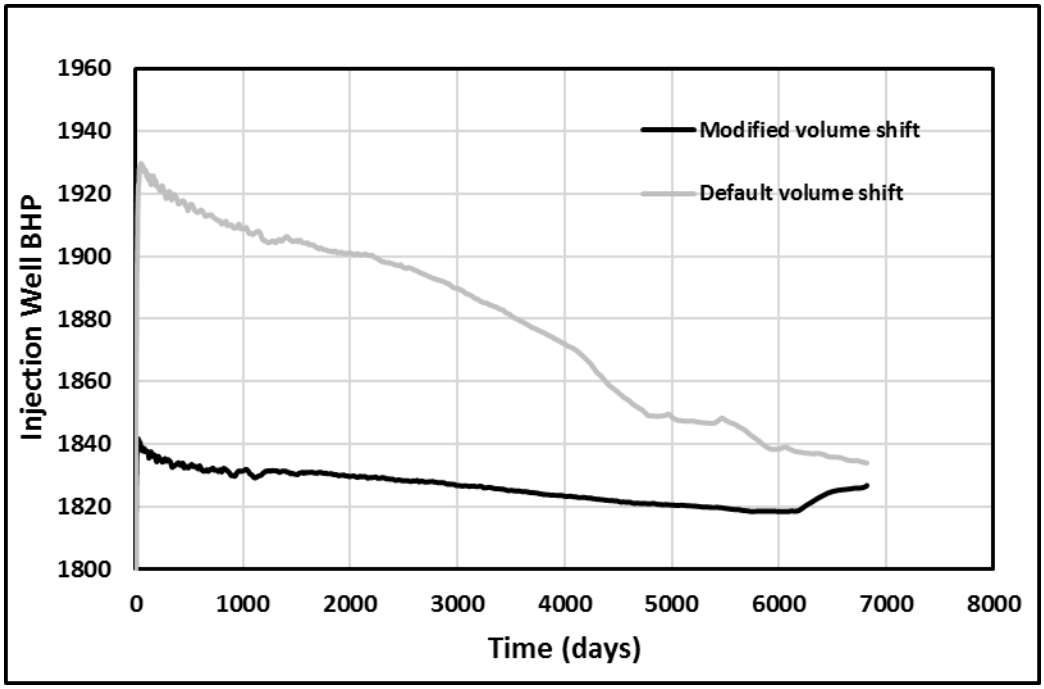

Figure 0.31 – Result of Figure A.30

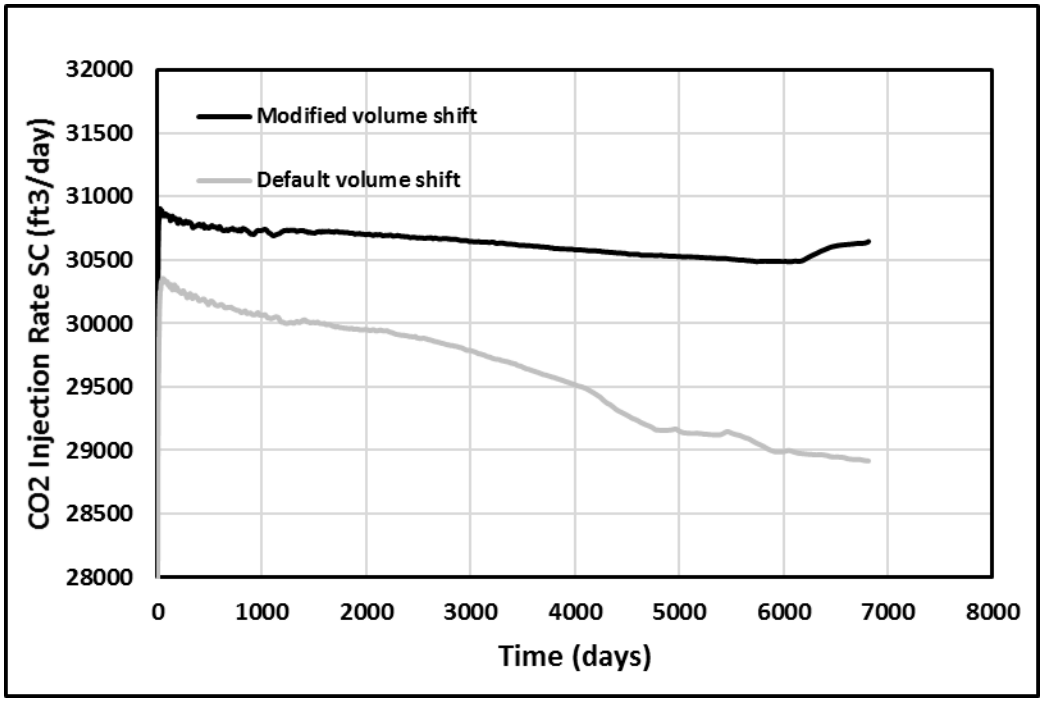

Figure 0.32 – Result of Figure A.30

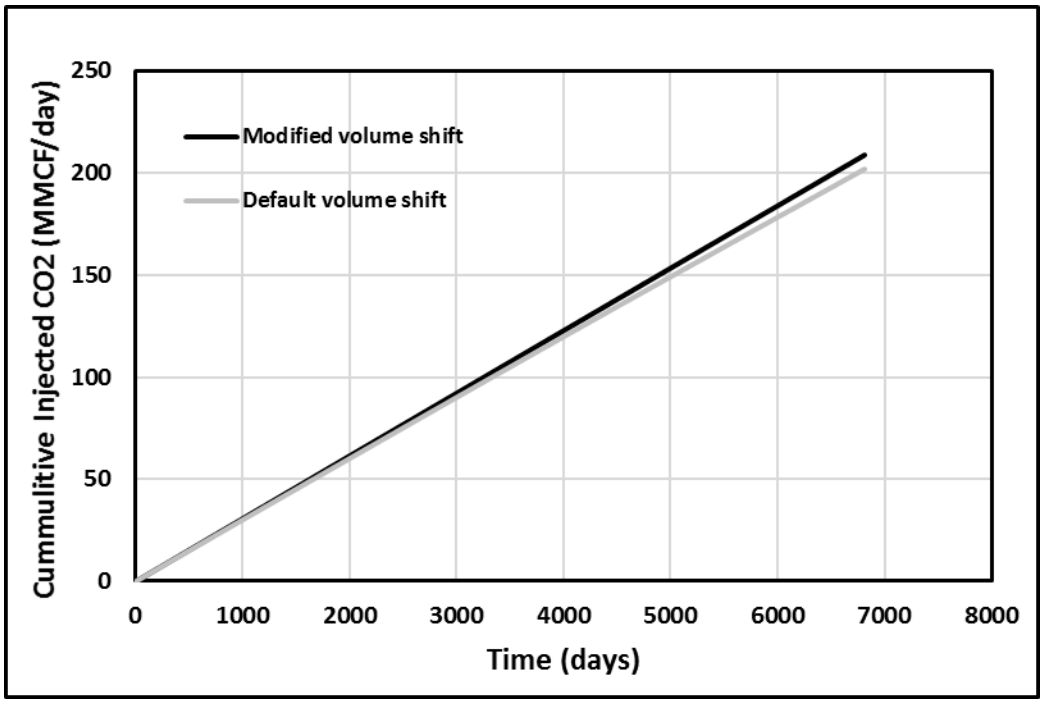

Figure 0.33 – Result of Figure A.30

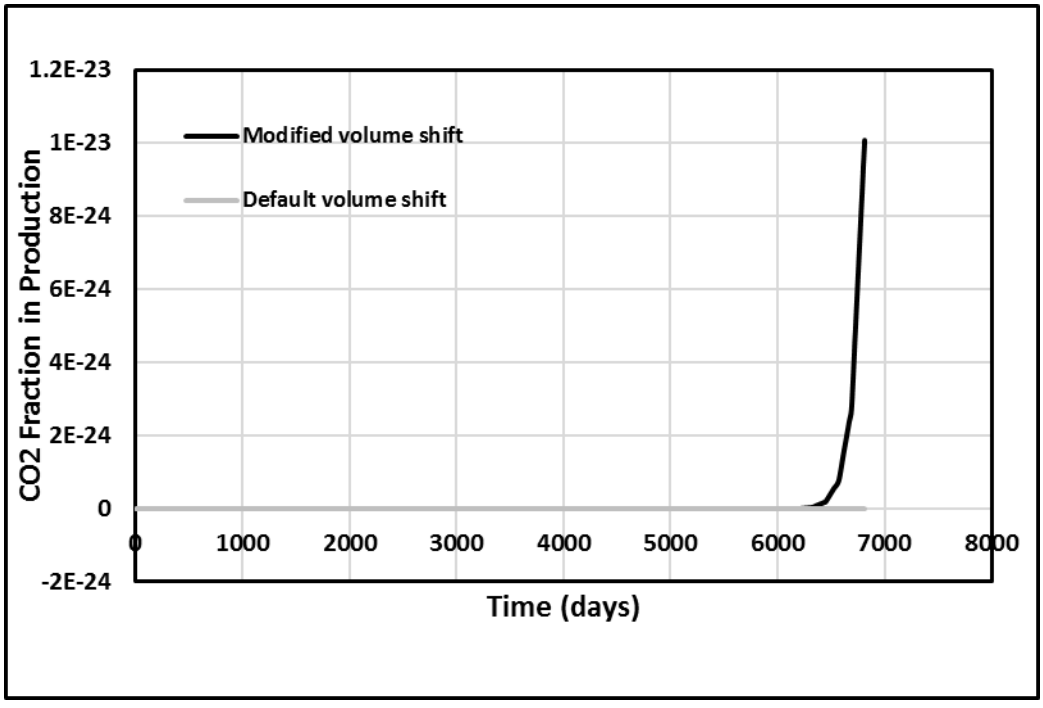

Figure 0.34 – Result of Figure A.30

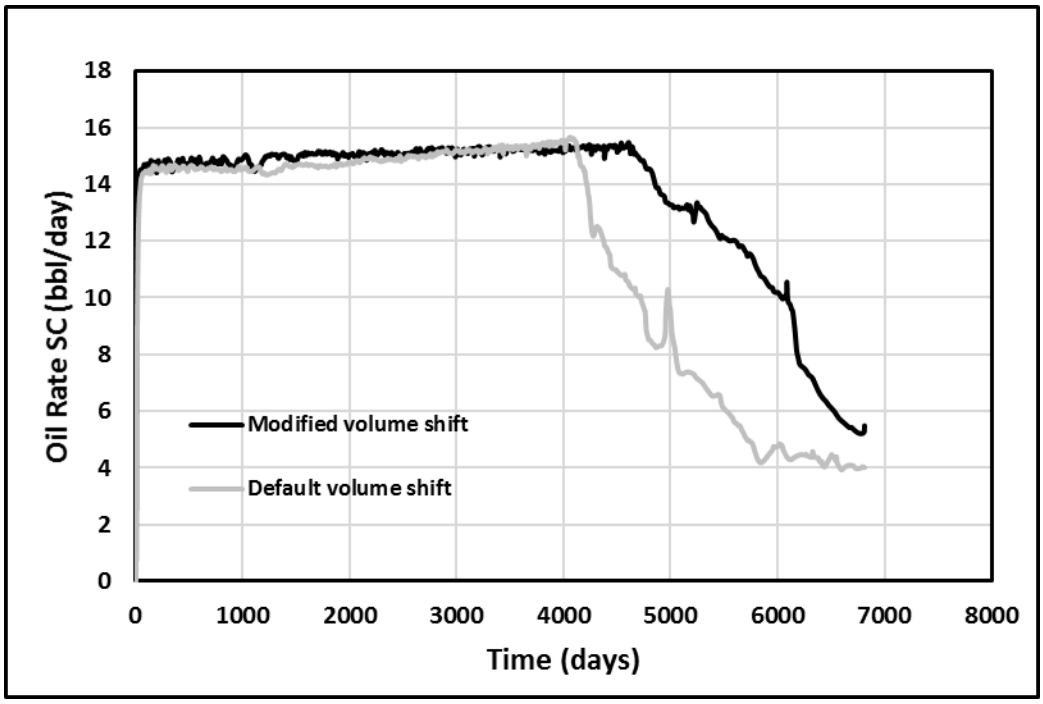

Figure 0.35 – Result of Figure A.30

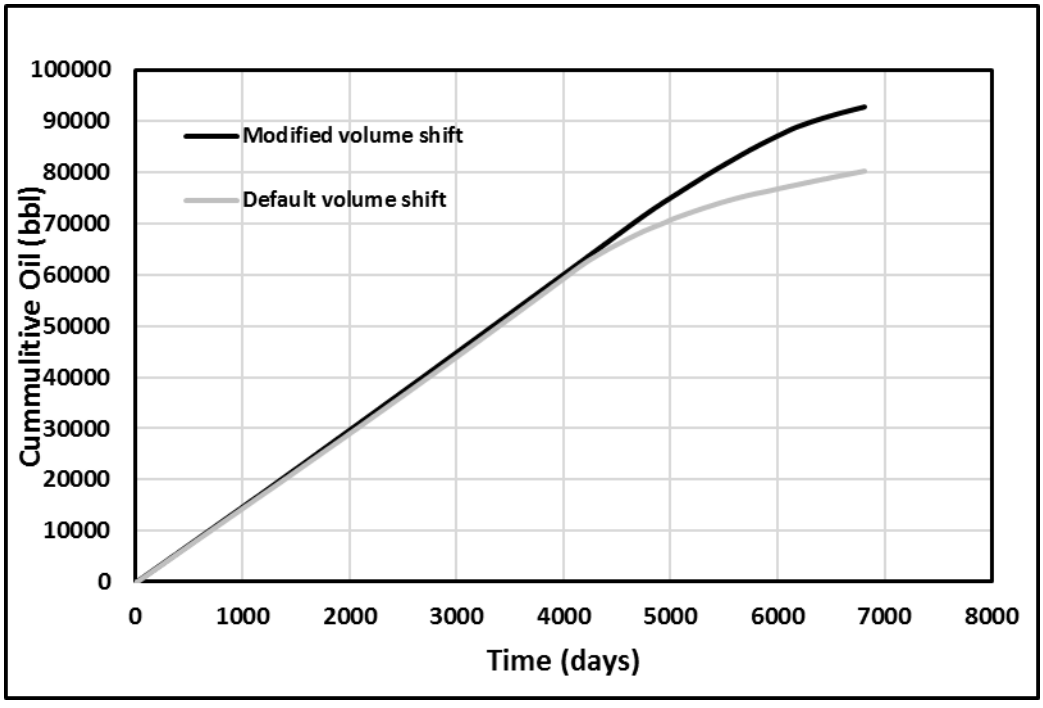

Figure 0.36 – Result of Figure A.30

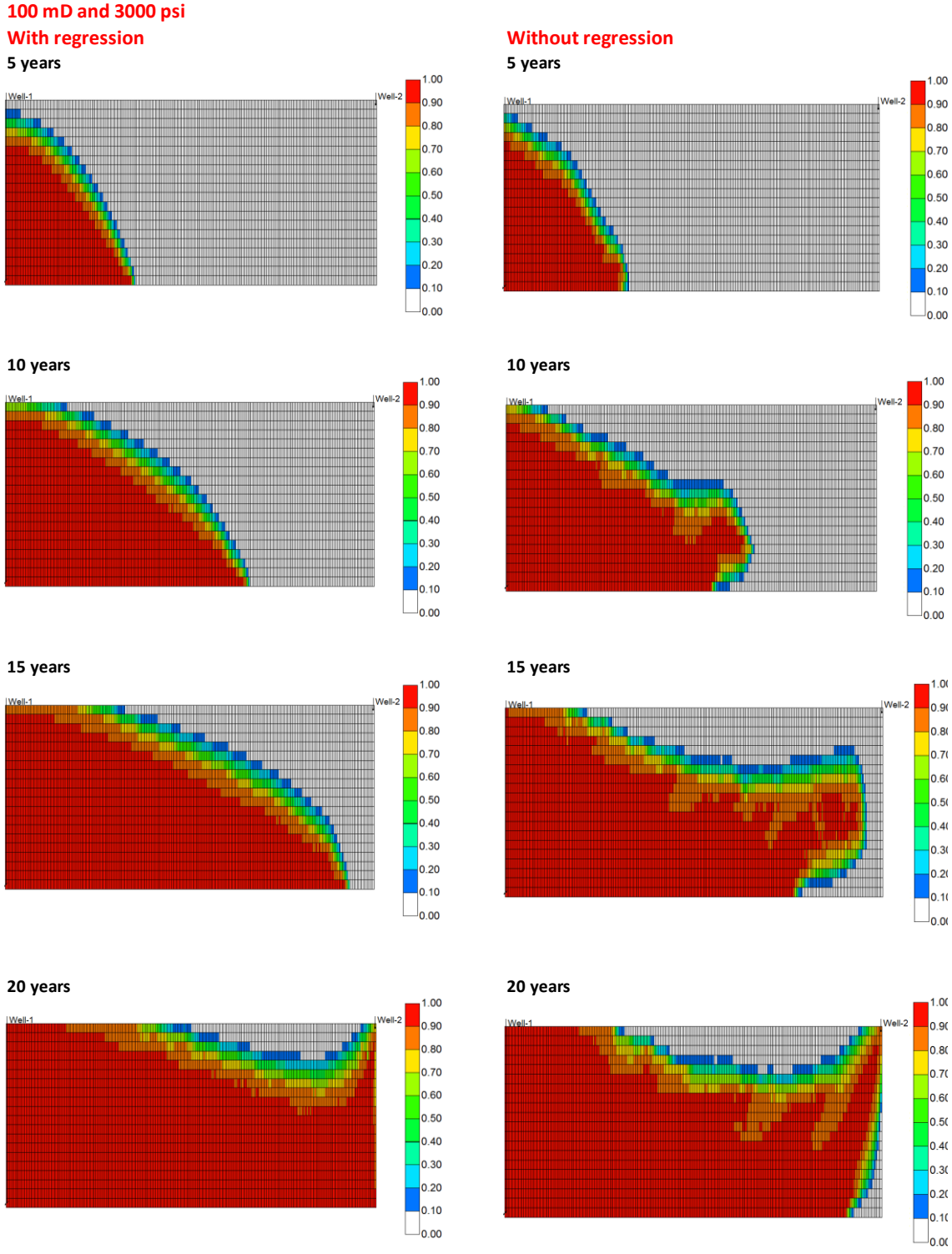

Figure 0.37 – K = 100 mD and P = 3000 psia.

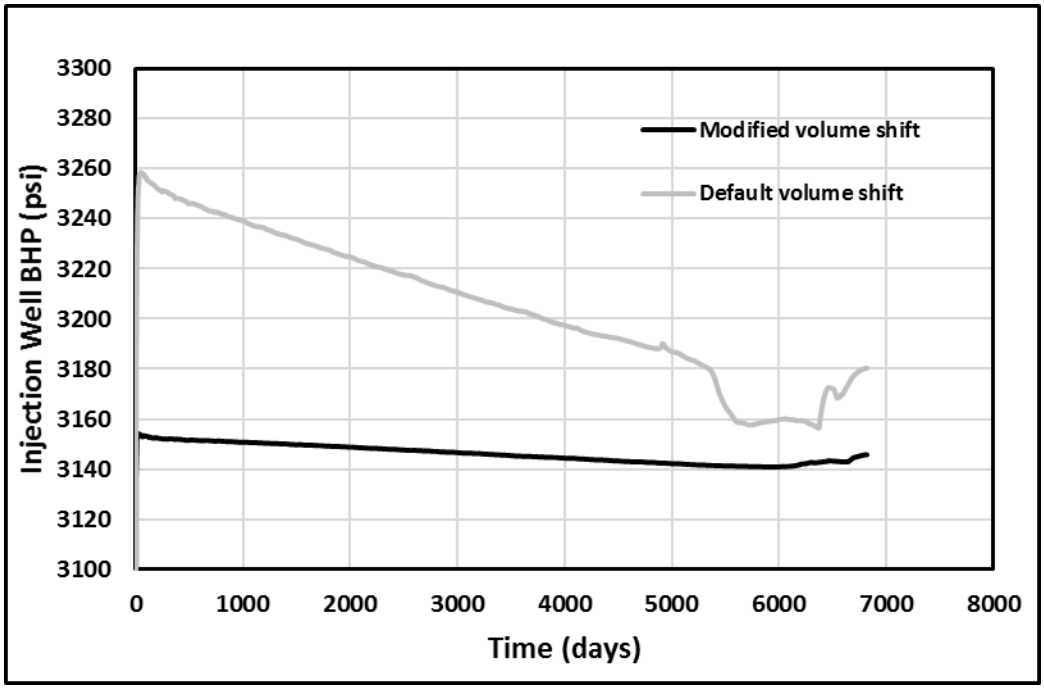

Figure 0.38 – Result of Figure A.37

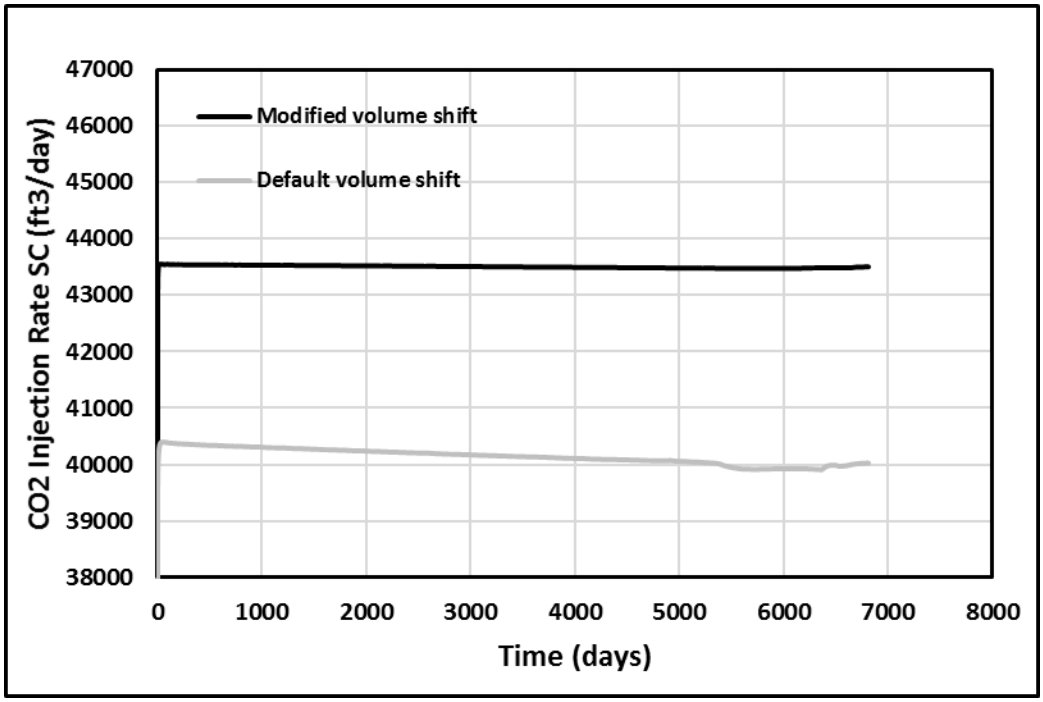

Figure 0.39 – Result of Fig. A.37

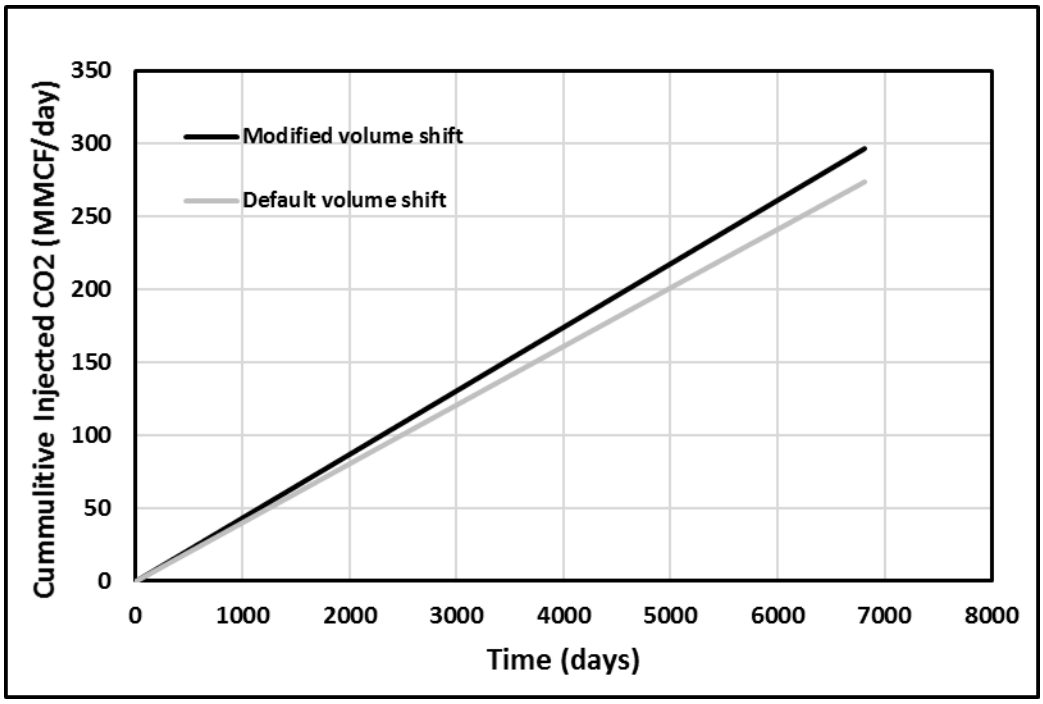

Figure 0.40 – Result of Fig. A.37

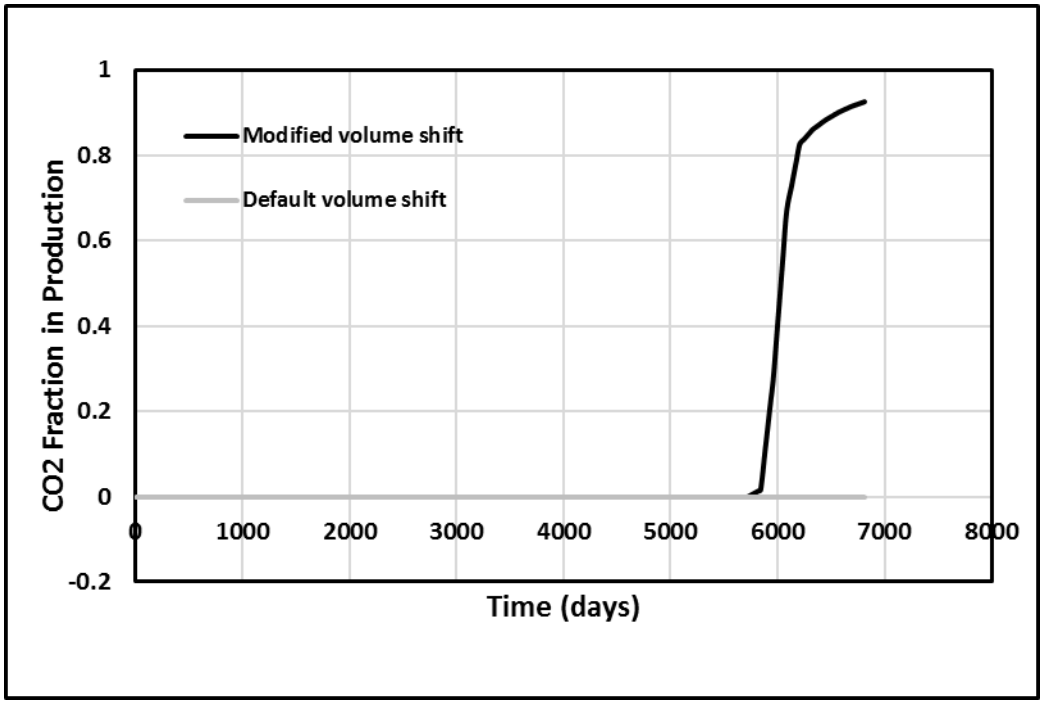

Figure 0.41 – Result of Fig. A.37

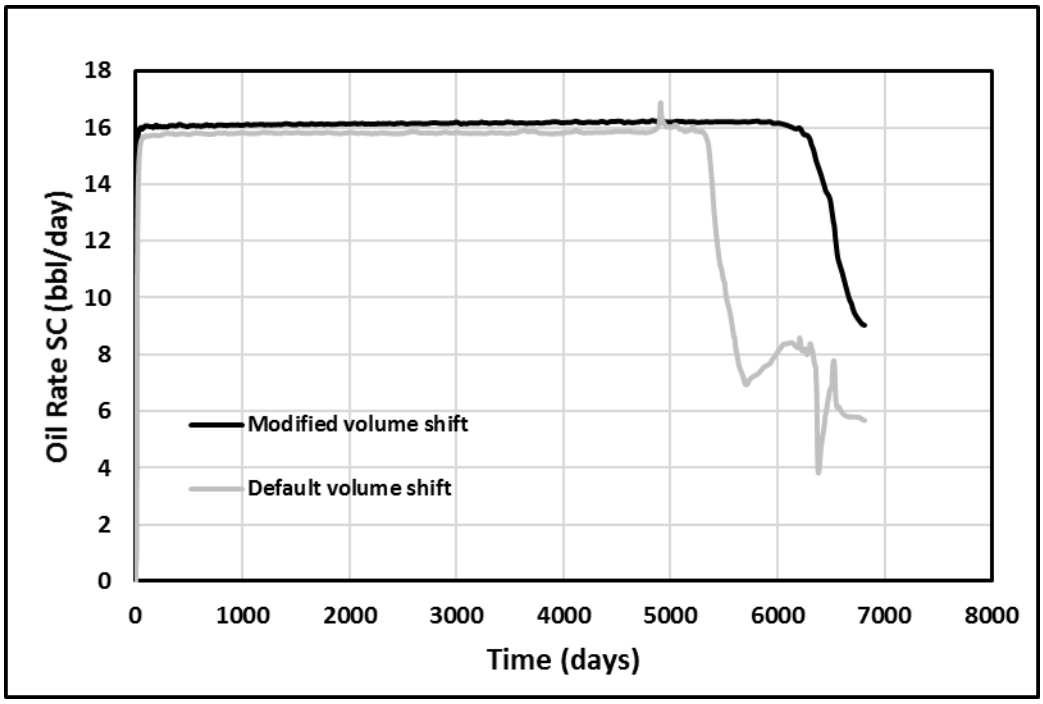

Figure 0.42 – Result of Fig. A.37

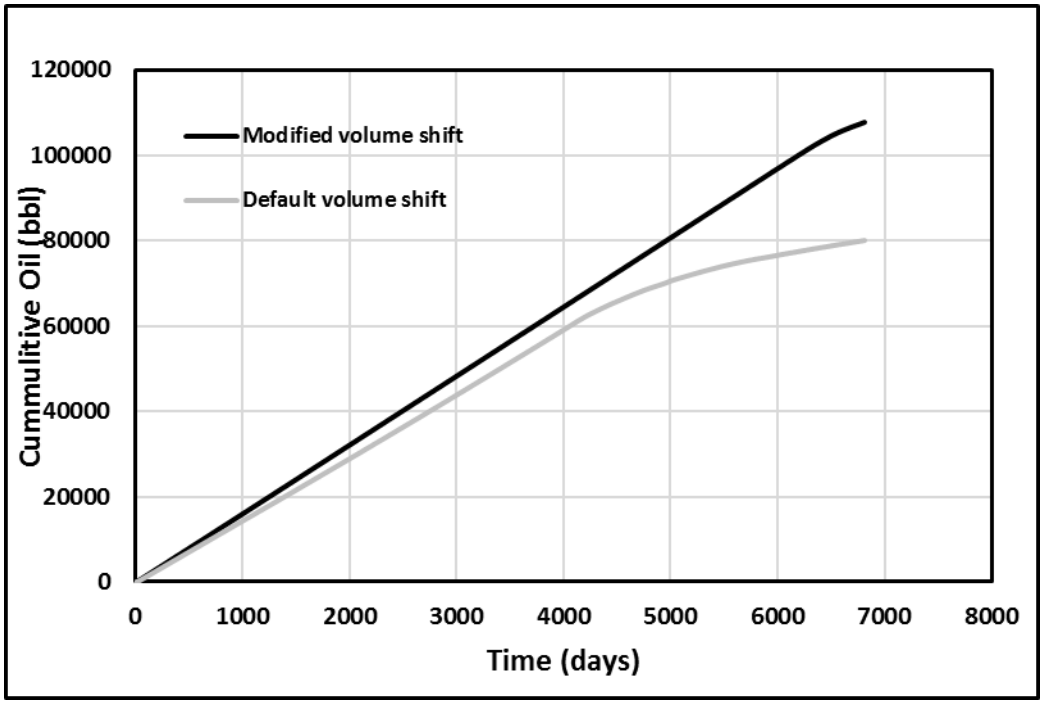

Figure 0.43 – Result of Fig. A.37

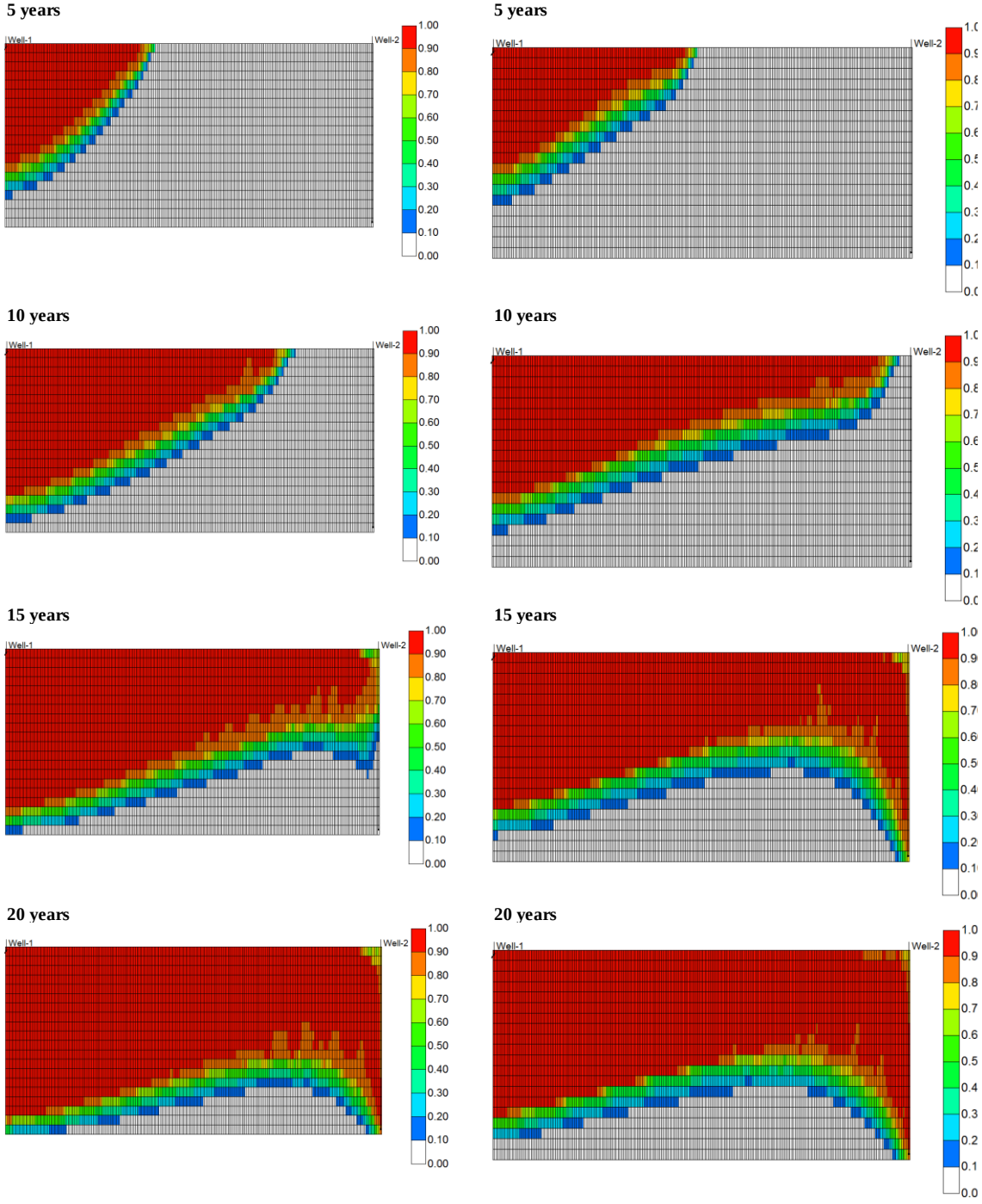

Figure 0.44 – K = 100 mD and P = 1700 psia. With and without density effect

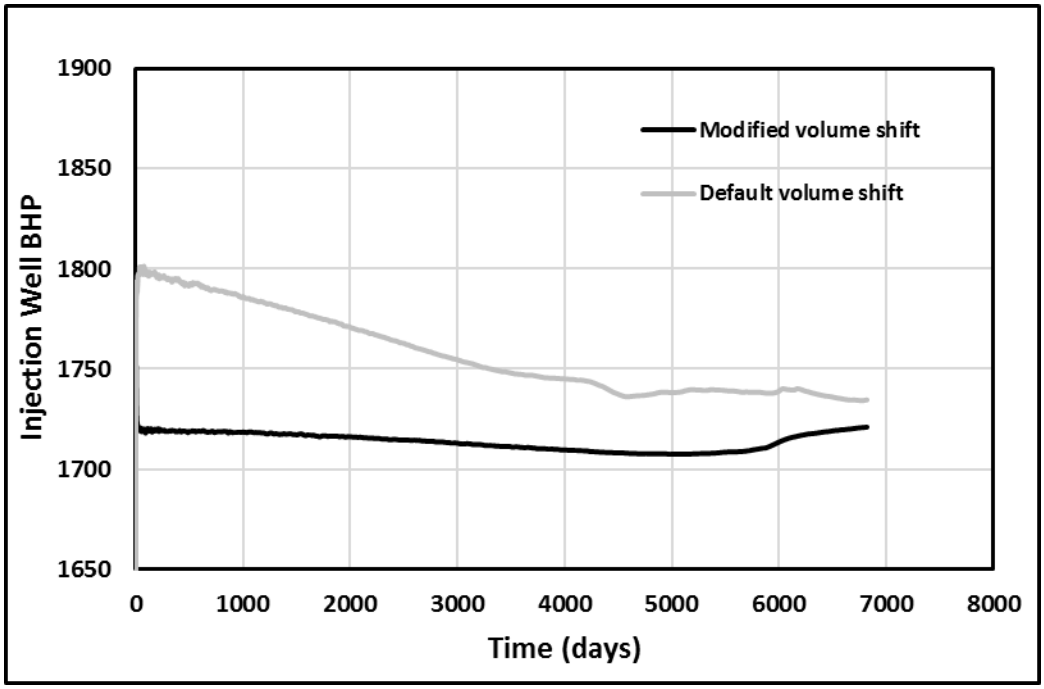

Figure 0.45 – Result of Fig. A.44

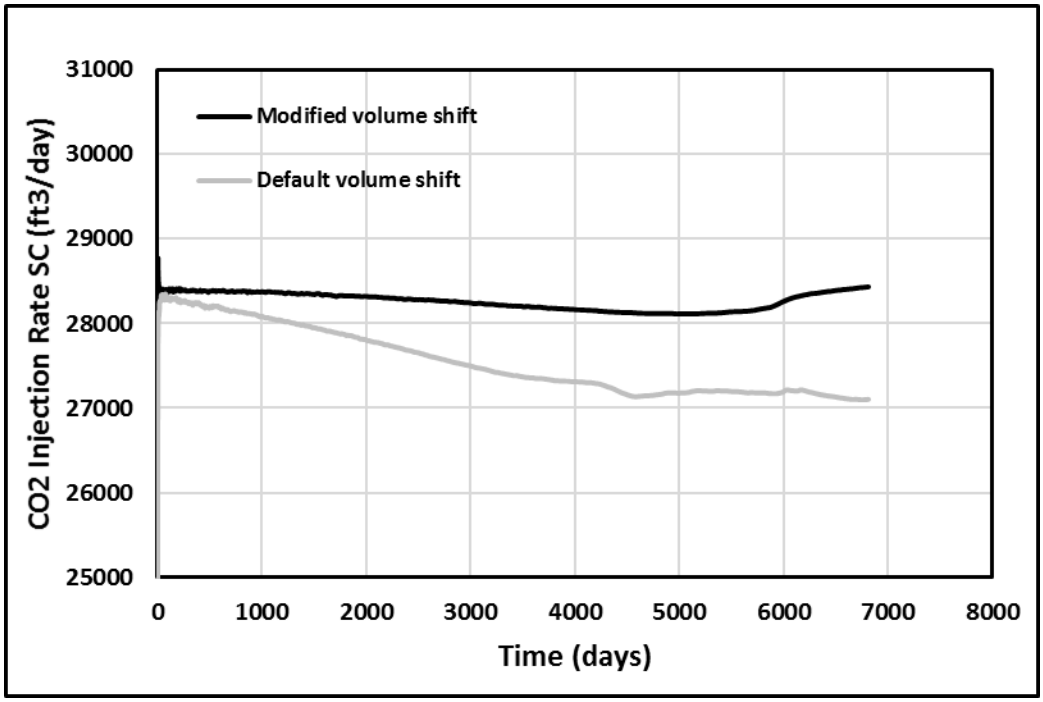

Figure 0.46 – Result of Fig. A.44

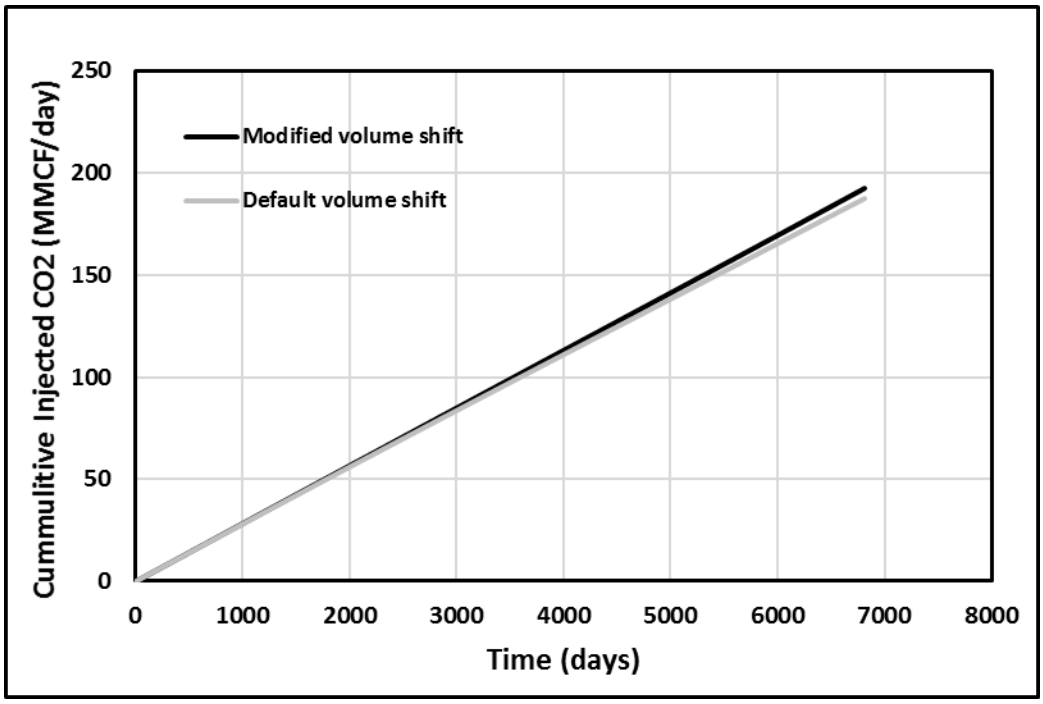

Figure 0.47 – Result of Fig. A.44

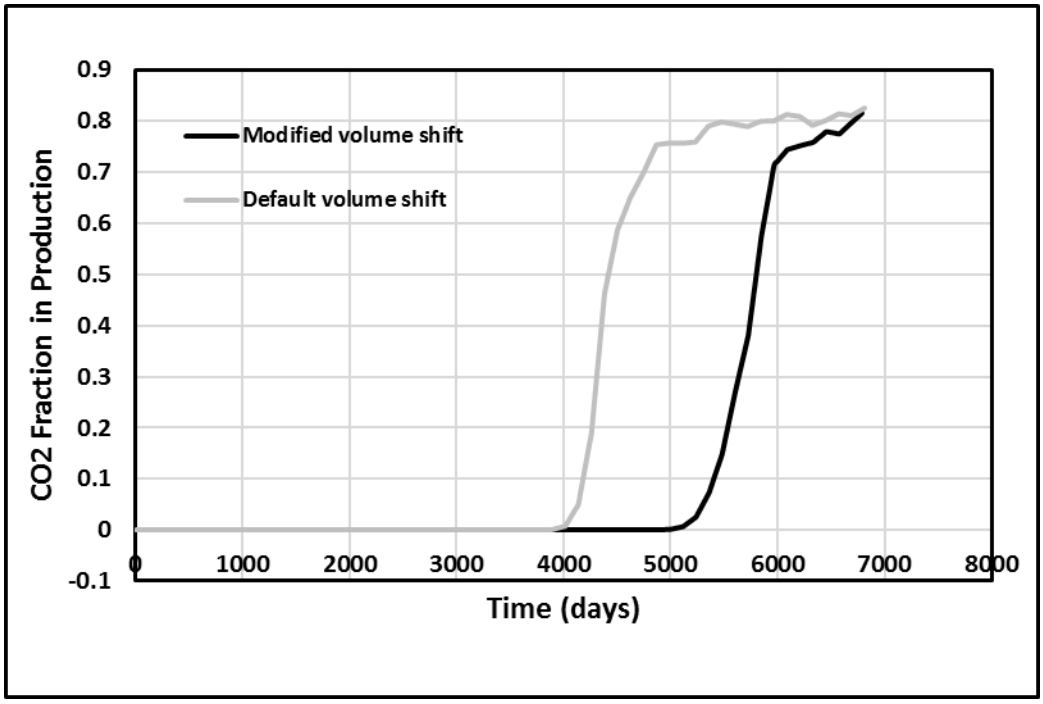

Figure 0.48 – Result of Fig. A.44

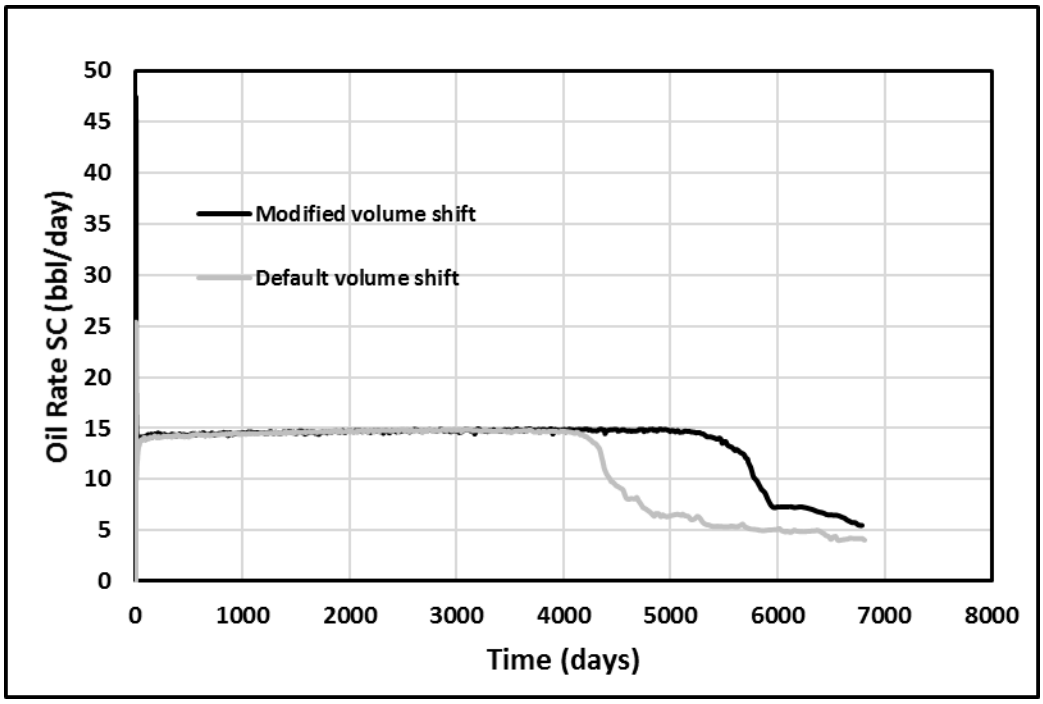

Figure 0.49 – Result of Fig. A.44

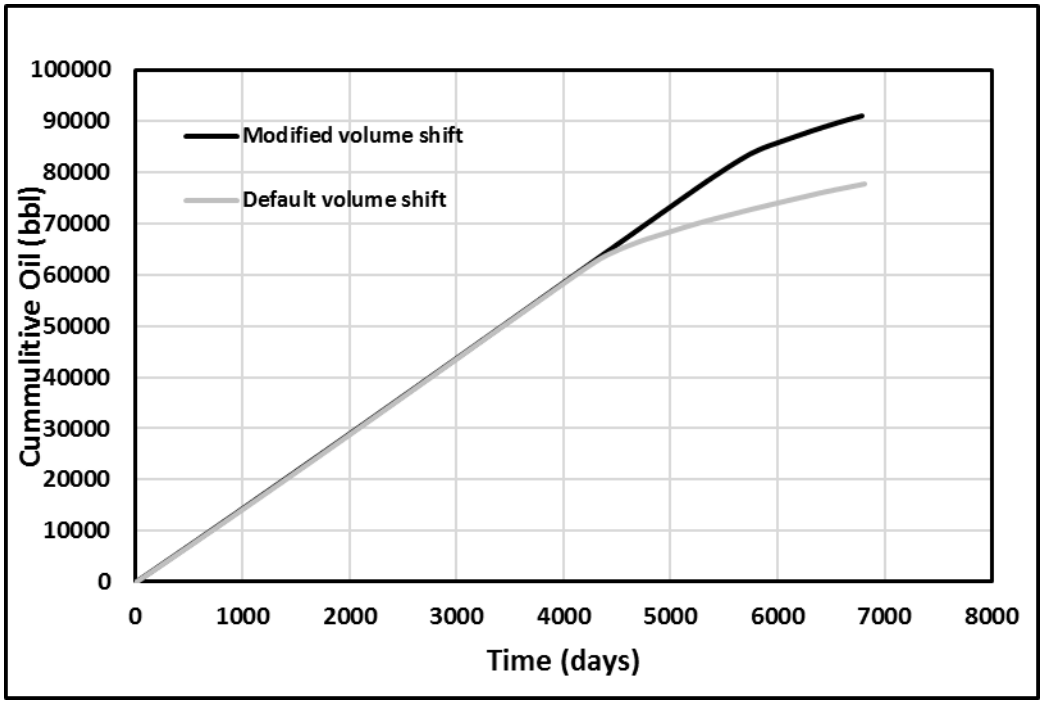

Figure 0.50 – Result of Fig. A.44

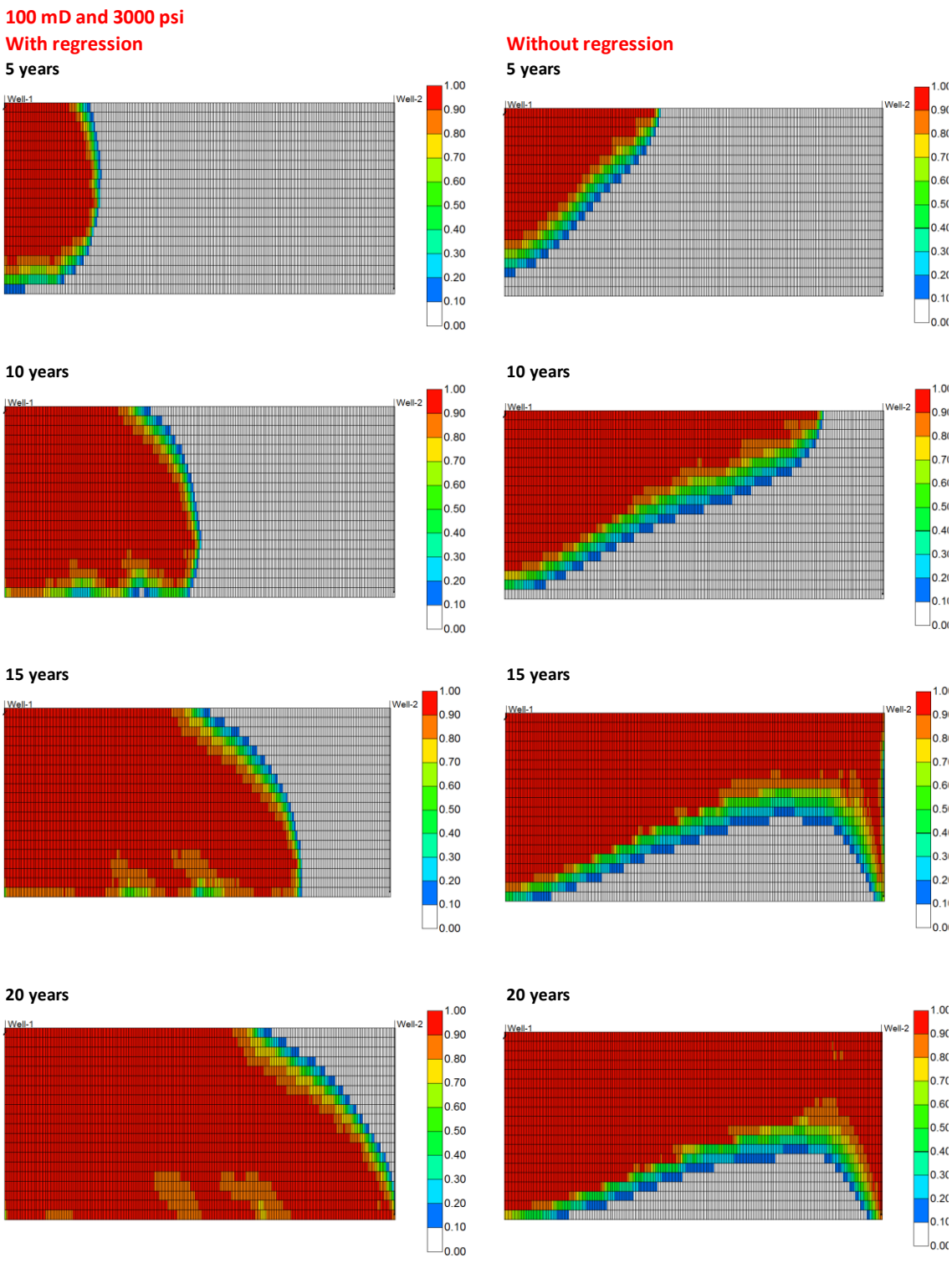

Figure 0.51 – K = 100 mD and P = 3000 psia. With and without density effect

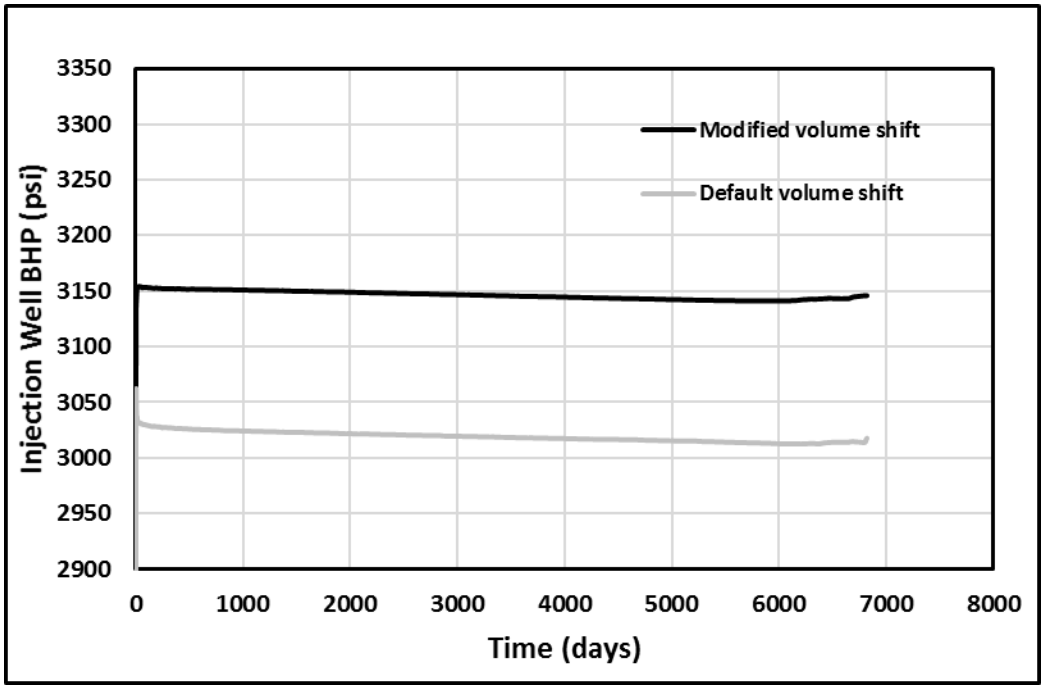

Figure 0.52 – Result of Fig. A.51

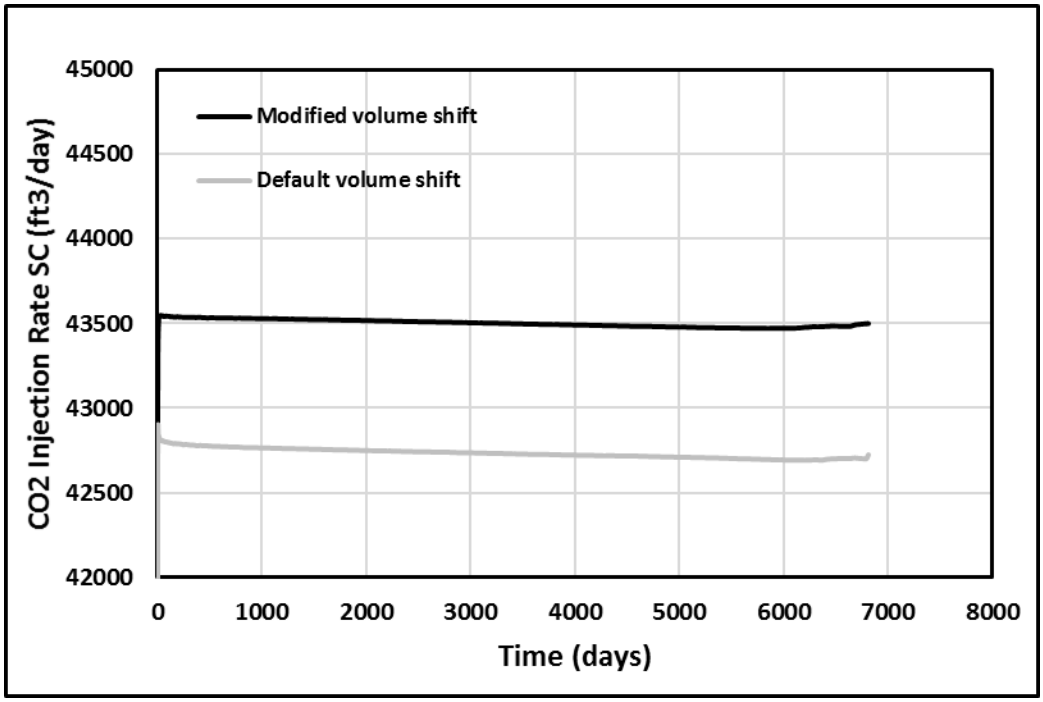

Figure 0.53 – Result of Fig. A.51

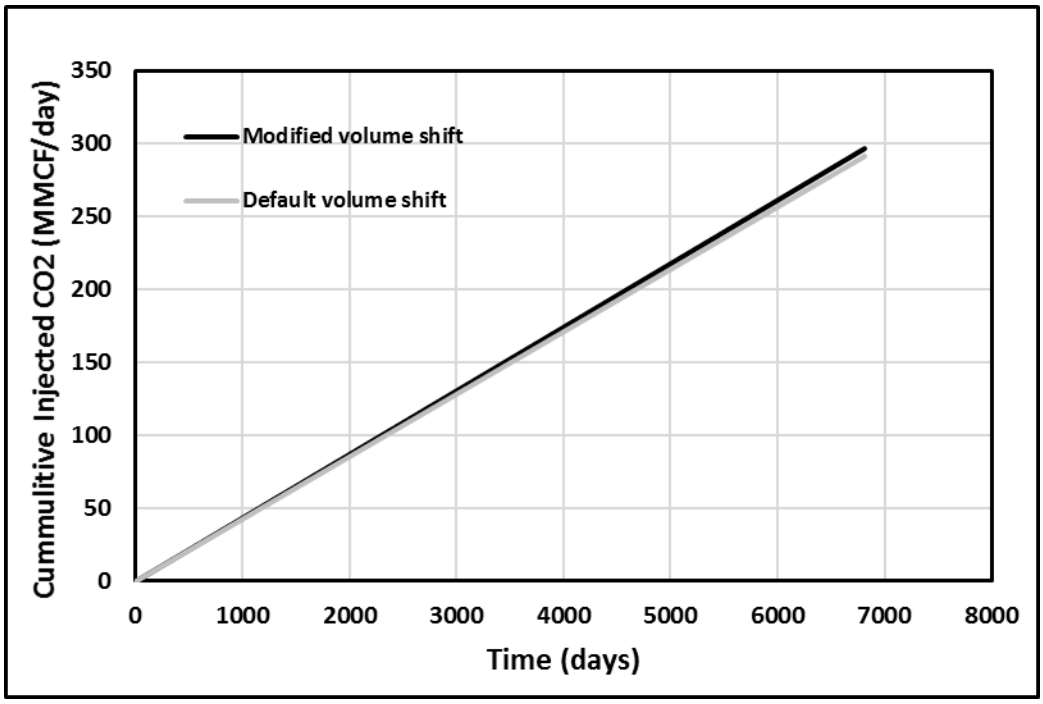

Figure 0.54 – Result of Fig. A.51

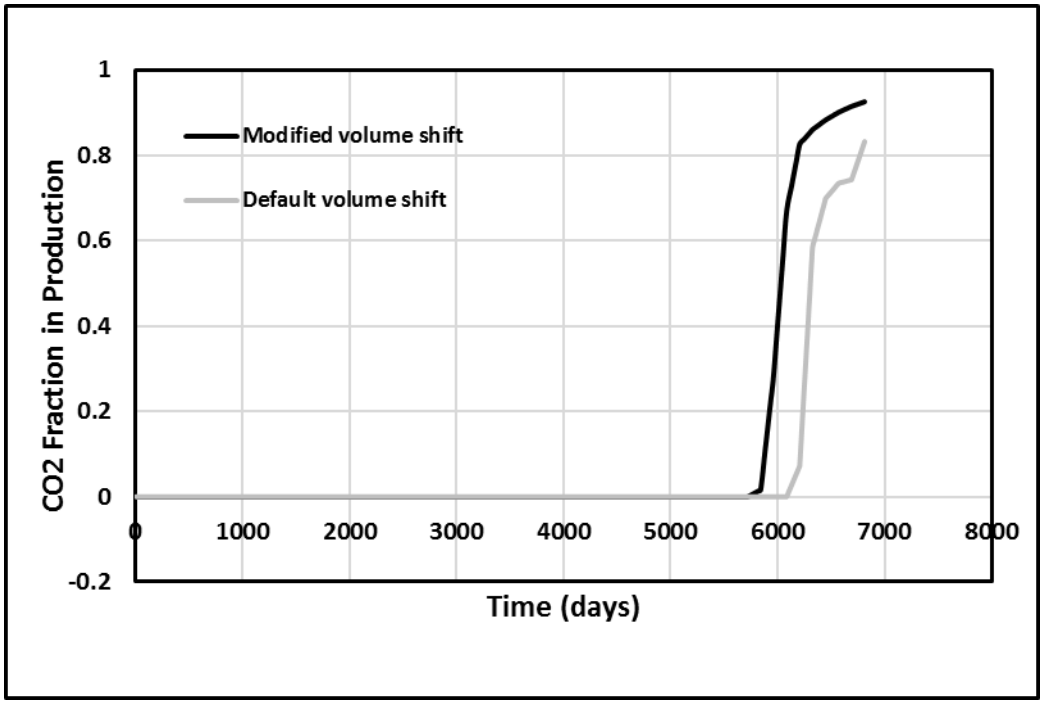

Figure 0.55 – Result of Fig. A.51

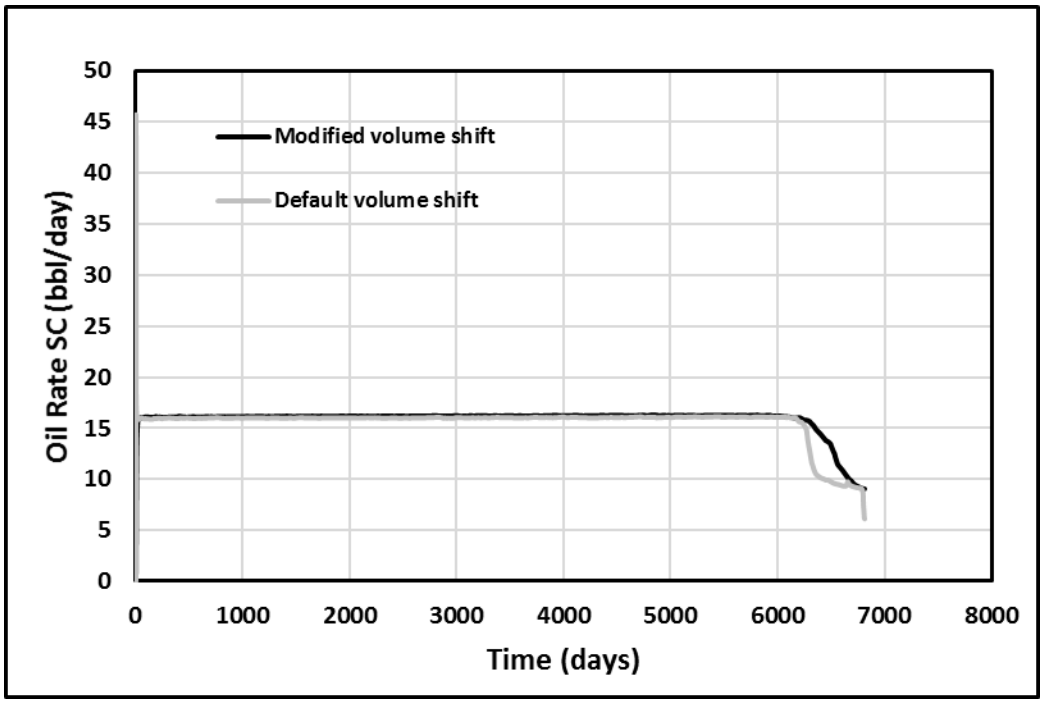

Figure 0.56 – Result of Fig. A.51

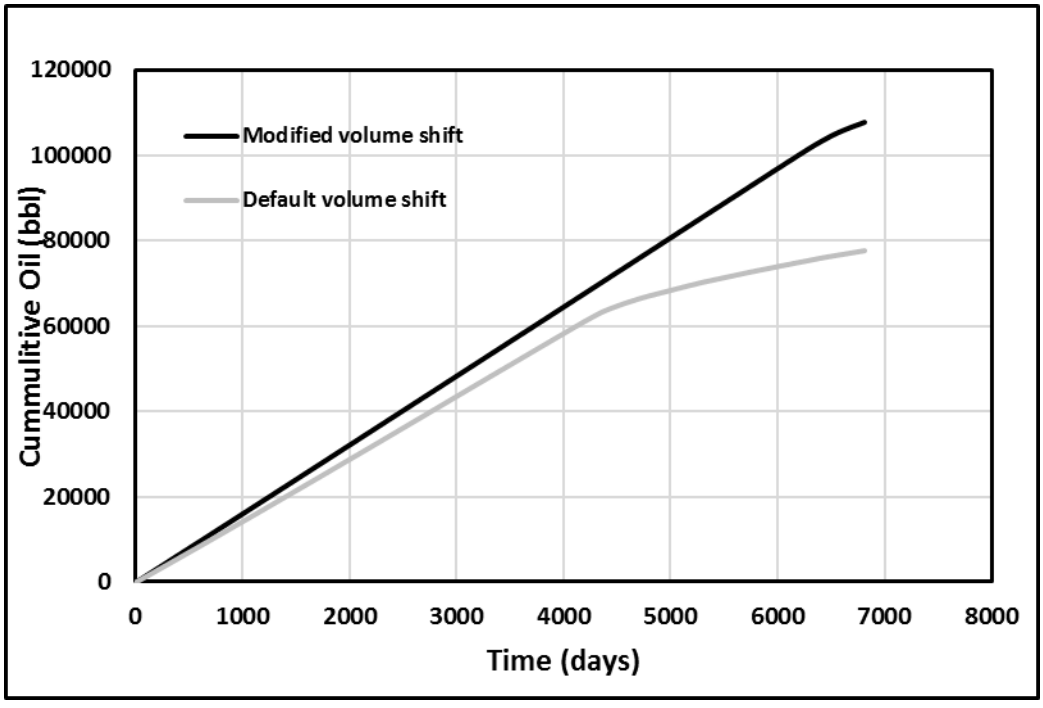

Figure 0.57 – Result of Fig. A.51